



University of HUDDERSFIELD

University of Huddersfield Repository

Promdee, Wanisa

TUNING OF THE RADIO FREQUENCY QUADRUPOLE FOR THE FRONT END TEST
STAND AT RUTHERFORD APPLETON LABORATORY

Original Citation

Promdee, Wanisa (2020) TUNING OF THE RADIO FREQUENCY QUADRUPOLE FOR THE FRONT END TEST STAND AT RUTHERFORD APPLETON LABORATORY. Doctoral thesis, University of Huddersfield.

This version is available at <http://eprints.hud.ac.uk/id/eprint/35611/>

The University Repository is a digital collection of the research output of the University, available on Open Access. Copyright and Moral Rights for the items on this site are retained by the individual author and/or other copyright owners. Users may access full items free of charge; copies of full text items generally can be reproduced, displayed or performed and given to third parties in any format or medium for personal research or study, educational or not-for-profit purposes without prior permission or charge, provided:

- The authors, title and full bibliographic details is credited in any copy;
- A hyperlink and/or URL is included for the original metadata page; and
- The content is not changed in any way.

For more information, including our policy and submission procedure, please contact the Repository Team at: E.mailbox@hud.ac.uk.

<http://eprints.hud.ac.uk/>



**TUNING OF THE RADIO FREQUENCY
QUADRUPOLE FOR THE FRONT END TEST STAND
AT RUTHERFORD APPLETON LABORATORY**

WANISA PROMDEE

DOCTOR OF PHILOSOPHY

2020

**TUNING OF THE RADIO FREQUENCY
QUADRUPOLE FOR THE FRONT END TEST
STAND AT RUTHERFORD APPLETON
LABORATORY**

University of
HUDDERSFIELD

Wanisa Promdee

International Institute for Accelerator Applications
University of Huddersfield

Doctor of Philosophy

May 2020

Declaration

- I. The author of this thesis (including any appendices and/or schedules to this thesis) owns any copyright in it (the "Copyright") and s/he has given The University of Huddersfield the right to use such Copyright for any administrative, promotional, educational and/or teaching purposes.
- II. Copies of this thesis, either in full or in extracts, may be made only in accordance with the regulations of the University Library. Details of these regulations may be obtained from the Librarian. This page must form part of any such copies made.
- III. The ownership of any patents, designs, trade marks and any and all other intellectual property rights except for the Copyright (the "Intellectual Property Rights") and any reproductions of copyright works, for example graphs and tables ("Reproduction"), which may be described in this thesis, may not be owned by the author and may be owned by third parties. Such Intellectual Property Rights and Reproductions cannot and must not be made available for use without the prior written permission of the owner(s) of the relevant Intellectual Property Rights and/or Reproductions.

Abstract

The Front End Test Stand (FETS) is a project that aims to accelerate a 60 mA beam of H^- ions to 3 MeV at 50Hz with an RF frequency of 324 MHz. It is designed to demonstrate a high beam current with fast chopping. It is also being considered for the ISIS II upgrade. The FETS RFQ is the main accelerating structure, and the 3 MeV final energy is reached at the end of this. It is a four-vane type and consists of four sections, one metre long each. There are sixty-four tuner ports, but only sixty-two are available for tuning. Four of them are for automatic tuners that are applied when the FETS RFQ is in operation. The other ports, fifty-eight, are allocated for the slug tuners, which must be adjusted manually.

The fields along the FETS RFQ have to be uniform (i.e. flat) at 324 MHz as it is a sensitive accelerating structure. The tuning system is used to do this and ensure that the RFQ is operating at the correct frequency. In order to correct the fields from the imperfectly machined RFQ, a bead pull measurement is introduced. Perturbation and tuning techniques have been studied to understand the ideas behind this technique. The inserted length from the tuner affects the overall frequency of the RFQ and local field distribution. If the tuner is inserted into the RFQ cavity leading to the decrease in cavity volume, the frequency will increase. On the contrary, to reduce the RFQ frequency, the tuner has to move out from the RFQ cavity. By using the bead pull measurement data, the new tuners' lengths can be calculated. After adjusting the tuners, measurements are taken to confirm the new fields. If the fields are not in a sufficiently uniform pattern, the tuning process is repeated.

The system was tested using a one-metre long FETS RFQ bead pull measurement away from the FETS area using section two of the RFQ. This gave experience with the bead pull technique and allowed the measurements to be studied. After that, the system was re-designed for the four-metre FETS RFQ and constructed in the limited space of the FETS area. One section and then all four sections of the FETS RFQ were installed for the first four-metre bead pull measurements. These have been taken to study the fields in the FETS RFQ and the effects of the tuners on the FETS RFQ cavity.

With one section of the RFQ, the measurements were taken for data preparation such as frequency resolution, tuner adjustment effects and direction of the bead pull. With the complete FETS RFQ, because of limitations in time, only the forward direction was chosen for the measurement. The sag effect is also important, especially with the long length pulley setup. The corrected measurement data might not match the programmed position because of the sag from the bead and string weights. It was demonstrated that this sag could be

corrected automatically during the measurements. Possible errors in the tuning measurement were studied and the largest determined to be in the measurement and adjustment of the manual tuners.

Using the FETS RFQ tuning algorithm, the field flatness was reduced from a spread of 7.42% to 0.8%, both with and without the RFQ cooling system in operation, at 324 MHz resonant frequency. With acceptable operation fields, the FETS RFQ is now ready for high power commissioning and beam tests.

Acknowledgement

First of all, I would like to thank the Thai Government for providing an undeniable opportunity to study abroad. Thank you Royal Thai Government staff for taking care of me since I have got a scholarship.

Thank you Professor Rob Edgecook, my best supervisor, for all the supports. You are a kindness, patient, generous and warm person. Thank you Professor Roger Barlow who always try to understand me. Thank you Professor Rebecca for encouraging me to do something new. I am really appreciating it.

Thank you my colleagues at RAL: Alan, Mike, Simon, Gary and Jim, and IIAA team at the University of Huddersfield who will always be great company.

I also thank my high school and undergrad friends for keeping in touch and cheering me up when I am feeling down. Thanks to my old housemates even though we rarely meet each other because I am a night person, I enjoyed living with you. Thanks to TJ team, I love working with you guys.

And last, my family. Though I am not in Thailand, I know all of you always have my back. I love you Mom, Dad and Jill.

Contents

Chapter 1. Introduction	16
1.1 Linear Accelerators (Linacs)	16
1.2 Low Velocity Accelerators	17
1.2.1 Sloan Lawrence Accelerator	17
1.2.2 Alvarez Accelerator	18
1.3 Radio Frequency Quadrupole (RFQ)	18
1.4 FETS Project	19
1.5 Aims of the Research	22
1.6 Summary	22
Chapter 2. Radio Frequency Quadrupole (RFQ)	24
2.1 Basic Principles of the RFQ	24
2.2 Functions of the RFQ	27
2.2.1 Focusing	27
2.2.2 Bunching	27
2.2.3 Acceleration	27
2.3 Structures of the RFQ	29
2.3.1 Radial Matcher (RM)	29
2.3.2 Shaper	29
2.3.3 Gentle Buncher	30
2.3.4 Accelerator	30
2.4 RF Structure of the RFQ	30
2.5 Types of the RFQ	31
2.5.1 Four-vanes Type	31
2.5.2 Four-rods Type	32
2.5.3 Other Types	32
2.6 Problems with RFQs	33

2.7	RFQ Applications	33
2.7.1	High Current injectors	34
2.7.2	Heavy Ion RFQs	34
2.7.3	Variable Energy RFQs	34
2.7.4	Other Applications	35
2.8	Summary	35
Chapter 3. FETS RFQ		36
3.1	The Design of the FETS RFQ	36
3.1.1	Four-Vane Structure	36
3.1.2	Modulation Parameters	37
3.2	Tuning system of the FETS RFQ	38
3.2.1	Slug Tuners	38
3.2.2	Automatic Tuners	39
3.3	The FETS RFQ Cold Model	40
3.4	Problems of the FETS RFQ	41
3.5	Summary	41
Chapter 4. Bead Pull System		42
4.1	Principles of the RF Cavity	42
4.1.1	Transverse Modes in the Cavity	42
4.1.2	S-parameters	43
4.2	Four-vane RFQ Cavity Eigenmodes	44
4.2.1	TE-like Mode	44
4.2.2	Quadrupole and Dipole Modes	45
4.2.3	Fields in the RFQ	46
4.3	Bead Pull Theory	47
4.4	Sag Effect of the Bead Pull System	48
4.5	Bead Pull Experiment	50
4.6	Examples of RFQ Bead Pull Measurements	50

4.7	Bead Pull System of the FETS RFQ	52
4.8	Summary	52
Chapter 5. Tuning System		54
5.1	RFQ Tuning System	54
5.2	Tuning Algorithm	55
5.2.1	Fields in Each Quadrant	55
5.2.2	Frequency Perturbations	56
5.3	FETS RFQ Tuning Algorithm	57
5.3.1	Measurement Data and Fitting	57
5.3.2	Calculation of New Frequency Shift	59
5.3.3	Tuning Diagram of the FETS RFQ	61
5.4	Summary	64
Chapter 6. Methods		65
6.1	Bead Pull Measurement	65
6.1.1	One-Metre Arrangement	65
6.1.2	Four-Metre Arrangement	69
6.2	Tuning Algorithm	76
6.3	Summary	81
Chapter 7. One-Metre of Bead Pull Measurement		83
7.1	Gaussian versus Lorentzian	83
7.1.1	Sweep Data	84
7.2	Frequency resolution	86
7.3	Forward and Reverse Direction	87
7.4	Tuner Effects	88
7.5	Summary	90
Chapter 8. Four-Metre of Bead Pull Measurement		91
8.1	One Section with Four-Metre of Bead Pull Measurement	91

8.1.1	Forward and Reverse Directions	91
8.1.2	Angle versus frequency shift	92
8.1.3	Temperature effect	94
8.1.4	Radius versus frequency shift	94
8.1.5	FETS RFQ Section one and two	96
8.2	Four Sections with Four-Metre of Bead Pull Measurement	97
8.2.1	Forward and Reverse Directions	98
8.2.2	Measurement Errors	98
8.2.3	Sag Correction	103
8.2.4	Temperature Effects	107
8.2.5	Manual Tuners	109
8.2.6	Automatic Tuners	111
8.2.7	Results with the Tuning Algorithm	112
8.2.8	Final Tuning Results	114
8.3	Summary	117
Chapter 9. Conclusions		119
9.1	Summary	119
9.2	Future Work and Suggestions	120
Chapter 10. References		122

Total word count: 24288

List of Figures

Figure 1.1: The simple diagram of a linear accelerator [4].	16
Figure 1.2: The principle of Sloan Lawrence accelerator [12].	18
Figure 1.3: The principle of Alvarez accelerator [12].	18
Figure 1.4: Ideal layout of a future plan of the FETS project [30].	19
Figure 1.5: FETS layout [37].	20
Figure 1.6: Model of the RFQ section one (right) connected with LEBT (left) [39].	21
Figure 1.7: FETS RF distribution layout [40].	21
Figure 2.1: Four electrodes with alternating voltages [41].	24
Figure 2.2: Alternating gradient focusing (G) with space (top) and time (bottom) periodicities [41].	25
Figure 2.3: Polarity of fields and parameters of modulation [41].	26
Figure 2.4: Diagram of how the vane modulation affects the particle [39].	28
Figure 2.5: Illustration of vane tips along the RFQ. There are four sections; radial matcher (RM), shaper, gentle buncher and accelerator, respectively [4].	29
Figure 2.6: TE ₂₁₀ mode in an empty cavity and a cavity with vane [42].	30
Figure 2.7: Four-Vane type of the RFQ [4].	31
Figure 2.8: Magnetic fields at the end of the RFQ in cross section (a), side (b) and top(c) views [4].	32
Figure 2.9: Four-Rod type of the RFQ [4].	32
Figure 2.10: Four vane with windows RFQ type [4].	33
Figure 3.1: Major vane (grey) and Minor vane (yellow) of the FETS RFQ [39].	36
Figure 3.2: Viton O-ring of the FETS RFQ (left) and End view of the FETS RFQ with O-ring (right) [39].	37
Figure 3.3: The design of FETS RFQ parameters [63].	37
Figure 3.4: Sixteen tuners in one module of the FETS RFQ [65].	38
Figure 3.5: Cross section of the slug tuner with a tuner (copper) and cooling tubes (red) [39].	39
Figure 3.6: An automatic tuning of the FETS RFQ: a welded bellow (left) and a stepper motor (right) which linearly control the length of tuner [65].	39
Figure 3.7: Feedback control of the automatic tuning system [65].	40
Figure 3.8: The four-vane FETS RFQ cold model: CAD model (left) and in manufacturer (right) [6].	40
Figure 4.1: The electric and magnetic fields in cylindrical cavity: TM ₀₁₀ , TE ₁₁₁ and TE ₂₁₁ [69].	43
Figure 4.2: S-parameters of two ports [72].	43
Figure 4.3: The longitudinal fields of simple TE (top) and TE _{nm0} –like modes (bottom) [69].	45
Figure 4.4: The magnetic fields in quadrupole and dipole modes of the RFQ [4].	46
Figure 4.5: The frequency spectrums of a 425 MHz RFQ [42].	46

Figure 4.6: Diagram of the pulley system [74].	47
Figure 4.7: The sag layout. A blue line is the thread before the bead is hung.	48
Figure 4.8: Block diagram of sag correction in FETS RFQ bead pull measurement.	50
Figure 4.9: Block diagram of the bead pull systems.	50
Figure 4.10: IPHI RFQ bead pull systems [81].	51
Figure 4.11: PXIE RFQ bead pull systems [82].	51
Figure 4.12: Diagram of one module bead pull measurement of the FETS RFQ [78].	52
Figure 5.1: Probe port of tuner in the outer wall (red circle) [39].	55
Figure 5.2: The brift diagram of tuning algorithm.	57
Figure 5.3: Quadrupole (left) and Dipole (right) signs.	60
Figure 5.4: Diagram of tuning algorithm part 1.	62
Figure 5.5: Diagram of tuning algorithm part 2.	63
Figure 6.1: The Bead pull measurement setup for one section of the FETS RFQ.	66
Figure 6.2: The LabVIEW window to setup and measure the parameters for the bead pull measurement of the FETS RFQ.	67
Figure 6.3: VNA pop-up window.	67
Figure 6.4: Bead pull analysis diagram of the one-metre FETS RFQ.	67
Figure 6.5: A tuner with its scale.	68
Figure 6.6: Old pulley system covering only one section of the FETS RFQ.	69
Figure 6.7: Pulley system on the FETS site.	69
Figure 6.8: The change of the wheels in the FETS RFQ bead pull measurements.	70
Figure 6.9: Bead pull analysis diagram of the four-metre FETS RFQ.	71
Figure 6.10: The new LabVIEW window to set the parameters for the bead pull measurement of the FETS RFQ.	71
Figure 6.11: The Zhome calculation.	72
Figure 6.12: The operating frequency or the first quadrupole mode from the VNA with a maker (Mkr1) to detect the peak of s-parameter.	73
Figure 6.13: Dynamic and manual tuners layout [93].	74
Figure 6.14: The instruments and way to adjust the slug tuner.	75
Figure 6.15: The instruments and way to adjust the automatic tuner.	75
Figure 6.16: The first ten dipole and quadrupole modes from VNA.	76
Figure 6.17: The results from algorithm code; Top left: the fields in each quadrant, Top right: the normalised quadrupole and dipole fields, Bottom left: Mode coefficients and Bottom right: the local frequency shift of each tuner.	78
Figure 6.18: The results of incorrect dipole signs.	79
Figure 6.19: The field shape in different Z starting points.	80

Figure 6.20: The results from algorithm code with a linear least squares optimisation.	81
Figure 7.1: Results from fitting Gaussian (left) and Lorentzian (right).....	84
Figure 7.2: Results of resonant frequency against Z position of section two, quadrant three of the FETS RFQ in July 2015 with 200 Hz frequency resolution.....	84
Figure 7.3: Sweep results of the reverse direction with 100 Hz frequency resolution in August 2015.....	85
Figure 7.4: Sweep results of reverse direction with 500 Hz frequency resolution in September 2016.	85
Figure 7.5: Results in different frequency resolutions of quadrant 1 in forward and reverse directions.	86
Figure 7.6: Fields against Z position in different frequency resolutions (1000, 200 and 100Hz) of the forward direction.	87
Figure 7.7: Result resonant frequency against Z position of quadrant 4 in September 2015 with 150 Hz frequency resolution.	88
Figure 7.8: The change of the tuner T3 of the quadrant 4 that affects the internal volume of the RFQ.	88
Figure 7.9: The results of adjusting the length of tuner 3 around 5, 10, 15 and 19 mm respectively from the internal surface of the RFQ in forward (top) and reverse (bottom) directions. Shown is the frequency as a function of longitudinal position.	89
Figure 8.1: Result resonant frequency against Z position of the FETS RFQ section 2 quadrant 4 in July 2016 with 500 Hz frequency resolution.	91
Figure 8.2: Angle measurement from a vertical line.	92
Figure 8.3: Angle against frequency in different Z position when the bead is 8 (top) and 10 (bottom) mm away from X and Y axes.	93
Figure 8.4: Frequency against temperature in different Z position when the bead is 10 mm away from X and Y axes.	94
Figure 8.5: Radius (mm) against frequency (Hz) in different Z position in mm when the bead is at 45°.	95
Figure 8.6: Normalised data in September 2016 along the Z position (in mm) in different radius (R in mm).	95
Figure 8.7: Normalised data in July and September 2016, R = 14.14, 21.21 and 28.28 mm as shown from the orange arrows.	96
Figure 8.8: The fields of section two in 2016 at r = (8,8) in the forward direction.	97
Figure 8.9: The fields of section one in 2018 at r = (10,10) in the forward direction.	97
Figure 8.10: The frequencies of quadrant two (left) and three (right), section two of FETS RFQ in forward and reverse directions in March 2019.	98
Figure 8.11: Results in number of frequency steps of four sections of the FETS RFQ in 2019.	99
Figure 8.12: The sweep data of quadrant one with the new bead pull code.....	100
Figure 8.13: The results when rotating wheel 1 and 2 and shift the Z by 180 degrees.	101
Figure 8.14: Different errors from one and different person in each tuner positions.	103
Figure 8.15: The average frequency in different Y position from 9 to -9 mm for the load of 610 g.	104

Figure 8.16: The average frequency in different Y position from 9 to -9 mm for the load of 2330 g.	105
Figure 8.17: Fitting of different frequency against Y distance for the load of 610 g.	106
Figure 8.18: The comparison of sag correction from the sag equation with and without the weight of the thread and the results from the measurements.....	106
Figure 8.19: The temperature at FETS area overnight from noon 25 th July to noon 26 th July 2019 by a thermocouple.....	107
Figure 8.20: The frequency of the FETS RFQ along Z position in each quadrant when running over 15 minutes (top), 1 hour (middle) and 4 hours (bottom).....	108
Figure 8.21: The ratio of frequency against the tuner's length from measurement and its average.	109
Figure 8.22: The quadrupole fields when inserting T15Q2 (left) and T5Q4 (right) by 2 mm.	110
Figure 8.23: Relationship between frequency and tuner's length of T15Q2 and T5Q4.	110
Figure 8.24: The field when the automatic tuners reach the inner and outer limit.	111
Figure 8.25: The quadrupole field results after tuning the RFQ with automatic tuners.	114
Figure 8.26: The frequencies of the RFQ before (a) and after (b) doing the field flatness in each quadrant.....	115
Figure 8.27: Quadrupole fields of before (blue) and after (orange) doing the field flatness in each quadrant. ...	115
Figure 8.28: The comparison of the quadrupole and dipole fields between before and after doing the field flatness.....	116
Figure 8.29: After added the cooling system.	117

List of Tables

Table 5.1: Frequencies and wavelengths calculation.	59
Table 6.1: A summary of bead pull measurements in different lengths and locations.	65
Table 6.2: The frequencies of each mode between measurement and prediction.	77
Table 7.1: The inserted length of the tuner 3 with the average frequency.	90
Table 8.1: The frequency of each sweep data from the bead pull measurement.	101
Table 8.2: The errors in step size of each motor.	102
Table 8.3: Errors between one and different person.	103
Table 8.4: The time period of the measurement in different time and quadrants.	109
Table 8.5: Data when moving the automatic tuners.	111
Table 8.6: Results of each field after applying the algorithm and adjusting the tuners.	113

Chapter 1. Introduction

Particle accelerators are used for many applications around the world, including in medicine, industry, security, the environment and for research [1-4]. In general, the particle electric charge interacts with electromagnetic fields [5]. Electric field can act in the direction of the particle motion and are used to accelerate the particle to achieve the required energy. Magnetic force acts transversely to the particle direction and hence are used for steering and focussing a particle beam.

The Front End Test Stand (FETS) project was proposed as part of studies of High Power Proton Accelerators. All the FETS elements, including the radio frequency quadrupole (RFQ), were designed to achieve the 2 ms, 50 Hz high current beam in 3 MeV energy. H^+ ion will be operated with fast beam chopping [6]. The RFQ is a significant part and will accelerate the particles from 65 keV to the final energy, 3 MeV. The electric fields along the RFQ need to be uniform at the level of 1% to meet the requirements. Thus, a tuning system is essential to correct the fields. This research project aims to study and provide the field flatness of the FETS RFQ.

1.1 Linear Accelerators (Linacs)

A linear accelerator or linac is an accelerator that accelerates particles in a straight line [7]. They are typically used when only low energies are required or as injectors for circular accelerators, though there are exceptions such as the European Spallation Source [8]. Figure 1.1 is a schematic diagram showing the main components of a linear accelerator [4]. It begins with a DC injector, which injects the particles into the linac structure. The main linac structure consists of RF cavities to accelerate the beam and magnets to focus and control it. The RF power system is used to supply electromagnetic energy to the cavity.

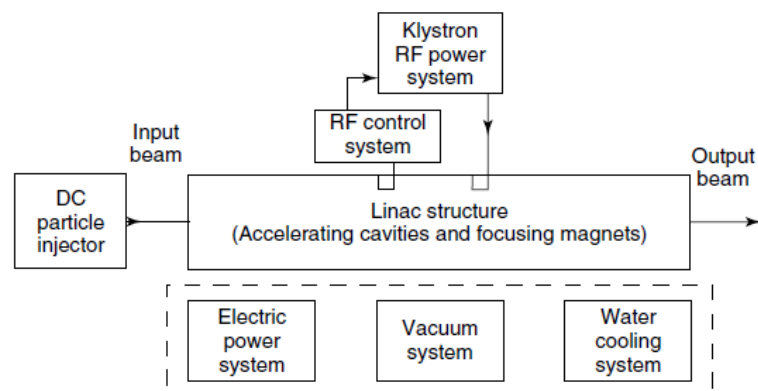


Figure 1.1: The simple diagram of a linear accelerator [4].

Linacs are briefly categorised into three main types: electrostatic, induction and RF accelerators [5]. This depends on what source is applied to accelerate the particles.

Electrostatic or high voltage accelerators are used in low energy applications [7]. A difference in potential is used directly to accelerate the beam. For example, a positive potential from a DC high voltage supply can be used to accelerate negative ions [9]. However, electrical break down limits the potential that can be achieved and hence the maximum energy of such an accelerator.

The induction accelerator was designed to do tasks that an RF accelerator cannot achieve [9]. The beam pulse is generated with low repetition rate but high currents. The linear betatron is an example of this accelerator type [5]. It is unsuitable for heavy ions.

RF accelerators are devices that can be considered as a resonator or waveguide when they are in operation. This is a time-varying operation where the accelerating electromagnetic fields are in the periodic sinusoidal form [10]. The operating frequency can be from low MHz until GHz range.

1.2 Low Velocity Accelerators

The Sloan Lawrence and Alvarez linear accelerators were early versions of low energy RF accelerators [11]. Both employed drift tubes with focusing from magnetic quadrupoles and acceleration from the electric fields related to a time-varying RF source [12].

In 1931, the Sloan Lawrence accelerator was first proposed for heavy ions, low velocity particles [13], while the idea of Alvarez linac was published in 1946 with higher performance at higher energy with protons [14]. Each of these accelerators is described below.

1.2.1 Sloan Lawrence Accelerator

The Sloan Lawrence or Wideröe accelerator is an RF Linac as shown in Figure 1.2. It accelerates the beam by the electric fields (red arrows) between drift tube gaps [12]. The drift tubes act as Faraday cages, so the frequency of the RF system and the length of tubes are arranged so that the beam always sees an accelerating field in a gap, while the wrong polarity only happens while the beam is in the tube [11]. The distance between two adjacent gaps (l_n) and the length of the tube has to be bigger with higher particle velocity.

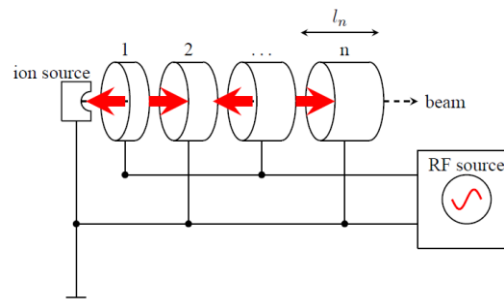


Figure 1.2: The principle of Sloan Lawrence accelerator [12].

An RFQ accelerator structure is categorised as this accelerator type because the way the accelerating fields are generated is similar [15]. The accelerating period of the RFQ is equivalent to the gap between the drift tubes.

1.2.2 Alvarez Accelerator

The Alvarez accelerator is basically the Sloan Lawrence accelerator in a cylindrical cavity, as seen in Figure 1.3 [12]. The electric fields (red arrows) are only in the accelerating direction because the fields are generated by the big cavity instead of from the drift tube itself.

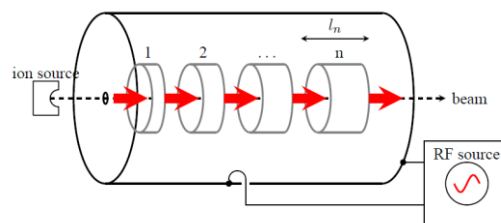


Figure 1.3: The principle of Alvarez accelerator [12].

1.3 Radio Frequency Quadrupole (RFQ)

The RFQ idea was published by Kapchinskii and Teplyakov or (K-T) in 1969 [16]. It is a sub-set of low velocity accelerators of the Sloan Lawrence type. It has four electrodes, and the modulation of these can create a longitudinal field in a similar way to the gaps of the Sloan Lawrence accelerator [15]. The advantage is these modulations can be much smaller, allowing acceleration at lower energies. Because of its better performance at high beam current with low energy, the RFQ has often been used to replace the Cockcroft-Walton DC pre-accelerators previously employed [17, 18].

The RFQ provides three functions simultaneously: focusing, bunching and acceleration. Firstly, the transverse beam focusing is performed using quadrupole fields from four electrodes placed at right-angles to each other (see Figure 2.1). The other functions are

created by adding the modulations along the electrodes to create longitudinal electric fields [16]. The output energy from the RFQ allows further acceleration using standard linear accelerator structures [11].

Many RFQs are in operation or being developed for high power accelerators around the world. For example, the RFQ III for J-PARC (Japan Proton Accelerator Research Complex) LINAC has been tested in Japan [19], and a high frequency RFQ is in development at CERN for medical applications [20]. In the UK, there are three RFQs. One is used in the ISIS injector [21], the second is the FETS RFQ at RAL, which is the subject of this thesis [6], and the third is under development for proton cancer therapy by the AVO company at the Daresbury Laboratory [22, 23].

1.4 FETS Project

The Front End Test Stand (FETS) project is under construction in R8 area at the Rutherford Appleton Laboratory (RAL), Oxfordshire. It could be used as a front end for a future ISIS II upgrade [24, 25], an FFAG prototype, a UK neutrino factory contribution [26] or other applications of the High Power Proton Accelerators (HPPAs) such as the production of medical isotopes, fusion materials studies, and etc. It is being developed as a part of the proposed Proton Accelerator Alliance, see Figure 1.4, which is a possible future plan for FETS [27, 28]. Another goal is to demonstrate fast beam chopping with high beam current and quality [6, 29].

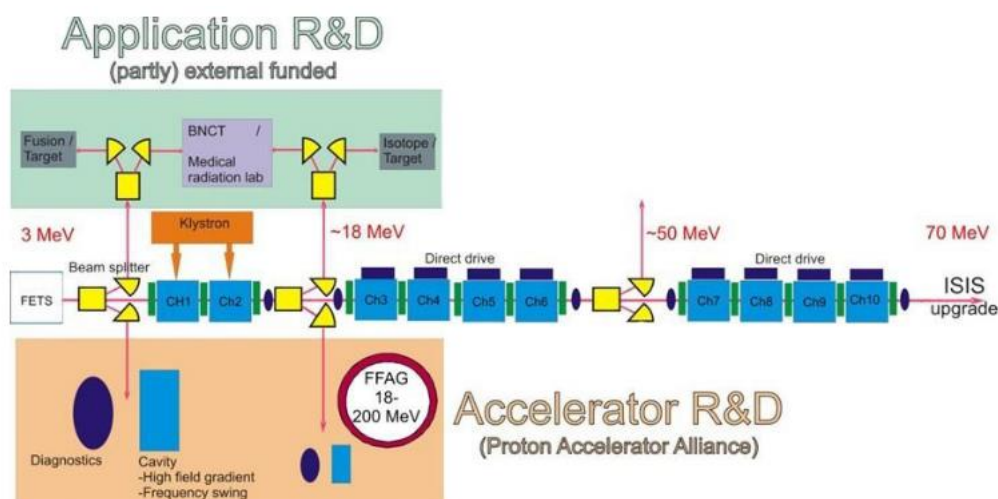


Figure 1.4: Ideal layout of a future plan of the FETS project [30].

Negative Hydrogen ion is a suitable choice for the high power proton accelerator applications especially when it is injected into a circular accelerator. It allows merging with the proton beam because the protons and H^- ions are bent in opposite directions by the same magnet. At the end of H^- transmission, the two electrons are removed via passing through a foil strip in that a proton is introduced. The H^- stripping provides a “dissipative force” that overcomes Liouville’s theorem and hence gives a lower emittance beam. This irreversible process is called a charge-exchange. The multiturn injection can also be designed in the process [31, 32].

The charge-exchange injection has been used in various machines such as tandem accelerators and cyclotrons [33]. It is also applied for the high intensity proton synchrotron as in a multiturn charge-exchange injection system for the ISIS synchrotron [34, 35]. For the FETS project, the H^- ion has been generated for the injection system because of its efficiency [27]. The FETS ion source was developed from the existing ISIS ion source. The duty cycle and beam emittance are optimized. The beam current increases from 35 mA to 65 mA [33, 36].

FETS consists of five main elements: an ion source, low energy beam transport (LEBT), radio frequency quadrupole (RFQ), medium energy beam transport (MEBT), and a diagnostic section, as shown in Figure 1.5. It was designed to achieve a beam of 60 mA H^- ions and 3-MeV acceleration. First of all, the ion source will produce the 60 mA H^- beam at 65 keV. Then, the LEBT, whose structure is three magnetic solenoids, will match the beam from the ion source to the RFQ. After that, the RFQ will accelerate the beam from 65 keV to 3 MeV. The output from the RFQ will be a long string of bunches of particles. However, to allow clean injection of these into a synchrotron, for further acceleration, it is necessary to remove some of these bunches in the MEBT. This will be done using two beam choppers and dumps. Next, the beam finally reaches the diagnostic section [28, 30, 37].

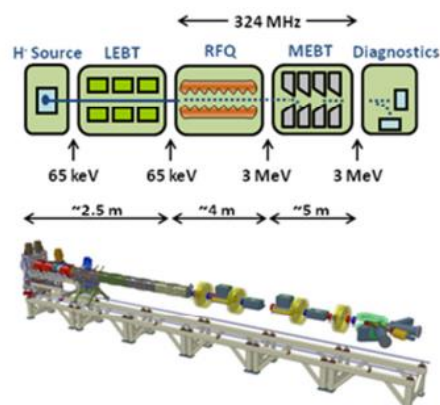


Figure 1.5: FETS layout [37].

The FETS RFQ has been under development for a decade. It is a four-vane type providing focusing, acceleration and bunching functions at the same time. The radio frequency (RF) power is from a Toshiba 324 MHz klystron. The FETS RFQ, which is typically placed between the LEBT and MEBT as shown in Figure 1.6, consists of four sections, each one-metre long [28, 30, 37-39].

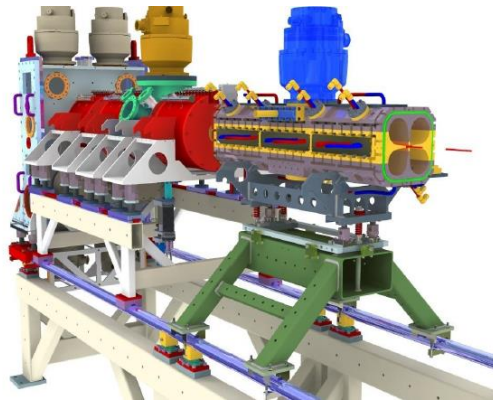


Figure 1.6: Model of the RFQ section one (right) connected with LEBT (left) [39].

The FETS RF system, seen in Figure 1.7, begins with a high power klystron (E3740 Toshiba) delivering power through a three-port circulator via a waveguide. The circulator consists of input, output and load ports. The purpose of the third port is to protect the klystron by forwarding any reflected power to a load, where it is absorbed. The WR2300 waveguides are used to connect the circulator to two coaxial lines used to deliver the power to the RFQ. This is done via two couplers, which are connected to the RFQ cavity [40].

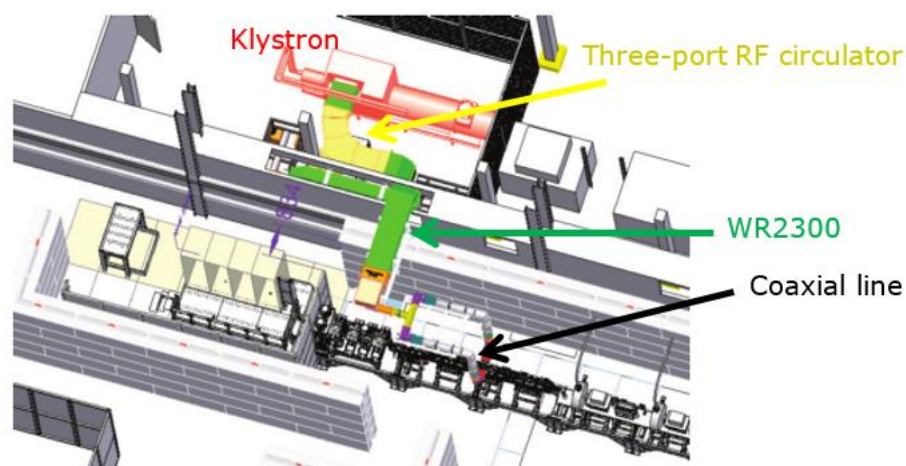


Figure 1.7: FETS RF distribution layout [40].

1.5 Aims of the Research

The current aims of the FETS RFQ project [30] are to complete the RFQ installation, testing and commissioning. The RFQ commissioning, however, has been delayed due to problems with the manufacturing of each RFQ section. Several tests have been done, such as low RF power tests. The field flatness tuning, RF tests and high power commissioning are the next stages.

This research will focus on the FETS RFQ tuning system to achieve sufficiently uniform fields. By applying the perturbation technique to measure the fields along the RFQ, the fields can be flattened by adjusting the length of tuners inside the RFQ. A bead pull measurement was constructed in RAL to correct the frequency and fields of the FETS RFQ from the imperfect structure by using a tuning algorithm. Many experiments have been conducted to understand the bead pull and tuning systems and to obtain the satisfactory field flatness at 324 MHz.

A one-metre bead pull measurement has been setup to test with one module of the FETS RFQ. This is to study and prepare for the full-range FETS RFQ. After that a four-metre pulley system was setup in the FETS area. The bead pull there started with one section of the FETS RFQ and then the whole FETS RFQ was constructed for the full bead pull measurement and tuner adjustment.

This thesis describes the FETS project, the principles of the RFQ and the FETS RFQ in Chapters 1, 2 and 3. The Bead pull theory and tuning algorithm are described in Chapters 4 and 5 to understand the basic concepts of the measurement. The methods to achieve the aims of the research are shown in Chapter 6. The results of bead pull measurement and the final uniform field are shown in Chapters 7 and 8. The conclusions and future work are included in Chapter 9.

1.6 Summary

Particle accelerators have been used in many applications. Linear accelerators are typically used to accelerate the beam at low energies. They can be divided into two main types: Sloan Lawrence and Alvarez accelerators, depending on the connection between the drift tubes and RF source leading to the different methods of longitudinal field creation. The RFQ is considered to be a Sloan Lawrence accelerator.

The RFQ concept was published in 1970s. It provides focusing, bunching and accelerating fields at the same time. The focusing function is from the quadrupole fields of four electrodes. The other functions are generated by the modulation of the electrodes along

the longitudinal direction. The RFQs have been developed for use in many applications. The FETS RFQ was designed for the FETS project at RAL.

The FETS project was proposed to accelerate H^- ions from 65 keV to 3 MeV at 324 MHz, 60 mA. It consists of five sections: an ion source, low energy beam transport, radio frequency quadrupole, medium energy beam transport and a diagnostic part. It is considered as a prototype of the ISIS II upgrade or other High Power Proton Accelerator applications.

The aims of this research are to study and apply bead pull measurement and a tuning system to the FETS RFQ to obtain the field flatness at 324 MHz. The measurements of one and four modules of the FETS RFQ have been done.

The principles of RFQs, the FETS RFQ, bead pull system and tuning algorithm are described. The method and results of the FETS RFQ bead pull measurements are illustrated in the following Chapters, with the conclusions and future work described.

Chapter 2. Radio Frequency Quadrupole (RFQ)

The RFQ, employing “spatially uniform quadrupole focusing”, was first proposed by Soviet researchers, K-T, in 1969 [16]. The aim was to reduce the required source energy, by accelerating the beam through the RFQ, while still obtaining high energy at the output of a linear accelerator. The structures of four electrodes were designed to accelerate, bunch and focus the beam at the same time. The second RFQ was built in the US in 1979 and called the proof of principle (POP) RFQ [11]. An RFQ is an alternative choice to Tandems or Cockcroft-Walton DC pre-accelerators because of its better performance with high current beams with low energy protons and ions, including lower cost and size reduction [17, 18]. In addition, the efficient bunching in an RFQ leads to very much smaller beam losses at higher energies.

Though the RFQ is considered a type of RF accelerator, its operation mode and structure are different from conventional accelerators [16]. The RFQ concept is to provide three functions, which are focusing, bunching and acceleration in the accelerator machine simultaneously. The transverse beam focusing is achieved by electric fields from the quadrupole electrodes. Both longitudinal acceleration and adiabatic bunching are performed by the electrode shapes called modulations. The basic principles of the RFQ are explained below.

2.1 Basic Principles of the RFQ

The ability of the RFQ is to accelerate particles at low energy with high beam current. Alternating voltages $V = \pm \frac{v}{2} \sin(\omega t + \varphi)$ applied to the four electrodes as seen in Figure 2.1, where, v is a peak voltage, ω is the RF frequency varying with time (t), and φ is the RF phase. Particles then travel along the longitudinal or Z axis with an alternating transverse electric fields resulting in an alternating gradient focusing [41].

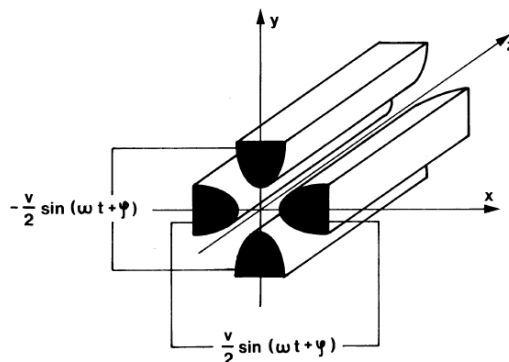


Figure 2.1: Four electrodes with alternating voltages [41].

This focusing effect is similar to the results from the conventional magnetic focusing from the change in polarities as seen in Figure 2.2. This figure shows the alternating gradient focusing on different periodicity. The top figure illustrates space varying fields from traditional magnetic quadrupoles, while the bottom is the gradient from an RFQ structure, with fields varying in time. This focusing effect is created by a long quadrupole with the AC voltage [41].

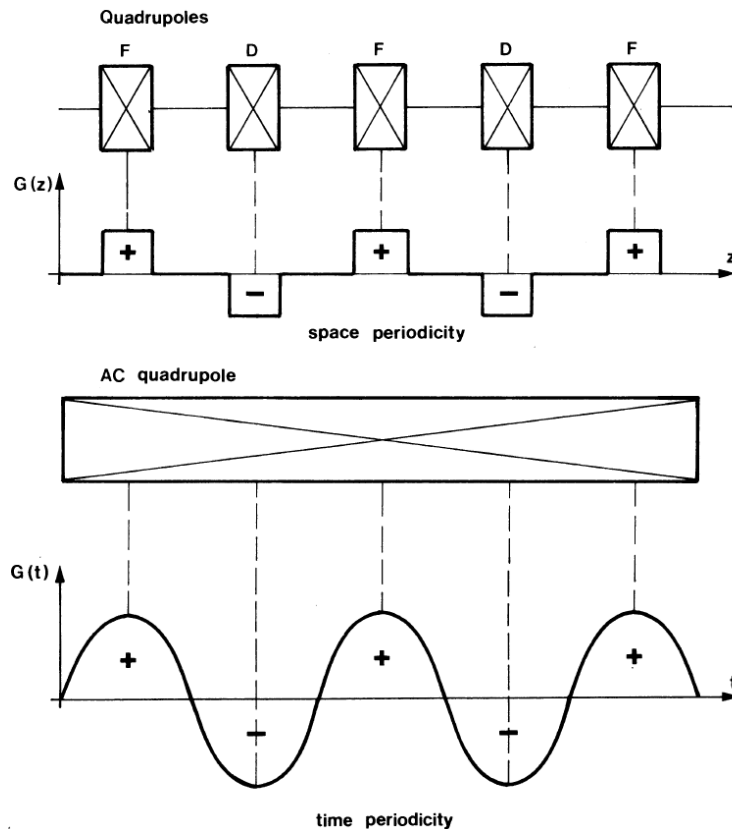


Figure 2.2: Alternating gradient focusing (G) with space (top) and time (bottom) periodicities [41].

The electrodes are not uniform along the accelerating axis, resulting in non-zero electric fields. The electrode modulation is designed to create longitudinal, accelerating fields. The distances from the centre to the tip between adjacent electrodes in a transverse section are unequal [4]. In order to build the longitudinal fields, the modulation phase of the adjacent electrodes, or called vanes in Figure 2.3, needs to be shifted by 90 degrees [41]. Thus, the phase of opposite vanes differs by 180 degrees. Half of the modulation period or $\frac{\beta\lambda}{2}$ is called the unit cell. Where β is a particle velocity, and λ is the wavelength of the RFQ cavity.

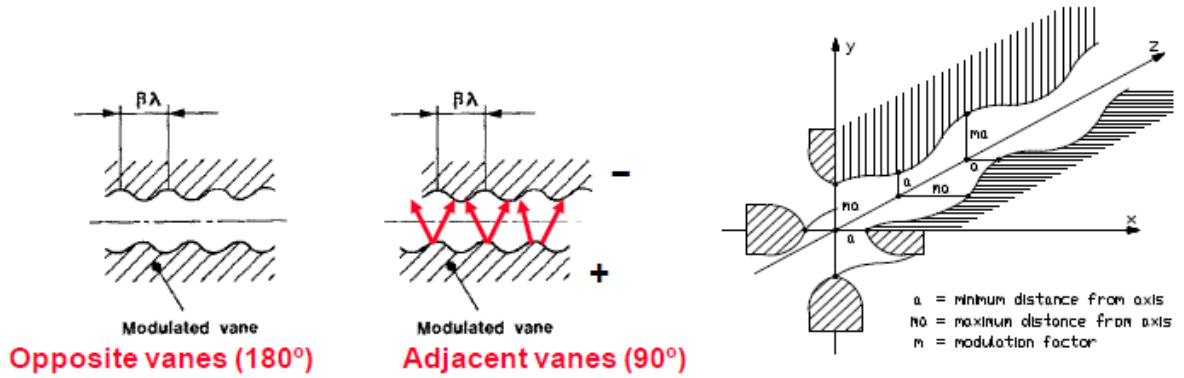


Figure 2.3: Polarity of fields and parameters of modulation [41].

For the longitudinal fields, the vane modulation period and RF voltage need to be synchronised by the RF period to accelerate the particles because this is a time-dependent system. If the potential is constant along the RFQ, the particles are practically not accelerated because there is no generated longitudinal field [4].

The potential (U), acceleration (A) and focusing (X) efficiency functions are written below,

$$U = \frac{V}{2} \left[X \left(\frac{r}{a} \right)^2 \cos 2\varphi + A I_0(kr) \cos kz \right] \sin(\omega t + \phi) \quad (2.1)$$

$$A = \frac{m^2 - 1}{m^2 I_0(ka) + I_0(mka)} \quad (2.2)$$

$$X = 1 - A I_0(ka) \quad (2.3)$$

where V is the peak potential between close pole tips, r is the vane displacement, a is the minimum radius from electrode tips to the centre of the RFQ axis, $I_0(kr)$ is the zero order of the modified Bessel function, ω is the angular RF frequency, m is the modulation parameter and $k = \frac{2\pi}{\beta_s \lambda}$ where β_s is the ratio of synchronous particle velocity and λ is RF wavelength [4].

From (2.2) and (2.3), the m and a parameters relate to the function of the RFQ. For instance, the more acceleration we need, the higher m needs to be. The focusing also depends on a . More focusing means smaller a .

The four electrodes are built as an RF resonator with a TE_{210} -like operation mode. With that mode, the fields will be uniform along the RFQ. The voltages of all four electrodes also

have to be the same to prevent the other modes contributions which could interfere with the desired one [18].

2.2 Functions of the RFQ

As stated above, the RFQ provides focusing, bunching and acceleration at the same time via the electric forces.

2.2.1 Focusing

The RFQ provides strong beam electrostatic focusing by the electric field from the four electrodes called electrostatic quadrupoles [16], while the conventional linear accelerator obtains the magnetic focusing from magnetic lenses. The magnetic quadrupoles well operate at a higher particle velocity (β) compared with the electric focusing that is good at lower β [11].

2.2.2 Bunching

The modulation of quadrupole electrodes is designed to accelerate and bunch the continuous beam from the ion source until the required energy [11]. The modulation provides a small effect, which can be ignored, on the electric focusing fields.

The lengths of modulation cells are slowly increased from the beginning with a small acceleration field. With a lot of short cells, the beam is gradually bunched and accelerated providing an adiabatic bunching. The bunching process covers most the RFQ's length while the acceleration is provided at nearly the end of the RFQ. [11]. Therefore, a number of unit cells with varying structures are required. Their period is short because there are no accelerating gaps as in conventional accelerators. The slow change between the phase of the longitudinal fields and particles relate to the increase in particle velocity [18].

2.2.3 Acceleration

The accelerating function depends on the shape of electrode modulation. The modulation depends on the RF frequency as the phase needs to be synchronised with the charged particle [4]. By changing the modulation parameters, the longitudinal fields start from small until they deliver the desired energy.

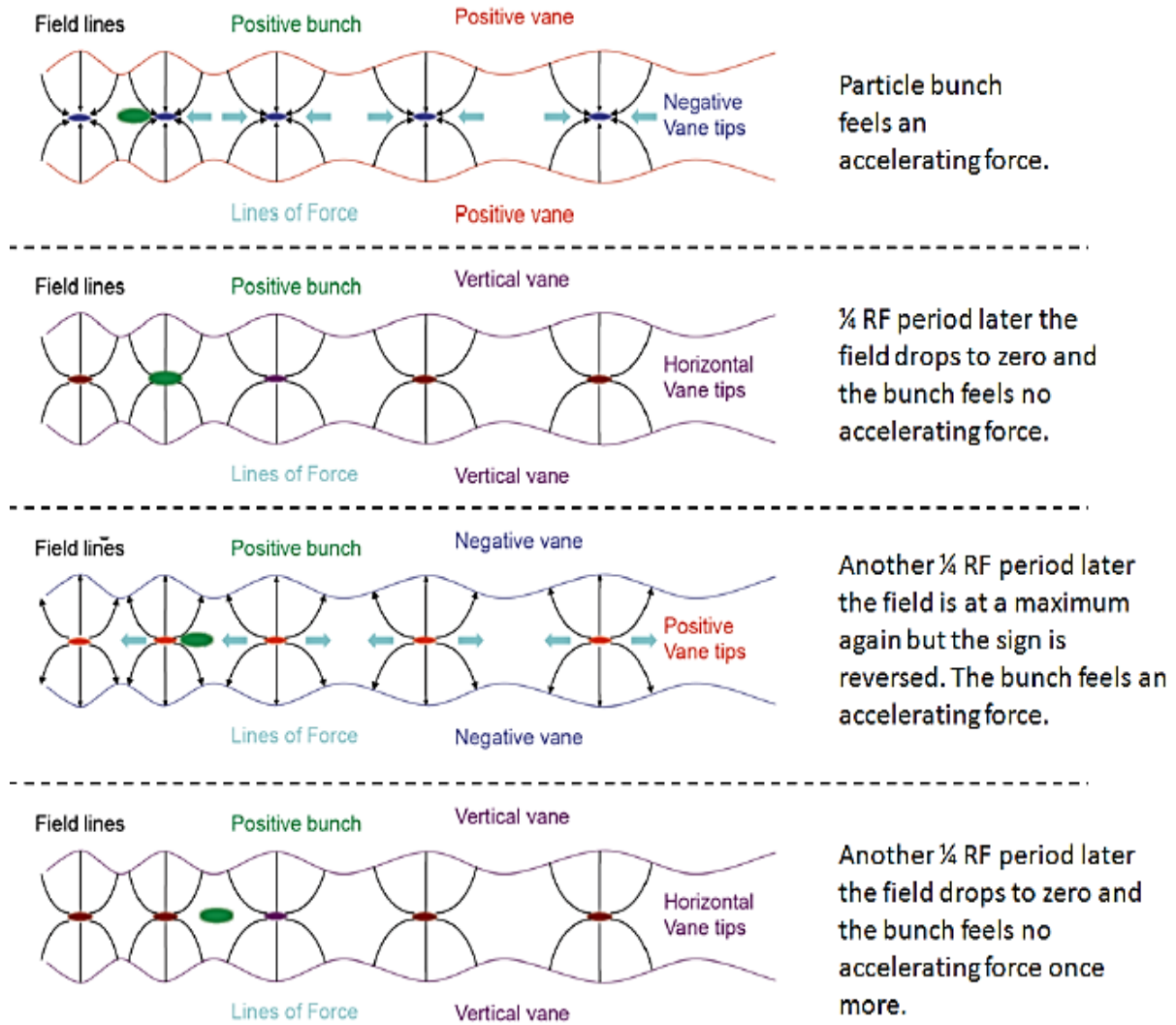


Figure 2.4: Diagram of how the vane modulation affects the particle [39].

Figure 2.4 shows the effect of the fields from the vane modulations on the particles as they are bunched and accelerated. The diagram begins with the particle bunch in a positive vane with an accelerating force (the line force in light blue colour). After a quarter of the RF period, the electric fields are zero leading to no force in the longitudinal direction. In other words, the particle will not be accelerated at that time. The particle bunch is at the centre between accelerating and decelerating electric forces and gets ready to the next stage. Then, the particle bunch will be accelerated again in another quarter RF period. This is because the negative vane voltage changes the direction of the fields to the opposite way [39]. Therefore, the particles will be accelerated along the whole RFQ.

By using the electrodes all along the RFQ, there are no gaps in the acceleration. The accelerating and focusing cells are shorter than the aperture leading to a high frequency design [18].

2.3 Structures of the RFQ

There are four sections in the RFQ: the radial matcher, shaper, gentle buncher and accelerator sections, see Figure 2.5. Each section provides different functions to accelerate and match the beam from the ion source to later parts of the linear accelerator. The beam from the ion source is a DC continuous beam. It needs to be bunched first and then accelerated [11].

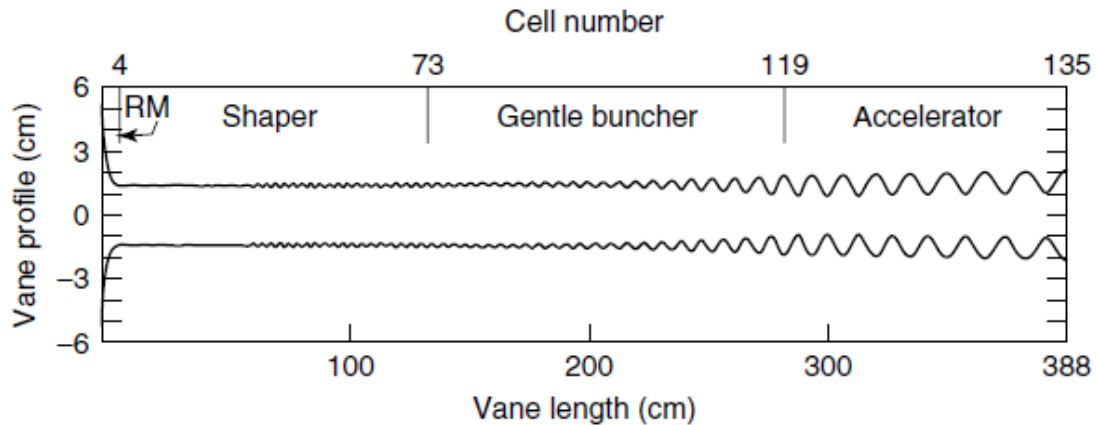


Figure 2.5: Illustration of vane tips along the RFQ. There are four sections; radial matcher (RM), shaper, gentle buncher and accelerator, respectively [4].

2.3.1 Radial Matcher (RM)

As the particles are transported from the Low Energy Beam Transport (LEBT) to the RFQ, the focusing structure needs to be matched as the pattern moves from a time-independent to a time-dependent structure. The radial matcher is put at the beginning of the RFQ to solve this problem. The RF focusing structure, increasing from zero to the final value, slowly forces the DC input beam to be a time-dependent pattern (sinusoidal term) [41]. The modulation structure is not applied in this section because the emphasis is on the transverse effect of the beam [4].

2.3.2 Shaper

After being matched by radial matcher, the beam is now prepared for adiabatic bunching and acceleration. The bunching function starts from a shaper section [11]. The aperture is constant to keep focusing the beam from now on [18]. The electrodes are

modulated but not in a way to provide much acceleration. This slowly shifts the synchrotron phase for the full bunching in the next section.

2.3.3 Gentle Buncher

This section still adiabatically bunches the beam until the beam is ready to be accelerated [11]. The synchrotron phase is increased until the beam is ready for acceleration, from -90 to -30 degree. The beam in the section is at an intermediate energy.

2.3.4 Accelerator

This is a proper acceleration station [11]. This section relates to the general design of the RFQ because this is the final stage of each parameter. The phase and focusing system are constant along the section.

The electrode modulation period or $\beta\lambda$ relates to the particle acceleration. The velocity (c) or βc of particles increases when accelerated. This means that the length of modulation period in the accelerator part also gets longer, as seen in Figure 2.5 [41]. The beam will be at the required energy at the end.

2.4 RF Structure of the RFQ

Apart from the traditional RF accelerators, the RFQ operates at Transverse Electric or TE mode. The particles are accelerated by the electric forces, which are created by the modulation of the electrodes. TE₂₁₀-like mode is the operation mode for the RFQ. Thus, the electric fields which are perpendicular to the longitudinal axis are considered as the focusing fields. Figure 2.6 shows how the electric and magnetic fields perform in an empty cavity (left) and a four-vane RFQ cavity (right) [41, 42]. Even though the electrodes or vanes are added in the resonant cavity, the mode is still TE₂₁₀. The modulation along the vane tips causes a minor effect for the determined mode.

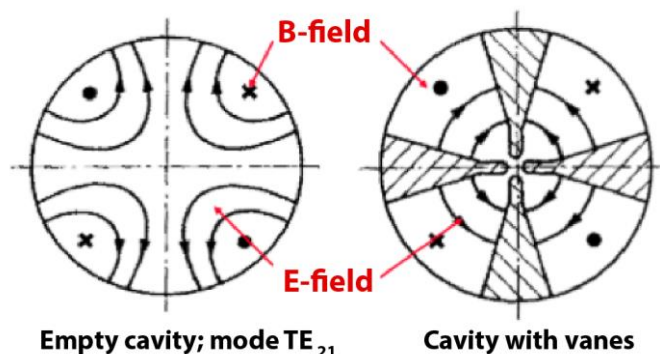


Figure 2.6: TE₂₁₀ mode in an empty cavity and a cavity with vane [42].

However, considered as the resonator, not only the TE_{210} mode is present in the RFQ cavity but other modes are also resonated at different frequencies. If the frequencies from adjacent modes are close, they sometimes mix. This can happen, for example, due to an imperfect RFQ structure being made by the manufacturer. To prevent interference between the desired mode and others, a perturbation technique is applied to eliminate or reduce this interference to sufficiently small levels [41]. After this is done, the fields will be sufficiently uniform and RF phase constant enough along the RFQ for operation. [18].

2.5 Types of the RFQ

RFQs can be roughly categorised by the shape of the electrodes, which are four-vane and four-rod types. They are based on a waveguide and lump components of a circuit (capacitances and inductances) in consequence [11].

2.5.1 Four-vanes Type

The four-vane RFQ, as seen in Figure 2.7, consists of four symmetrical electrode vanes in the cavity providing the quadrupole TE_{210} -like mode. As there is no TE_{210} mode in reality, it is from the TE_{211} mode by tuning the end of the vane to obtain the uniform field [4].

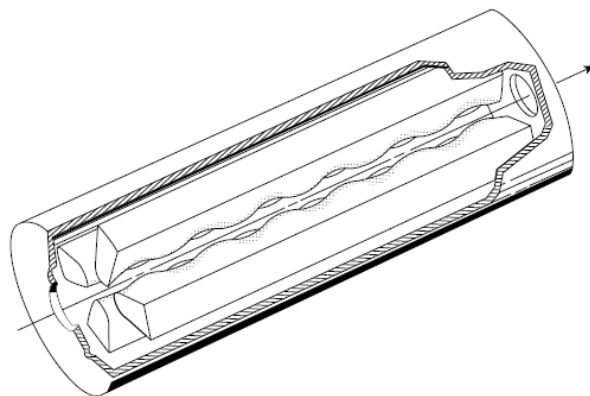


Figure 2.7: Four-Vane type of the RFQ [4].

It is used at the high frequency ($\sim 100 - 425$ MHz). Due to its large vane cross section, a conventional cooling system can be applied in this RFQ type [43]. However, this mode can be disturbed by a dipole mode (TE_{110}), which leads to poor operation. This is because both dipole and quadrupole modes can mix or be degenerate. Consequently, the dipole mode will be stronger on the axis and cannot be ignored. All the unwanted modes need to be sufficiently reduced by a tuning process [11].

Moreover, the vane voltage should be constant along the vane. The ends of the RFQ need to be designed to allow the magnetic fields across the vane cutback to meet the

boundary condition [44]. This is because the magnetic fields should be in parallel with the end cover, see Figure 2.8 [41].

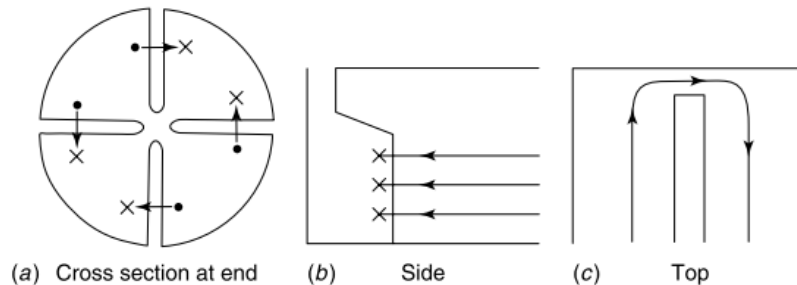


Figure 2.8: Magnetic fields at the end of the RFQ in cross section (a), side (b) and top(c) views [4].

2.5.2 Four-rods Type

The four-rod type, as seen in Figure 2.9, is the simplest RFQ model because there is no problem from the dipole mode (TE_{110}). Because of its shape, the rods (even and odd) which are tied together do not support the dipole mode. However, this RFQ type is used at the low frequency of the heavy ion accelerators. The voltage for the opposite pairs has to be the same. This device can be with a circular electrode or rectangular bar which also has the vane modulations [9, 11, 45]

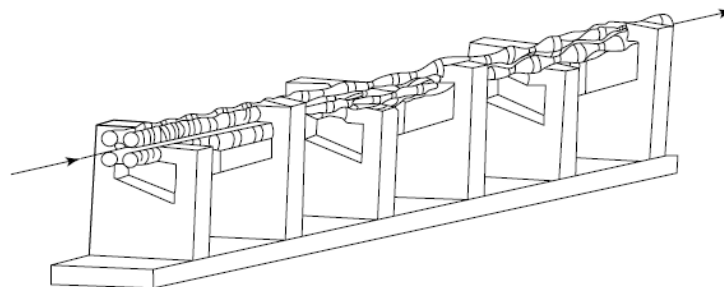


Figure 2.9: Four-Rod type of the RFQ [4].

2.5.3 Other Types

Four-vane and four-rod type are commonly used in linear accelerators. However, there are others that are designed to be applied in many applications.

The four-vane with windows RFQ structure is between a four-vane and four-rod RFQ. It can be four-vane with windows or four-rod with supporting stems as seen in Figure 2.10. It is used in the intersection frequency between the common types. The windows are designed to move the operating mode far away from the unwanted frequencies. Compared with the same frequency, the RF power efficiency of four-vane with windows is more than the four-rod RFQ but not the four-vane RFQ [4].

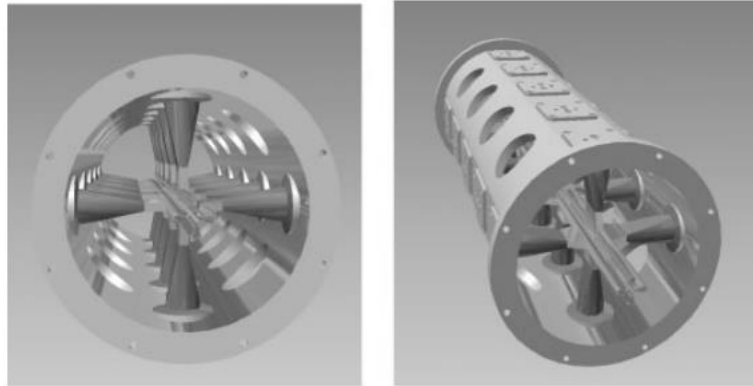


Figure 2.10: Four vane with windows RFQ type [4].

2.6 Problems with RFQs

When building an RFQ, many researchers face very high challenges [46]. Moreover, the design sometimes is restricted by the funding available. As a result, various RFQs have had obstacles during the construction. For instance, the radial matching was not included in the High Intensity Proton Injector (IPHI) RFQ design leading to an increase in the frequency (by more than 10 MHz) [47]. Quadrupole fingers were installed to solve that problem. That needed the extra time to design the new quadrupole to match the current RFQ. Though the results provided a significant improvement, there still was a difficulty in the tuning system [46].

The High Intensity Neutrino Source (HINS) RFQ also had a problem with the incorrect frequency while measuring the field distribution [48]. In this case, some of the vane cutback material had to be eliminated from the output to maintain the frequency. In addition, there was a field tilt from the vane modulations [46]. Thus, each vane tip had to be moved into the centre by 50 μm . The tuning process could not solve the problem of the non-uniform fields because the tuner length was over the limit.

Another example is from the Japan Proton Accelerator Research Complex (J-PARC) RFQ which also had a problem in the field tilt [49]. However, it could be solved by adjusting the slug tuners as their design left sufficient adjustment, around 5 mm from the inner surface.

2.7 RFQ Applications

Many RFQs are being developed for various applications around the world. The RFQ was first considered to replace Cockcroft-Walton injectors because of its good performance for high energy accelerators [50]. First of all, the RFQ was built to prove the new idea of strong focusing in a particle accelerator at low energy using electric fields. It could accelerate

protons or deuterons as a pre-injector part of accelerator machine. After that, it was designed for the specific use such as for spallation neutron sources, future accelerator driven system, or material test in fusion devices [45].

2.7.1 High Current injectors

For the design of injectors for the high energy acceleration system, we need to meet the high energy and high current by preparing the beam in the injector [18]. The first Russian RFQ that was applied as an injector was the URAL 30 RFQ at the Institute for High Energy Physics (IHEP) [51]. It was used in a linear proton accelerator with 80 mA in 1983. During that year, the CERN RFQ 1 was also set up for the same current [52]. After that some RFQs, such as the BNL-RFQ and HERA RFQ, were built but their currents are not more than 50 mA [18]. However, in 1993, the 200 mA CERN RFQ 2 was the first RFQ exceeded the URAL 30 RFQ current [53]. It was designed to achieve high performance with low emittance.

2.7.2 Heavy Ion RFQs

It is difficult to achieve a heavy ion accelerator [11]. The velocity in heavy ion applications is lower than with protons or electrons leading to shorter length of the acceleration cells. The length of the RFQ is generally short if compared with the conventional accelerator. Therefore, the energy of the injection can be very low.

Considered as a low current accelerator, the very first RFQ for heavy ions was the LBL heavy ion RFQ in 1984 [54]. It was a four-vane type RFQ. The accelerated ions could be varied from helium to silicon. Another example of the heavy ion RFQ was the CERN heavy ion RFQ [55]. It is the four-rod structure which is commonly used in the heavy ion applications. This RFQ is for Pb ion acceleration.

2.7.3 Variable Energy RFQs

An RFQ normally operates in fixed output energy and velocity profile. However, in some experiments, variable energy is useful, for example, ion implantation, atomic physics areas and material research [18]. The change in velocity profile could be from the length of modulation period or the phase of group cells. This can be achieved in a post accelerator. The structure will be divided into individual sub units. In addition, the frequency variation without changing its electrode structure also could change the velocity profile. The latter solution is a concept of a variable energy (VE) RFQ.

A VE RFQ example is the four rod RFQ with tunable frequency in Frankfurt for a cluster post accelerator [56]. The movable tuning plate from the RFQ base plate was designed to tune the capacitance and inductance in the cavity to change the output energy. The VE RFQ

can be combined with an electron cyclotron resonance ion source to perform charged ions in keV range [57].

2.7.4 Other Applications

RFQs were first designed for accelerating light ions for the pre-acceleration purpose. They are not only used for scientific research but also can be applied in several applications [18, 45]. RFQs are being studied as a part of a cancer therapy source for hospitals. At airports, the small compact RFQs can be seen as a source of positron emission tomography (PET) for detecting the dangerous items. They are also adapted for use in material industries such as ion implantation in semiconductors.

2.8 Summary

The RFQ provides three functions: focusing, bunching and acceleration. The focusing function is from the four electrodes. The lengths of vane modulation cells are gradually increased, allowing the continuous beam from the ion source to be bunched and accelerated in the RF structure along the RFQ.

The radial matcher matches the DC beam from the ion source to the time-varying focusing system. After that, the beam is passed to the shaper section to prepare for acceleration and to start bunching. The beam is continued to be bunched in the gentle buncher until it is ready for acceleration. The last section of the RFQ is the accelerator which accelerates the beam up to the final energy.

An RFQ can be considered as TE_{210} -like mode resonator. It is mainly categorised as the four-vane and four-rod RFQ type. The four-vane RFQ operates at high frequency, about 100 – 425 MHz, while the four-rod RFQ, which has a more straightforward design, can be used in lower frequency. Another type is the four-vane with windows, which is between the other two.

The RFQ can be used for various application such as a high current injector, heavy ion accelerator and variable energy. It can also be applied in industry and medicine.

Chapter 3. FETS RFQ

The FETS RFQ has been under development since 2005 [58]. It was proposed as a part of the Front End Test Stand (FETS) project at RAL for future high power proton accelerators. At first, the design was based on the four-rod RFQs of the Rutherford RFQ test stand [59] and the ESS (European Spallation Source) [60]. After that, the structure of the FETS RFQ was changed to a four-vane type because of the higher efficiency of the RF distribution and the reduced complexity of the cooling system design [61].

3.1 The Design of the FETS RFQ

The FETS RFQ accelerates the H^- beam from 65 keV to 3 MeV at 324 MHz. The operating frequency was chosen from the available Toshiba pulsed klystron [6]. Therefore, the four-vane type is more suitable for the frequency range produced by the klystron. The FETS RFQ consists of four sections, each one-metre long. The total length is about 4.2 metres.

3.1.1 Four-Vane Structure

The four-vane FETS RFQ design also considered the ability to reassemble the major and minor vanes, see the grey and yellow colour, respectively in Figure 3.1, by avoiding permanent brazing. To ensure vacuum tightness, an O-ring was introduced to the joints of the vanes, as seen in Figure 3.2 [29].

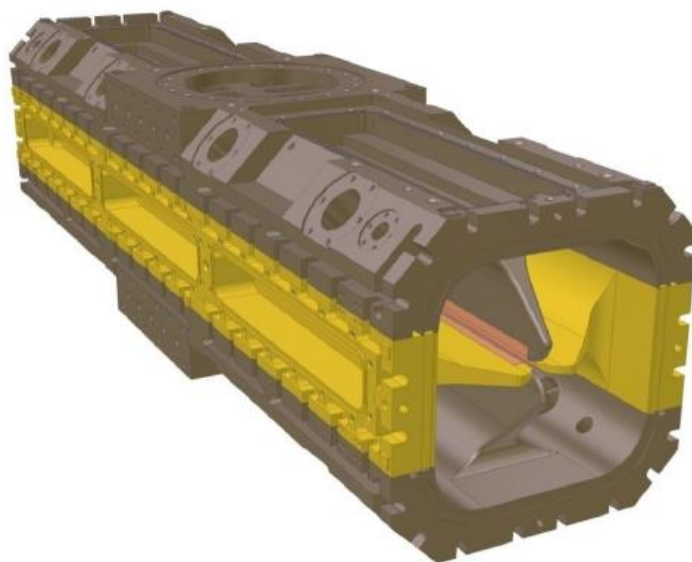


Figure 3.1: Major vane (grey) and Minor vane (yellow) of the FETS RFQ [39].

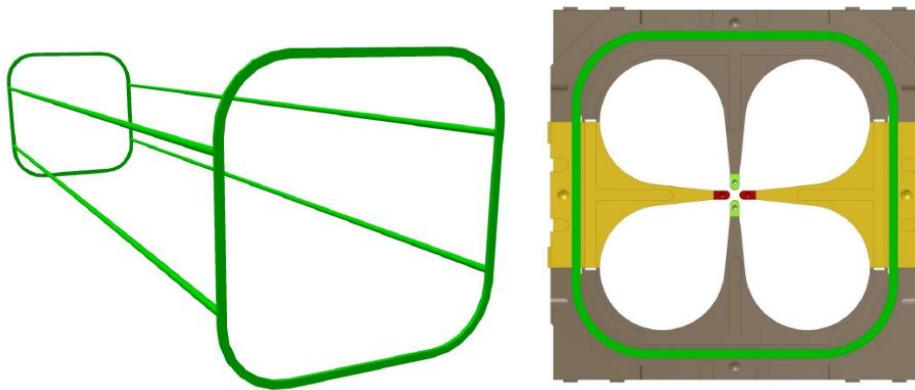


Figure 3.2: Viton O-ring of the FETS RFQ (left) and End view of the FETS RFQ with O-ring (right) [39].

By replacing the vacuum brazing by the O-ring, the FETS RFQ is more convenient to transport, install and maintain [39]. This can reduce the risk of damage when compared with shipping a complete RFQ which cannot be dismantled. In addition, the operation frequency could be changed because the RFQ's parts were not permanently jointed. This is useful for the future modification of the RFQ.

3.1.2 Modulation Parameters

The modulation parameters define the functions of focusing, bunching and accelerating of the RFQ. Using the RFQSIM programme [62], Figure 3.3 shows the results for the FETS RFQ parameters along with its cell numbers [63]. The energy (W) of the FETS RFQ increases from the middle of the structure until it reaches the desired energy of 3 MeV.

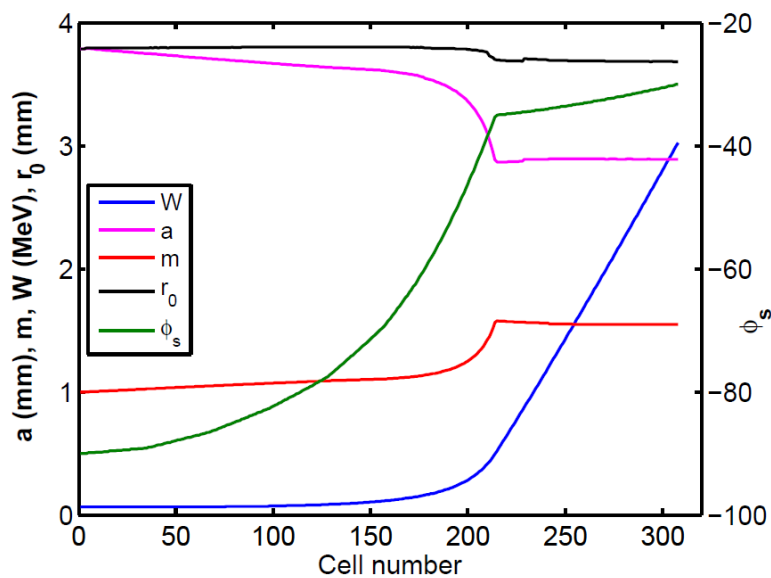


Figure 3.3: The design of FETS RFQ parameters [63].

a , m and r_0 are aperture, modulation parameter and the mean of the distance from vane tips to beam axis respectively [64], see Figure 2.3 and Equation (2.1). They were calculated separately for each structure of the FETS RFQ. For instance, a , m and r_0 are nearly constant for most of the accelerating section at the end of the RFQ. The synchrotron phase (ϕ_s) is increased from -90 to -30 degree for the maximum energy of 3 MeV.

3.2 Tuning system of the FETS RFQ

Both manual and automatic tuners are inserted in the FETS RFQ to correct the frequency and electric fields from the imperfect structure [39]. There are sixty-four tuner ports in the whole FETS RFQ, sixteen per module, as seen in Figure 3.4. However, two of them are used as RF ports for the power input. Thus, sixty-two tuner ports are available to flatten the fields along the RFQ: fifty-eight static and four dynamic tuners. The static tuners need to be tuned by hand, while the dynamic tuners are computer controlled and can be used for tuning during the RFQ operation.

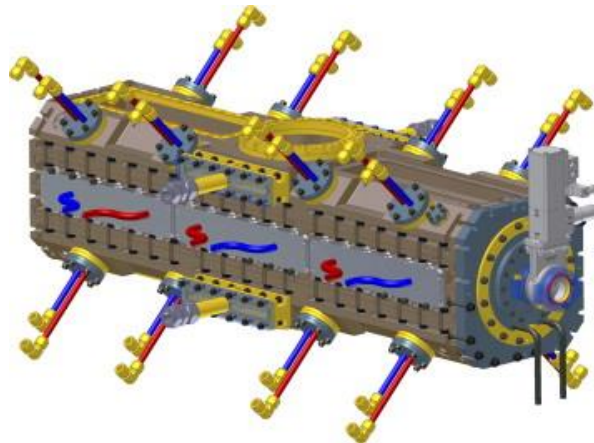


Figure 3.4: Sixteen tuners in one module of the FETS RFQ [65].

As it is extremely complicated to calculate by hand the correct position of each tuner due to their number, a perturbation technique is considered to tune the fields. Even though the static tuners can correct the field to be uniform, the automatic tuners are still necessary in case of any changes in the environment, such as temperature [65].

3.2.1 Slug Tuners

Sixty-two slug tuners, see Figure 3.5, will be inserted along the RFQ to provide the field flatness. They are cylindrical in shape and are mounted only on the major vanes. There are 16 tuner ports per RFQ section [39]. The red tubes of Figure 3.5 are designed for the cooling system. The static tuners are adjusted manually and then left through the beam operation.

The nominal position of static tuners is to have them flush with the inner surface of the FETS RFQ cavity. If the tuner length is inserted into the cavity, the volume of the cavity decreases leading to a frequency increase, both locally around the tuner and globally for the whole RFQ. The local frequency changes from the tuner affect the fields which can be tuned to be flat by applying the bead pull system [66].

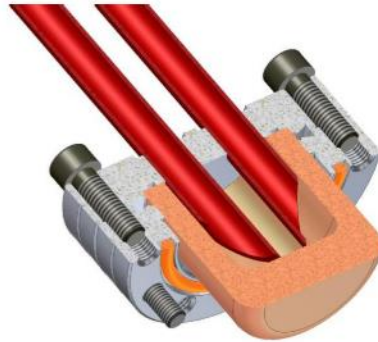


Figure 3.5: Cross section of the slug tuner with a tuner (copper) and cooling tubes (red) [39].

3.2.2 Automatic Tuners

The automatic tuners, see Figure 3.6, replace one of the slug tuners in each RFQ quadrant [39]. They are located at the middle of the FETS RFQ because changing their length has less effect in field distribution. However, it allows the overall frequency to be shifted due to the change in the cavity volume. The frequency will be corrected using these tuners from unpredictable causes such as temperature changes while the beam is in operation.



Figure 3.6: An automatic tuning of the FETS RFQ: a welded bellow (left) and a stepper motor (right) which linearly control the length of tuner [65].

The dynamic tuner is driven by the stepper motor and automatically corrected by a feedback control circuit, see Figure 3.7 [65]. When the electric field's phase varies, the phase detector will send a signal to the control system to manipulate the stepper motor.

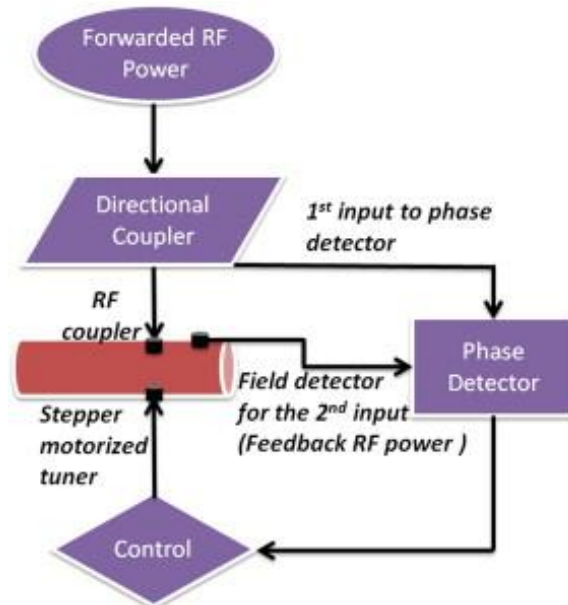


Figure 3.7: Feedback control of the automatic tuning system [65].

3.3 The FETS RFQ Cold Model

A four vane RFQ cold model, as shown in Figure 3.8, was built to compare the actual performance with simulations, and to study tuning and manufacture in preparation for building the full RFQ [6]. The development of the bead pull system started from a pillbox cavity and was tested on the cold model.

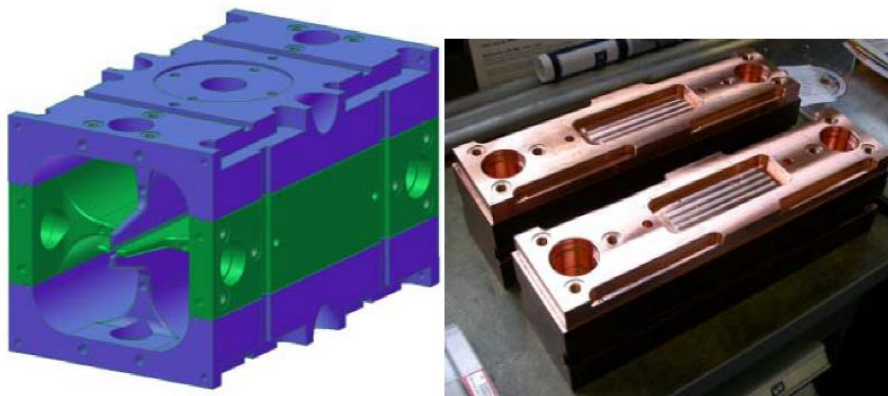


Figure 3.8: The four-vane FETS RFQ cold model: CAD model (left) and in manufacturer (right) [6].

The cold model consisted of four parts [67]. The Aluminium material was produced for one part to test the manufacturing process. After that, the copper model was formed with two major and two small minor vanes, see Figure 3.8 (right). This was 0.4 m long. All the vanes were joined together by a brazing method. There was no modulation of the vanes.

3.4 Problems of the FETS RFQ

There were a number of problems during the manufacture of the actual RFQ. After the first section had been finished by the manufacturer, an error was found in the vane modulations [28]. The modulations were shifted in both the transverse and longitudinal directions from an error setting up by the Computer Numerical Control (CNC) machine which is a automatic device that controls the machining tools by using computer programming. This led to a change in the resonant frequency that cannot be corrected by the tuning system. Thus, the section one of the FETS RFQ needed to be sent back to the manufacturer for modifications. Moreover, internal stresses occurred in the second section of the FETS RFQ due to machining. Sections three and four needed some corrections due to these problems. These processes took time leading to a delay in the overall schedule.

3.5 Summary

The FETS RFQ is designed for the Front End Test Stand project. It accelerates the H⁻ beam from 65 keV to 3 MeV at 324 MHz. It is the four-vane RFQ with O-ring sealing. It consists of two major and two minor vanes, and there are sixty-four tuning ports. Fifty-eight slug and four dynamic tuners are used for tuning. The other two tuning ports are for the RF feed. The problems from the RFQ machining caused a major delay in the FETS project.

Chapter 4. Bead Pull System

The use of the bead pull system for tuning the RFQ is explained in this chapter. The practical bead pull measurement and some experiments of the RFQ bead pull measurement will be shown. This includes the sag effect from the bead mass over the long range of the pulley system. The actual measurements are shown in later Chapters.

4.1 Principles of the RF Cavity

In a particle linear accelerator, a simple cylindrical cavity is used to analyse the electromagnetic fields in the RF cavity [4] starting from Maxwell's equations. The resonant mode is sufficient to specify and study the functions of the fields in the cavity.

The transverse mode, especially electric transverse mode, and s-parameters, which are frequently mentioned in the measurements, are briefly explained in this chapter.

4.1.1 Transverse Modes in the Cavity

In free space, electric and magnetic fields are perpendicular to the longitudinal axis of the RFQ and are of transverse electromagnetic types (TEM), as a result. However, only transverse electric (TE) or magnetic fields (TM) are allowed in empty cavities for the propagation fields [41]. In the longitudinal direction (Z axis), if the electric field (E_z) is zero, the magnetic field (H_z) should not be zero [68]; otherwise, there is no propagation field in the cavity. These are called TE modes. On the other hand, TM mode is introduced when $H_z = 0$ and $E_z \neq 0$ in the propagation direction. In the RFQ, TE mode is applied to the operation.

The subscript of TE and TM mode is shown as TE_{mnp} and TM_{mnp} mode where $m_{\theta=0,1,2,\dots}$, $n_r=0,1,2,\dots$ and $p_z=0,1,2,\dots$ are the number of periods in the azimuthal (θ) component, zeros in radial (r) axis and half periods of longitudinal (Z) direction, respectively [69, 70].

The fields in a cylindrical cavity in different modes are shown in Figure 4.1. The circle is the cross section of the cavity and the rectangular presents the longitudinal or the beam propagation direction. TM_{010} shows the accelerating mode because there is an electric field on the longitudinal axis [69]. TE_{111} and TE_{211} are dipole and quadrupole modes, respectively.

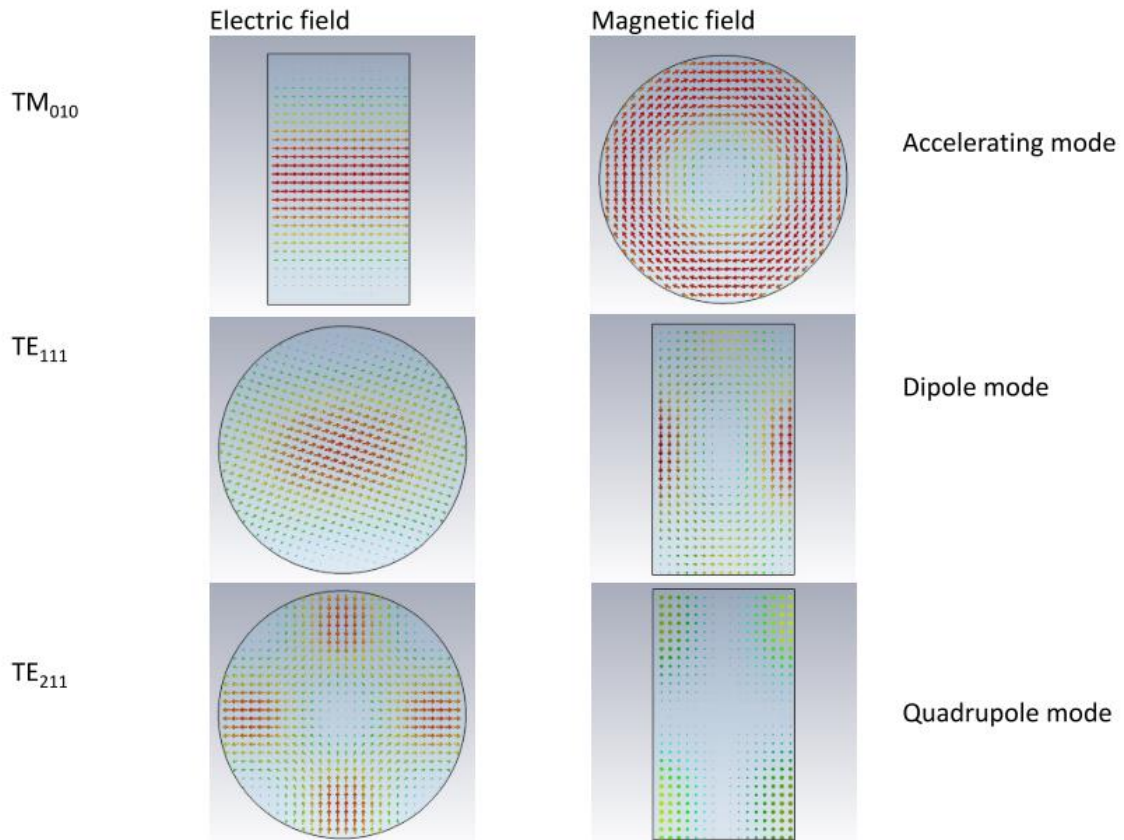


Figure 4.1: The electric and magnetic fields in cylindrical cavity: TM_{010} , TE_{111} and TE_{211} [69].

4.1.2 S-parameters

The scattering or S parameter describes the wave transmission, reflection and propagation in the RF system [4]. The subscript numbers of the s-parameters provide the efficiency of reflection or transmission. Figure 4.2 shows the incident (a) and outgoing (b) waves between two ports [71, 72].

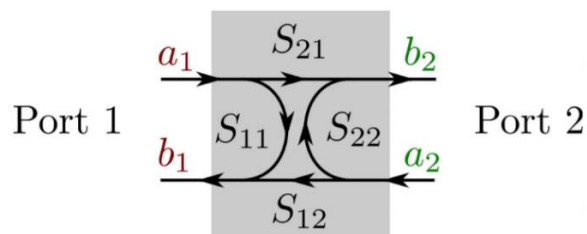


Figure 4.2: S-parameters of two ports [72].

From Figure 4.2, the equations of the s-parameters are written below [72],

$$\begin{aligned} b_1 &= S_{11}a_1 + S_{12}a_2 \\ b_2 &= S_{21}a_1 + S_{22}a_2 \end{aligned} \quad (4.1)$$

where S_{11} and S_{22} are the reflection coefficients and S_{21} and S_{12} are the forward and reverse transmission coefficients, respectively.

In addition, the parameters generally are written in matrix form, as seen in Equation (4.2).

$$\bar{b} = S\bar{a} \quad (4.2)$$

$$\begin{bmatrix} b_1 \\ b_2 \end{bmatrix} = \begin{bmatrix} S_{11} & S_{12} \\ S_{21} & S_{22} \end{bmatrix} \begin{bmatrix} a_1 \\ a_2 \end{bmatrix} \quad (4.3)$$

where S is the matrix of s-parameters. This is the linear term. If the number of ports N is more than two, Equation (4.1) will be solved N times with S being an $N \times N$ matrix in Equation (4.3).

To measure the s-parameters for a cavity, the coupling probe has to be inserted into a port on the cavity to transmit the electromagnetic energy from a microwave source. With the energy in the cavity, the s-parameters can be measured using the appropriate output ports [4].

4.2 Four-vane RFQ Cavity Eigenmodes

An alternating voltage is applied for the focusing, bunching and accelerating fields in the four-vane RFQ [68]. These fields occur in the RFQ cavity as an RF resonator which consists of the vanes inside. The RFQ has to operate at a precise frequency. Microwave techniques are studied to understand the RFQ as a radio frequency device.

4.2.1 TE-like Mode

The RFQ operates at a TE_{210} -like mode which is impossible in a simple cavity. The basic TE mode cannot provide the flat fields through the cavity because the first or lowest quadrupole mode is TE_{211} [69]. The structure of the vane has to be designed by cutting back to achieve TE_{210} mode, as shown in Figure 2.8. Figure 4.3 shows the longitudinal fields of normal TE and TE-like modes. The top figure is the longitudinal modes of the normal TE fields in a simple cavity. Considering $p = 1$ is the blue line, the field is not flat. When applying the vanes' edge modification, the fields are as shown in the bottom figure. In this pattern, $p = 0$ is allowed in the cavity providing a uniform field.

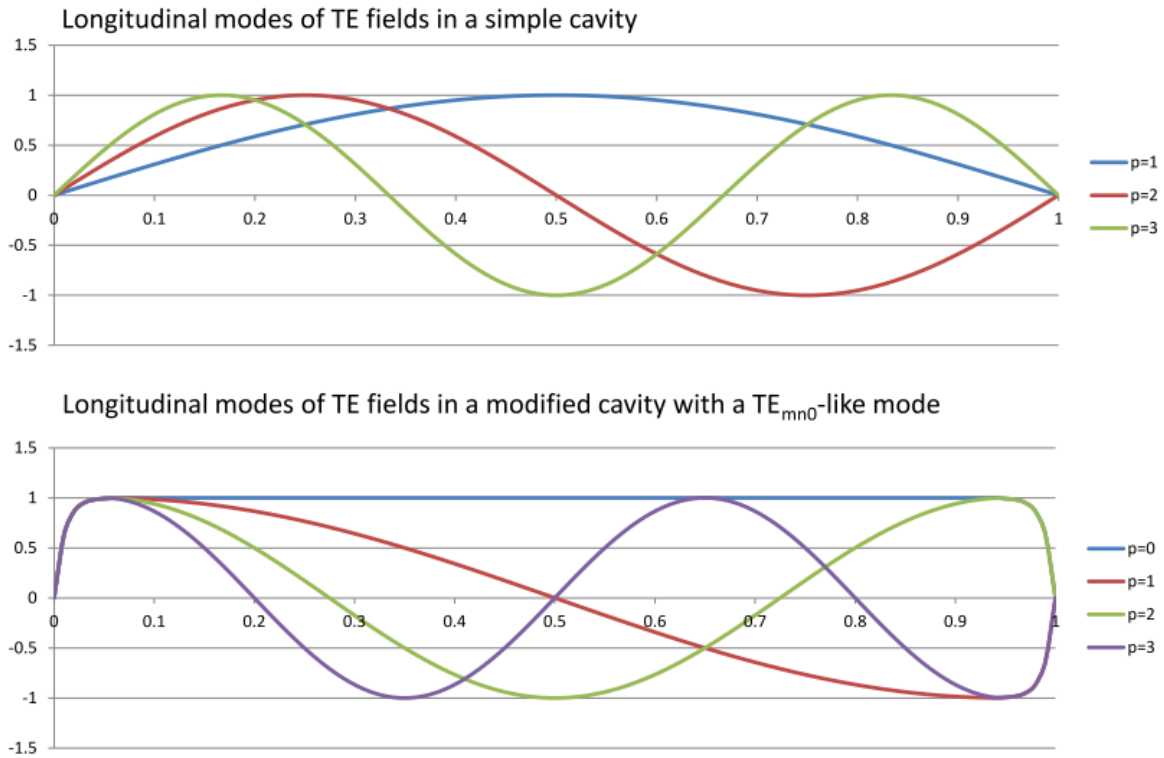


Figure 4.3: The longitudinal fields of simple TE (top) and TE_{nm0} -like modes (bottom) [69].

4.2.2 Quadrupole and Dipole Modes

The operating quadrupole mode in the RFQ can be considered as a bandpass because only one frequency is needed without any interfering from other frequencies. The gap in frequency between the cutoff frequency (ω_0) and its nearest longitudinal modes are very close [4]. This can be written as in an Equation (4.4) below,

$$\left(\frac{\omega_n}{c}\right)^2 = \left(\frac{\omega_0}{c}\right)^2 + \left(\frac{n\pi}{l_v}\right)^2 \quad (4.4)$$

where ω_n and ω_0 are the frequencies of the n^{th} and 0^{th} modes, $n_{|0,1,2,\dots}$ is the longitudinal mode and l_v is the length of the vane. If the RFQ is longer, the difference in frequency between n th and operation modes is lower [42], and the stability of the RFQ will deteriorate.

In the four-vane RFQ, the dipole modes also occur when the RFQ is in imperfect condition [41]. This might be because of errors in machining or the mispositioning of the vanes [42]. Thus, in these cases, there are TE_{21n} and TE_{11n} modes in the RFQ which mix together.

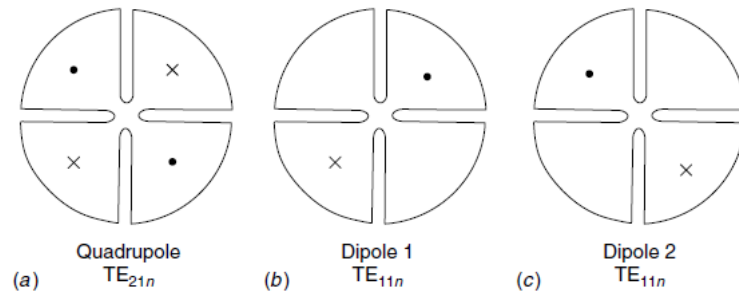


Figure 4.4: The magnetic fields in quadrupole and dipole modes of the RFQ [4].

Figure 4.4 shows the magnetic fields in the RFQ. The quadrupole or TE_{21n} mode is the ride hand side, where n is the beam propagation mode. The fields from the others, (b) and (c), which are orthogonal in orientation, are polarised that means there are two frequencies in one dipole mode [42].

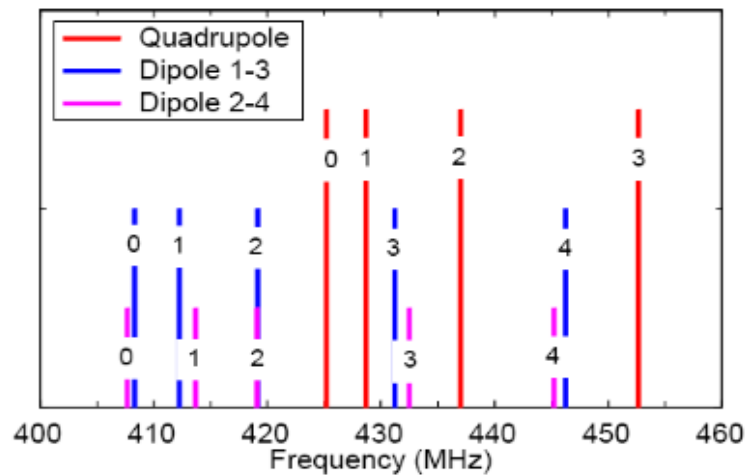


Figure 4.5: The frequency spectrums of a 425 MHz RFQ [42].

Figure 4.5 shows the frequencies in different modes of the RFQ [42]. The operation mode is a quadrupole 0 (red line) which is about 425 MHz. Dipole 1 and 2 modes are illustrated by blue and magenta lines, respectively. Apart from the resonant mode (quadrupole 0), the other frequencies need to be moved away by using the tuning system.

4.2.3 Fields in the RFQ

From Figure 4.3, the fields of the required mode in the cavity should not be mixed with other modes. The mixing depends on how strong the other modes are and how close they are in frequency. This mixing leads to the non-uniformity of the RFQ fields.

Thus, the fields in the RFQ can be written as in (4.5) below [69, 73],

$$E(z) = \sum_{p=0}^N [A(p) * TE_{21p} + B(p) * TE_{11p} + C(p) * TE_{11p}] \quad (4.5)$$

Where $A(p)$, $B(p)$ and $C(p)$ are the parameters that tell us how much the frequency interferes the operating mode. TE_{nmp} is the fields in each mode.

From Equation (4.5), the fields in the RFQ are the summation of fields in each mode. However, the accelerator needs only one mode to operate efficiently. In the ideal RFQ, the quadruple TE_{210} is the desired mode, so, $A(p)$ of TE_{210} must be 1. The other $A(p)$, $B(p)$ and $C(p)$ have to be 0. A primary aim of the tuning procedure is to achieve this.

4.3 Bead Pull Theory

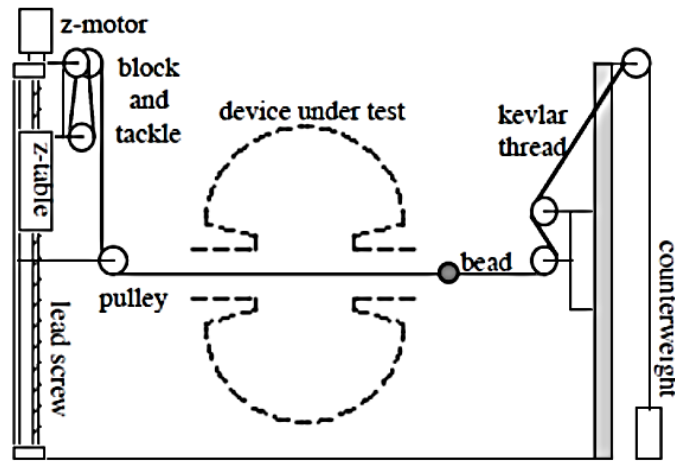


Figure 4.6: Diagram of the pulley system [74].

The bead pull measurement is a method to calculate the field distribution in the RFQ by using a perturbation technique to map the fields. The frequency will shift when the cavity volume is decreased by a small object. This is explained by Staler Perturbation Theorem as below

$$\frac{\Delta\omega_0}{\omega_0} = \frac{\int_{\Delta V} (\mu_0 H^2 - \epsilon_0 E^2) dV}{\int_V (\mu_0 H^2 + \epsilon_0 E^2) dV} = \frac{\Delta U_m - \Delta U_e}{U} \quad (4.6)$$

where $\Delta\omega_0$ is the perturbed angular frequency, ω_0 is the unperturbed angular frequency, μ_0 is the permeability of vacuum, ϵ_0 is the permittivity of vacuum, H is the magnetic field, E is the electric field, V is the volume of the cavity, U is the unperturbed stored energy, ΔU_m and ΔU_e are the stored magnetic and electric energies, respectively [75, 76].

In a bead pull measurement, a dielectric or metallic bead is pulled through the cavity, see Figure 4.6. Subsequently, the fields will be measured by observing the change of the resonant frequency, which depends on the local field strength. Each type of bead represents a different tactic. The dielectric bead only measures the electric field while the metallic bead does both the electric and magnetic fields [9].

4.4 Sag Effect of the Bead Pull System

As the bead is suspended on a thread passing through the cavity to perturb the local field, the string will be weighed down by the mass of the bead and the mass of thread itself. This can create a sagging or catenary effect [77]. However, the weights of the bead and wire are much smaller than the load's at the end of the pulley system. The catenary curve is hardly seen by eyes. In addition, the length of the pulley system is much longer than the sag which is only in millimeters. Therefore, the straight line is considered instead of the complicated curve in the sag calculation (see Figure 4.7).

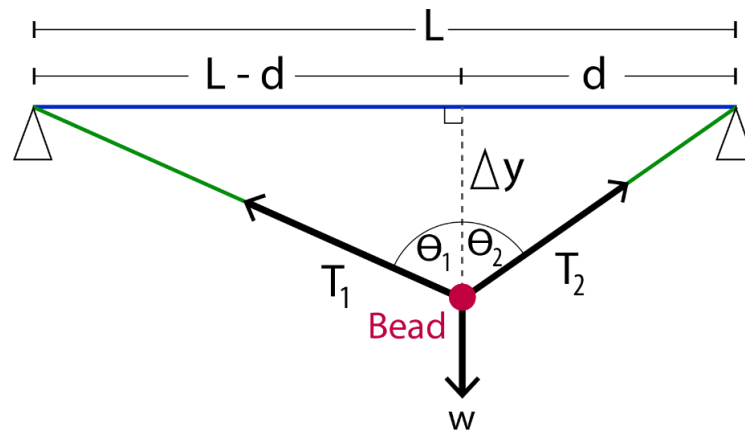


Figure 4.7: The sag layout. A blue line is the thread before the bead is hung.

The sag (Δy) is shown in Figure 4.7. A blue line is a longitudinal length (L) of the pulley system. When the bead is set, the line is dropped by the bead weight (w) as shown in the green line. Z position of the bead is indicated by d which is the distance from the end of the pulley system to the bead. T_1 and T_2 are the tensions from the bead with θ_1 and θ_2 respectively.

Assuming that the sag from the wire is much less than the distance of the bead from the end of the pulley, a sag expression can be approximated making the calculation simpler. By ignoring the curve from the wire, the expression is shown as below.

From Pythagoras's Theorem,

$$\cos \theta_1 = \frac{\Delta y}{\sqrt{(L-d)^2 + (\Delta y)^2}} \quad (4.7)$$

$$\cos \theta_2 = \frac{\Delta y}{\sqrt{d^2 + (\Delta y)^2}} \quad (4.8)$$

From the pulley layout d or $(L-d)$ is between at least 100 mm and up to 2000 mm which is much longer than Δy (which is not more than 1 mm approximately). The error is small. Δy^2 can be omitted.

Thus, $\Delta y \ll L-d$ and $\Delta y \ll d$,

$$\cos \theta_1 = \frac{\Delta y}{L-d} \quad (4.9)$$

$$\cos \theta_2 = \frac{\Delta y}{d} \quad (4.10)$$

Considering at the bead position or an equilibrium point, for the single wire, tensions of both side from the bead is equal.

So, $T_1 = T_2 = T$,

$$T \cos \theta_1 + T \cos \theta_2 = w \quad (4.11)$$

$$\frac{\Delta y}{L-d} + \frac{\Delta y}{d} \approx \frac{w}{T} \quad (4.12)$$

$$\therefore \Delta y = \frac{w}{T} \left(d - \frac{d^2}{L} \right) \quad (4.13)$$

The wire mass could be added together with the bead mass (w); however, its effect does not impact the sag because of the small weight. Thus, it is ignored for the calculation, see the comparison in Chapter 8.2.3.

In the FETS RFQ bead pull measurement, the sag correction from (4.13) is included in the LabVIEW script. The motors of Y position will be moved to the corrected position automatically in each Z position. Some information such as bead and load masses need to be added in the LabVIEW control program before running the experiments. The motors of Y position will be moved to the corrected position automatically in each Z position as seen in Figure 4.8. This process has to be done before taking the data from the Vector Network Analyser or VNA.

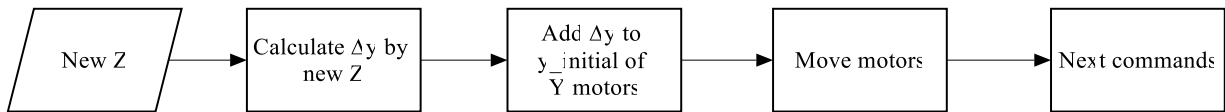


Figure 4.8: Block diagram of sag correction in FETS RFQ bead pull measurement.

Some information such as the bead and load masses need to be collected in the LabVIEW control program before running the experiments. The positions of the Y motors (y_{initial}) are set from the beginning. It is the centre position of the RFQ. The new sag (Δy) will be added to this data.

4.5 Bead Pull Experiment

A schematic of a bead pull system is shown in Figure 4.9. The cavity is connected to a Vector Network Analyser (VNA) which is used to supply RF power and determine the RF response. Low power RF is applied to the cavity and scanned through a range of frequencies across the resonance to allow the frequency of this to be determined. The pulley system consisting of the bead and thread is manipulated by motors which control of the transverse position and move the bead through the cavity in steps. All the data are then recorded by a software (such as LabVIEW) running on a P.C. [78, 79].

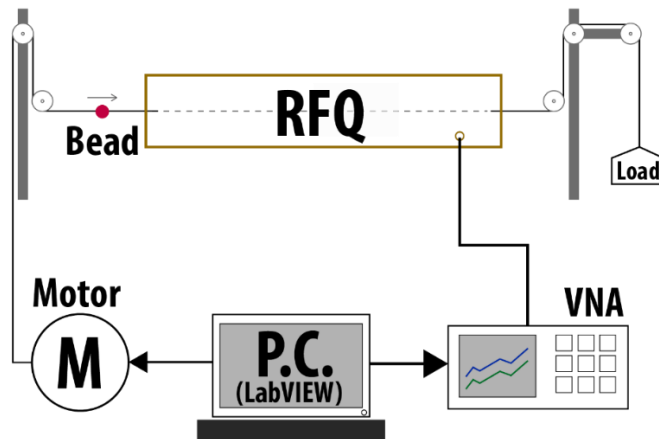


Figure 4.9: Block diagram of the bead pull systems.

4.6 Examples of RFQ Bead Pull Measurements

In the RFQ, the inter-vane gaps are narrow, so the bead cannot be passed along the axis but must be used near the centre of each quadrant instead [75, 80]. Traditionally, the string is set in four lines, one in each quadrant to perform the bead pull measurement, such

as the IPHI bead pull systems, see Figure 4.10 [81]. The beads at four quadrants are pulled at the same time. This reduces the time duration.

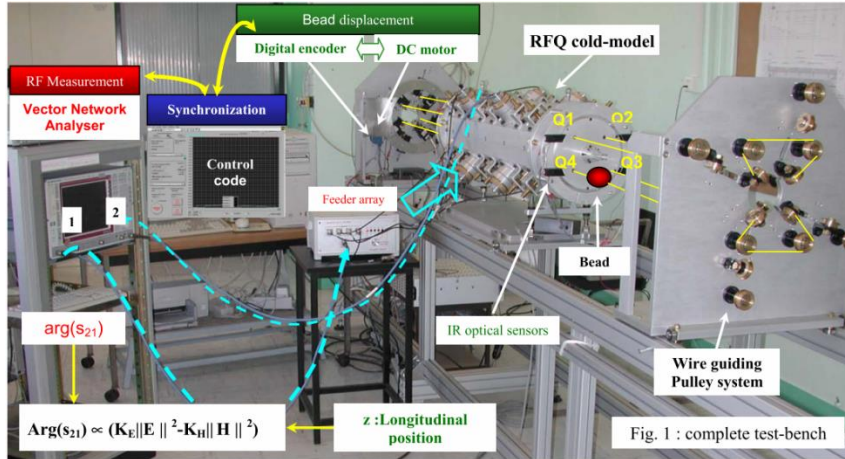


Figure 4.10: IPHI RFQ bead pull systems [81].

In contrast, the PXIE (Project X Injector Experiment) RFQ bead pull measurement was designed by using only one line, see Figure 4.11. The bead could be moved to the desired position in any quadrant by the motors. The thread was set in a loop with the actuators and motors [79, 82]. This bead pull method decreases the number of strings used in the measurement.

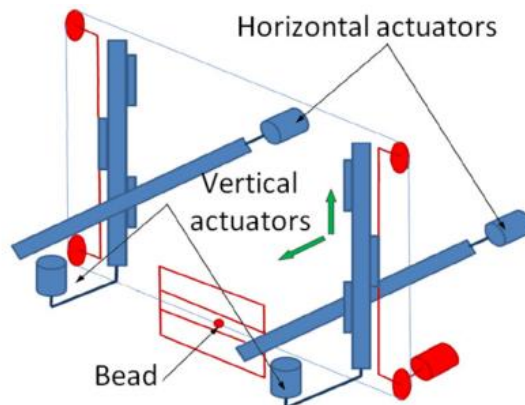


Figure 4.11: PXIE RFQ bead pull systems [82].

The FETS RFQ bead pull system also used only one bead on the measurement [66]. However, it is not a closed loop system such as the PXIE bead pull [82]. This will be expanded upon in the next section.

4.7 Bead Pull System of the FETS RFQ

The FETS RFQ bead pull measurement was originally setup at Royal Holloway, University of London (RHUL) before moving to RAL. It was developed from a pill box cavity system and then used on the cold model [67]. The bead position was movable by the stepper motor in the longitudinal direction and servo motors in the transverse directions. The string was not trod in a loop, as this would have made it more complicated, with specific hardware, when the pulley was moved to other cavities. A mass was introduced opposite the stepper motor to tension the thread. This, in addition, also reduces the slipping of the thread on the motor controlling the horizontal motion (read back errors) [78].

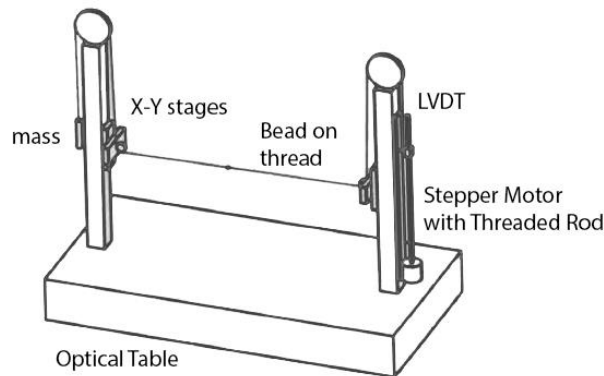


Figure 4.12: Diagram of one module bead pull measurement of the FETS RFQ [78].

However, the design of the pulley, including data collection, had been modified to suit the FETS area and the full length of the FETS RFQ. More details will be discussed in the Methods chapter.

4.8 Summary

As a resonator, a cavity can resonate in different modes. It is categorised by the pattern of the fields in each direction of the cavity. The electric and magnetic fields are perpendicular in direction. That means, in the cavity, there is neither electric nor magnetic field in the longitudinal direction which are called transverse magnetic and electric fields, respectively. The s-parameter is important in RF measurement. It can determine how well the wave can propagate, transmit and reflect through the multiple network.

The RFQ cavity is designed to satisfy the TE_{210} mode. This aims to get the fields in the longitudinal direction for accelerating and bunching the beam. The fields in the RFQ cavity is the summation of the field components in different modes. To get a flat field, the other modes have to be small and not affect the operation frequency.

The fields in the RFQ consist of the field strength in different components, especially quadrupole and dipole modes. The $A(p)$, $B(p)$ and $C(p)$ parameters, which are extracted from the field equation, show how well of each mode dominates in the overall field.

The Staler Perturbation Theorem is used to study the frequency shift when a small object is inside the cavity. This is applied to the RFQ bead pull measurement. The fields are then measured as the small bead is moved along the RFQ cavity. The material of the bead affects the fields. The catenary effect must also be considered in a long RFQ measurement as the curve on the string leads to the change of bead position. The sag is corrected to prevent the miscalculation.

RFQ bead pull measurements can be done by four or one beads running in the RFQ cavity. The IPHI RFQ bead pull system used four beads moving together to determine the fields in the RFQ, which decreases the measurement time. The PXIE RFQ system applied only one bead for the measurement. The bead can be independently moved to any position.

The FETS RFQ bead pull measurement uses only one bead to move around the RFQ. The bead is controlled by servo and stepper motors in transverse and longitudinal directions, respectively. It has been developed to measure the four-metre FETS RFQ in the restricted space of the FETS area.

Chapter 5. Tuning System

The tuning system is the method used to adjust the length of the tuners to obtain the desired frequency and electric fields. In order to get a corrected length for each tuner, an algorithm based on a perturbation technique is used.

5.1 RFQ Tuning System

In order to ensure that the RFQ has a constant flat field, a tuning system is particularly important. For the four-vane RFQ, when focusing on the bead pull area, the electric field structure is in the form of a standing wave [9]. The relationship between local field and local frequency can be derived starting with a wave equation of one dimension [83, 84].

$$\frac{\partial^2}{\partial z^2} E(z) + k^2 E(z) = 0 \quad (5.1)$$

Where $E(z)$ is a longitudinal field, k is a wave number which is $\frac{\omega}{c}$. c is a speed of light while ω is an angular frequency which equal to $(\omega_0^2 - \omega^2(z))$ [85].

In RF cavity, the local perturbation frequency $\omega(z)$ and electric field along the longitudinal axis are shown as

$$\omega(z) = \omega_0 + \delta\omega(z) \quad (5.2)$$

$$E(z) = E_0 + \delta E(z) \quad (5.3)$$

Where ω_0 and E_0 are the resonant frequency and electric field of the cavity and $\delta\omega(z)$ and $\delta E(z)$ is the shift of local resonant frequency and electric field. For the small perturbation, the $\delta E(z)$ is very small, so, $\delta E(z) \ll E_0$.

From Equations (5.1)-(5.3), the local field deviation $\frac{\delta E_0(z)}{E_0}$ can be presented as below

$$\frac{\partial^2}{\partial z^2} \left(\frac{\delta E_0(z)}{E_0} \right) = \frac{8\pi^2}{\lambda^2} \left(\frac{\delta f_0(z)}{f_{average}} \right) \quad (5.4)$$

where $\delta f_0(z)$ is the variation of local frequency due to errors in the mechanical structure and $f_{average}$ is the average frequency of the whole cavity [9].

Thus, from Equation (5.4), the second derivative of the local electric field depends on the variation of the local frequency. The local field strength is measured by the frequency

along the cavity. Therefore, the change in tuner's length related to the local resonant frequency determines the change of field strength.

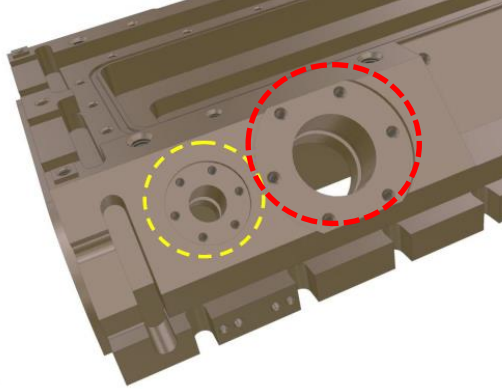


Figure 5.1: Probe port of tuner in the outer wall (red circle) [39].

Furthermore, there is a relationship between the internal volume of the RFQ and its frequency as shown in Equation (4.6). The frequency will rise when the internal volume is decreased [39]. Generally, the tuners will be inserted from the outer wall of the RFQ to reduce the volume of the RFQ cavity, see Figure 5.1, which is the FETS RFQ tuner port [9]. This means we can only tune the frequency of the RFQ when it starts lower than the expectation.

5.2 Tuning Algorithm

The idea behind the tuning system is to provide the field flatness from the expected local frequency. The fields in each quadrant are collected from the VNA. After that, they will be decomposed in term of quadrupole and dipole fields to calculate the new frequency shift that can provide the field flatness.

5.2.1 Fields in Each Quadrant

The overall fields consist of the fields in each mode (p) [69, 73]. The TE_{210} is the only mode for the RFQ operation. Therefore, the other modes have to be tuned out. From Equation (4.5), the fields in each quadrant can be defined by

$$E(z, q) = \sum_{p=0}^N [A(p)qq(p)(-1)^{q-1}f(z, p) \pm B(p)d_1(p)f(z, p) \pm C(p)d_2(p)f(z, p)] \quad (5.5)$$

where q is the number of each quadrant, $qq(p)$ is a normalisation factor, which is the stored energy of the mode in the cavity in quadrupole mode, $d_1(p)$ and $d_2(p)$ are normalised factors of the dipole modes, $f(z, p)$ is a sinusoidal function of the field, which depends on the mode, and

$$f(z, p) = \cos\left(\frac{2\pi(z - z_0)}{\lambda_g}\right) \text{ if } \omega_p > \omega_{q0} \quad (5.6)$$

$$f(z, p) = \cosh\left(\frac{2\pi(z - z_0)}{i\lambda_g}\right) \text{ if } \omega_p < \omega_{q0} \quad (5.7)$$

where,

$$z_0 = \frac{L}{2} - \lambda_g \frac{p}{4} \quad (5.8)$$

$$\frac{1}{\lambda_g} = \frac{1}{2\pi c} \sqrt{\omega_p^2 - \omega_{p0}^2} \quad (5.9)$$

From Equations (5.8) and (5.9), ω is an angular frequency where ω_p and ω_{q0} is the angular frequencies of the free space and operating modes, respectively, z_0 is the offset of the longitudinal direction, λ_g is the waveguide wavelength of mode p and L is the length of the RFQ.

For the tuning purpose, $A(0)$ has to be equal to one, and other normalisation factors have to be 0 to obtain the flat fields. This can be written as below,

$$A(0) = 1, A(p)|_{p=0, \dots, n} = 0, B(p)|_{p=0, \dots, n} = 0 \text{ and } C(p)|_{p=0, \dots, n} = 0$$

5.2.2 Frequency Perturbations

The frequency perturbation ω_k is the frequency from a small perturbation, where $z=k$. Therefore, the perturbation from the amount of mode p is formed as (5.10) [69].

$$\text{Amount of mode } p = \frac{\omega_k^2 - \omega_{p0}^2}{\omega_p^2 - \omega_{p0}^2} * |\text{mode } p|_{z=k} \quad (5.10)$$

Where $|\text{mode } p|_{z=k}$ is the pattern of the mode p along the Z position, normally it is in a cosine function ($f(z, p)$).

Thus, the coefficients $A(p)$, $B(p)$ and $C(p)$ are calculated below, see Equation (5.11).

$$A(p) = -\frac{1}{L} \int_0^L \left(\frac{\omega_z^2 - \omega_{p0}^2}{\omega_{qp}^2 - \omega_{p0}^2} f(z, p) \right) dz \quad (5.11)$$

$$B(p) = -\frac{1}{L} \int_0^L \left(\frac{\omega_z^2 - \omega_{p0}^2}{\omega_{d1p}^2 - \omega_{p0}^2} f(z, p) \right) dz \quad (5.12)$$

$$C(p) = -\frac{1}{L} \int_0^L \left(\frac{\omega_z^2 - \omega_{p0}^2}{\omega_{d2p}^2 - \omega_{p0}^2} f(z, p) \right) dz \quad (5.13)$$

By integrating over the tuner diameter along Z position of the RFQ with fixed $A(p)|_{p>0}$, $B(p)$ and $C(p)$, the frequency shift (ω_p) can be solved in the least squares form.

Therefore, if we know the frequency perturbation values and their location [73], the tuners can be moved to cancel the perturbation effects.

5.3 FETS RFQ Tuning Algorithm

The FETS RFQ tuning algorithm can be divided into two parts: fitting data and calculating the new frequency shift. In order to correct the fields, the new tuners' length is calculated from the frequency shift. The brift diagram is represented in Figure 5.2. The measurement data is fitted to determine the quadrupole and dipole fields as a function of longitudinal position. Then the measured fields are decomposed to map the expected new local frequency of each tuner that provides the uniform fields.

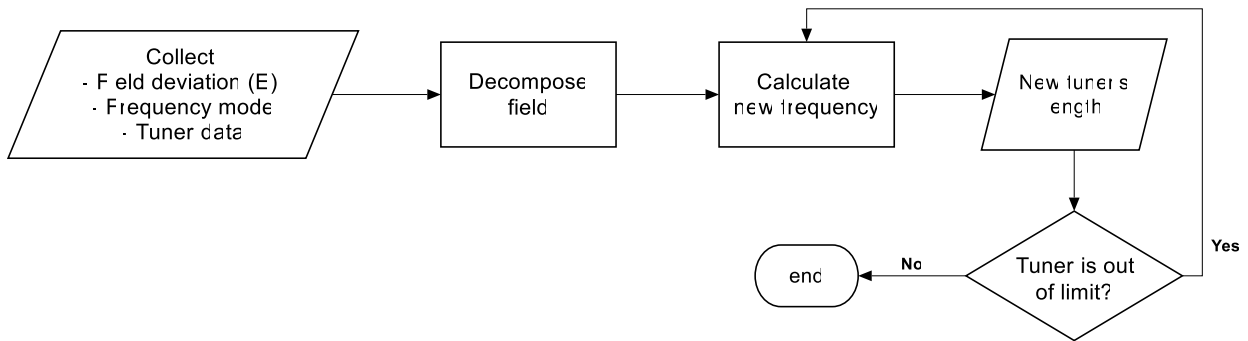


Figure 5.2: The brift diagram of tuning algorithm.

5.3.1 Measurement Data and Fitting

The field data from the bead pull measurement, which is in a discrete form, need to be fitted with Equation (5.10) to provide the new frequency shift. In the FETS RFQ, the field shapes (E) are calculated from the measured frequency as

$$E(z) \propto \sqrt{\frac{|f(z) - f_0|}{f_0}} \quad (5.14)$$

where f_0 is the unperturbed frequency and $f(z)$ is the longitudinal frequency. The field composes of various longitudinal modes. Both quadrupole and dipole mode components are considered because their frequencies can easily interfere. The field components in each quadrant need to be added up together depending on what kinds of fields is: quadrupole or dipole fields. This is because the signs of the fields are considered.

To begin with, number of modes to be used are determined depending on the number of tuners. The number of equations have to be enough to solve the frequency shift of each tuner. Since only quadrupole and two dipole components are extracted from the field, number of considered modes has to be at least one-third of number of the tuners.

The quadrupole and dipole field strengths are calculated. For the quadrupole aspect, the quadrupole field (Q) is the average of the fields in all four quadrants, see eq. (5.15), while the dipole components (D_1 and D_2) are calculated from only two quadrants, see eq. (5.16) and (5.17) [86, 87].

$$Q = \frac{(E_{q1} + E_{q2} + E_{q3} + E_{q4})}{4} \quad (5.15)$$

$$D_1 = \frac{(E_{q1} - E_{q3})}{2} \quad (5.16)$$

$$D_2 = \frac{(E_{q4} - E_{q2})}{2} \quad (5.17)$$

where E_{qi} is the field strength in quadrant i from the bead pull measurement. Then Q , D_1 and D_2 are normalised by the mean of Q to get the quadrupole mean equal to one.

The frequencies of the first five modes in each longitudinal components are taken from the measurement by measuring the quadrupole and dipoles frequencies. The rest of the frequencies (f_p) has to be calculated including the waveguide (λ_g) and free space (λ_p) wavelengths from Equation (5.9). The zero mode of waveguide wavelength is infinity. It can be set in very high number in the analysis. The other higher modes are calculated from the equation below.

$$\lambda_g = \frac{2L}{p} \quad (5.18)$$

The Table 5.1 shows how to calculate frequencies and wavelengths from the measured frequencies. This can be applied to quadrupole and dipole components.

Table 5.1: Frequencies and wavelengths calculation.

Mode number (p)	0	1-4	n
Frequency (f_p)	measured	measured	$\frac{c}{\lambda_p}$
Free space wavelength (λ_p)	$\frac{c}{f_p}$	$\frac{c}{f_p}$	$\frac{\lambda_g + \lambda_{p0}}{\sqrt{\lambda_g^2 + \lambda_{p0}^2}}$
Waveguide wavelength (λ_g)	∞	$\frac{\lambda_p}{\sqrt{1 - \left(\frac{\lambda_p}{\lambda_{p0}}\right)^2}}$	$\frac{2L}{p}$

Note: c is speed of light and λ_{p0} is The zero mode of λ_p .

The longitudinal offset from Equation (5.8) can be calculated. Then the field is decomposed by Equation (5.5). Therefore, we can calculate the magnitude mode patterns in the sinusoidal term, $f(z, p)$, from Equations (5.6) and (5.7). The least squared method is applied to solve the magnitude of $A(p)$, $B(p)$ and $C(p)$ from the measured data along the Z position. The data is already normalised from the beginning, so, the normalised factors are unity. This shows how much the undesired modes affect the FETS RFQ. In addition, the calculated $A(p)$, $B(p)$ and $C(p)$ are placed in the Equation (5.5) to confirm how well the fitting works with the measured data. The diagram of this analysis is represented in Figure 5.4.

5.3.2 Calculation of New Frequency Shift

From the above topic, $A(p)$, $B(p)$ and $C(p)$ of measured data are calculated. In order to flatten the field, these longitudinal coefficients need to be zero excepting $A(0)$ that has to be one. The new frequency shifts have to cancel out those coefficients in that they are set in opposite sign as $-A(p)$, $-B(p)$ and $-C(p)$.

The mode coefficients, from Equations (5.11)-(5.13), can be calculated by the integration with the function of frequency shift over the diameter of each tuner in Z position. The set of frequency perturbation (ω_z) for each tuner then is computed by the least square sense.

First of all, W_{result} is as seen in Equation (5.19). This will be used to in the least square process. Then apart from W_{result} , the integration over the tuner position from Equations (5.20)-(5.22) is applied. The longitudinal coefficient in each mode consists of the frequency

changes from each tuner along the RFQ. Thus, the number of considered mode is important. It should be enough to cover the frequency shift parameters from each tuner.

$$W_{result} = \omega_z^2 + \omega_{p0}^2 \quad (5.19)$$

$$A(p) = -\frac{1}{L} \int_0^L \left(\frac{W_{result}}{\omega_{qp}^2 - \omega_{p0}^2} f(z, p) \right) dz \quad (5.20)$$

$$B(p) = -\frac{1}{L} \int_0^L \left(\frac{W_{result}}{\omega_{d1p}^2 - \omega_{p0}^2} f(z, p) \right) dz \quad (5.21)$$

$$C(p) = -\frac{1}{L} \int_0^L \left(\frac{W_{result}}{\omega_{d2p}^2 - \omega_{p0}^2} f(z, p) \right) dz \quad (5.22)$$

In addition, as the tuners are placed in four quadrants of the RFQ, the location of the tuner is also considered. As seen in Figure 5.3, the sign of dipole component is important. The additional factor has to be multiplied for the dipole mode calculation. This depends on where the tuner is and the sign of the quadrupole and dipole at that moment. If the sign is the same, the factor is +1. In contrast, the factor is -1 when the sign is different. Thus, $B(p) = -B(p)$ when the tuner is in quadrant two and $C(p) = -C(p)$ when the tuner is in quadrant three where the quadrant starts clockwise from top right.

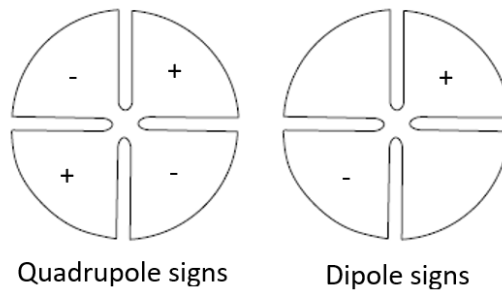


Figure 5.3: Quadrupole (left) and Dipole (right) signs.

All the longitudinal mode coefficients without $A(p)$ have to be zero. Then W_{result} of each tuner's position is obtained by the least squares optimisation method to map the negative sign of measured coefficients. The new coefficients are then cancelling out the measured one leading to the zero value. From (5.2)-(5.9) and $\omega = 2\pi f$, the local frequency $\delta f(z)$ is then calculated by the equation below

$$\delta f(z) = \sqrt{\frac{W_{result}}{(2\pi)^2} + f_{p0}^2} - f_{p0} = f_{local} \quad (5.23)$$

This local frequency shift, or f_{local} , of each tuner can compensate the measured data. The new set of local frequency shift will be converted to the global frequency (f_{global}) to apply into the RFQ cavity as

$$f_{global} = \frac{f_{local} * L_T}{L} \quad (5.24)$$

Where L_T is a length of tuner's diameter.

The global frequency is used for calculating the length of the tuner. This relationship is measured from the measurement. If the tuner is out of length, the new local frequency will be calculated again by ignoring that tuner position.

When obtaining the satisfied length of the tuners, they will be applied in the FET RFQ. A new bead pull measurement is then done to investigate how flat the field is. The tuning process iterates until the required flatness is obtained or no further improvement due to the measurement or other errors. The calculation of the new frequency shift and tuner's length process is illustrated in Figure 5.5.

5.3.3 Tuning Diagram of the FETS RFQ

The tuning diagram of the FETS RFQ is divided into two parts. The first part, see Figure 5.4, represents the analysis from Chapter 5.3.1 while the diagram of Chapter 5.3.2 is shown in Figure 5.5.

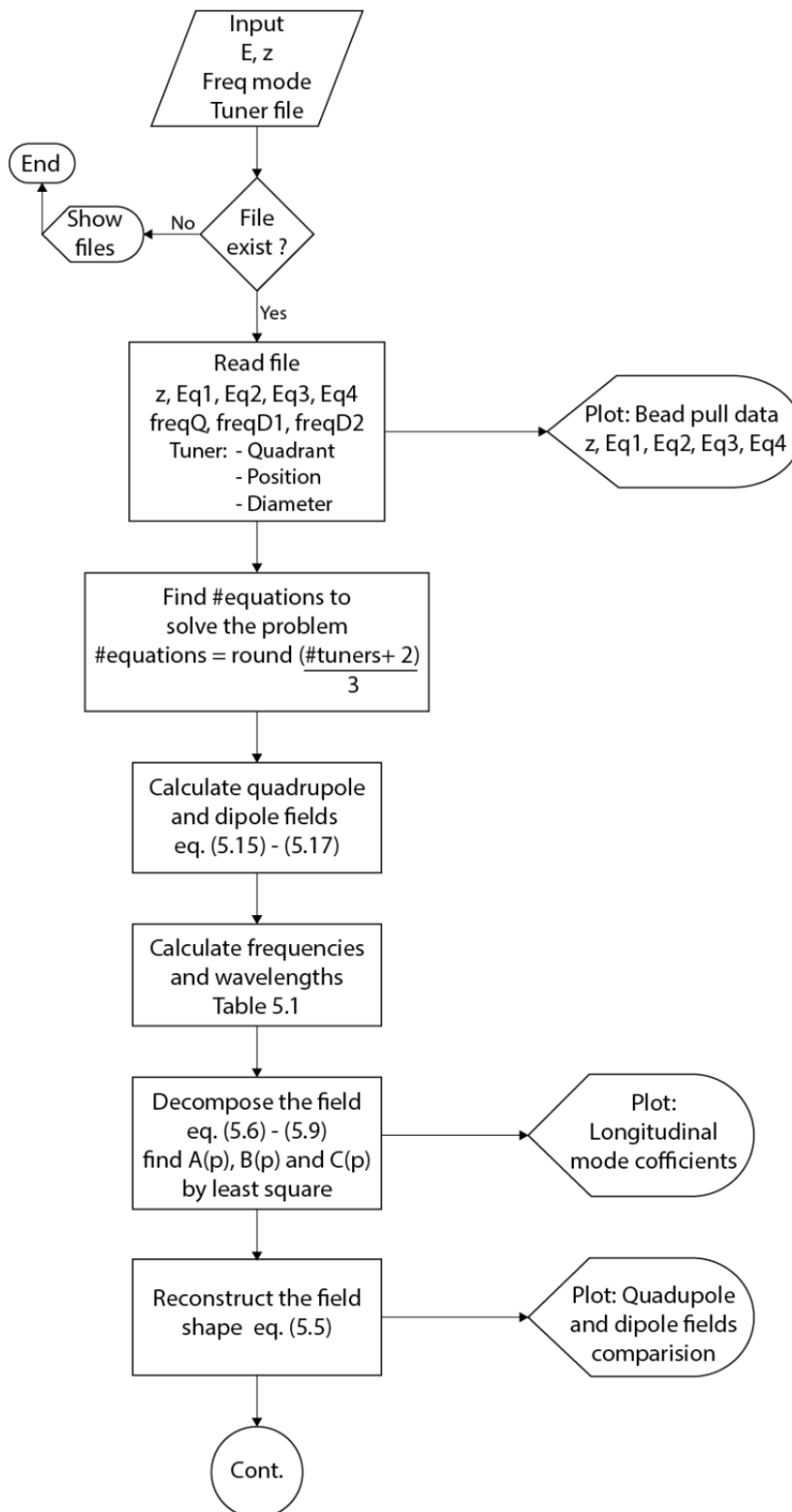


Figure 5.4: Diagram of tuning algorithm part 1.

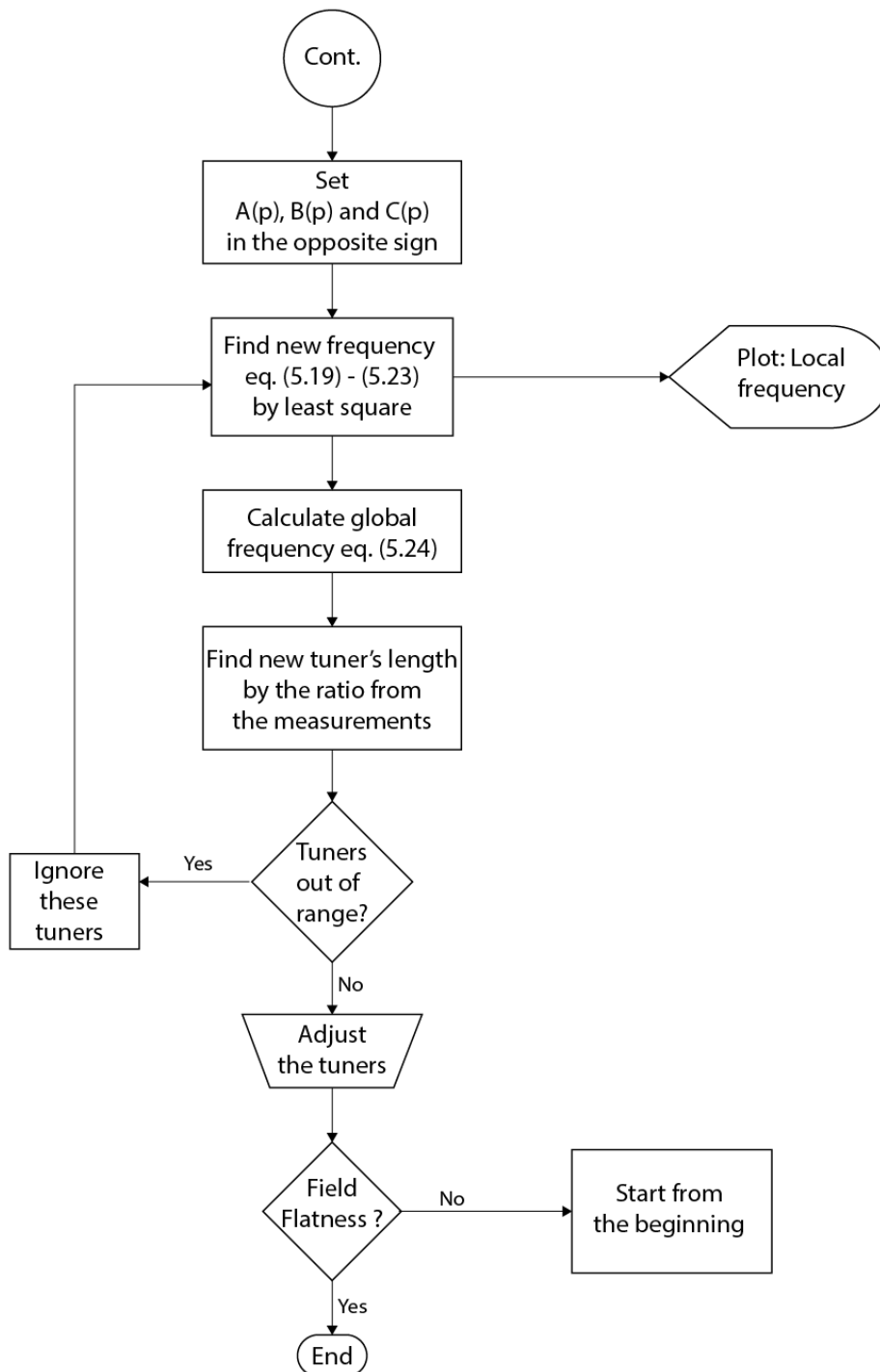


Figure 5.5: Diagram of tuning algorithm part 2.

5.4 Summary

The tuning system is the process used to tune the fields in the FETS RFQ from the imperfect manufacturing. By changing the length of the tuners, which are inserted into the RFQ, the frequency changes can be calculated from the theory.

The tuner length is also related to the inner volume of the RFQ that affects the overall frequency. The frequency goes up when increasing the length of the tuner into the RFQ.

In the FETS RFQ, the first five modes of the measured frequencies are applied while the higher modes are calculated from theory. The field shapes are computed from the measured frequency. Then, they are deconstructed into the factors: $A(p)$, $B(p)$ and $C(p)$ which determine how much the operation mode is disturbed by the other modes. These coefficient parameters are used to calculate the new frequencies shift by the least squares method after that the new length of each will be applied to correct the field.

Chapter 6. Methods

In order to obtain flat fields, understanding both the bead pull measurement and the tuning algorithm is important. As a result, measurements have been made in a series of steps to study the pulley system and to understand the response of the RFQ. A one-metre pulley system has been installed first for one-section of the FETS RFQ, and then it was modified to cover the whole length. After that, the tuning algorithm was applied to provide the information necessary to change the tuner's length. These measurements are described in this chapter.

6.1 Bead Pull Measurement

The bead pull measurement has been tested with a pill box cavity and the cold model of the FETS RFQ at RHUL [78] before being moved to RAL. The first bead pull measurement at RAL was made on a purpose-built test stand away from the FETS area. It was setup for a one-metre measurement. The idea behind this was to study and improve the measurement technique and the control software. To achieve flat fields, the bead pull measurement then was installed in FETS area for measuring the four sections of the FETS RFQ. Table 6.1 briefly demonstrates the location and sections of the RFQ used in the measurements as a function of time.

Table 6.1: A summary of bead pull measurements in different lengths and locations.

Year	Location	RFQ Section	Overall Length
2015	Beside the FETS area	2	~ 1.5 m
2016	FETS area	2	~ 4.5 m
2018	FETS area	1	~ 4.5 m
2019	FETS area	1-4	~ 4.5 m

6.1.1 One-Metre Arrangement

In 2015, the bead pull measurement was tested with the test stand in R8, RAL. Although it was not complete, section two of the FETS RFQ was available to conduct the measurements.

6.1.1.1 Bead Pull Measurement

The one-metre bead pull system, as seen in Figure 6.1, consists of the VNA, pulley system and LabVIEW software, which was written by Gary Boorman [67, 78, 88] from RHUL.

It was developed from the test on pill box cavity and the cold model of the FETS RFQ. The pulley system includes a metallic coated bead, cotton thread and motors. The vertical Aluminium rods have to be long enough to allow the complete motion of the bead through the RFQ and also strong enough to support the weight of the load used to stop the bead from sagging. The measurement was controlled from the LabVIEW window, see Figure 6.2. This moved the bead and controlled and readout the VNA.

All essential parameters could be changed from the left column of the window, including the VNA setup. The upper middle column shows the current position and status of the motors: M1 and M3 control the X axis (horizontal), M2 and M4 control the Y axis (vertical) and M5 controls the Z position (longitudinal). The lower middle column illustrates the frequency against S-parameter of the current Z position. The last column is the operating frequencies against Z position.

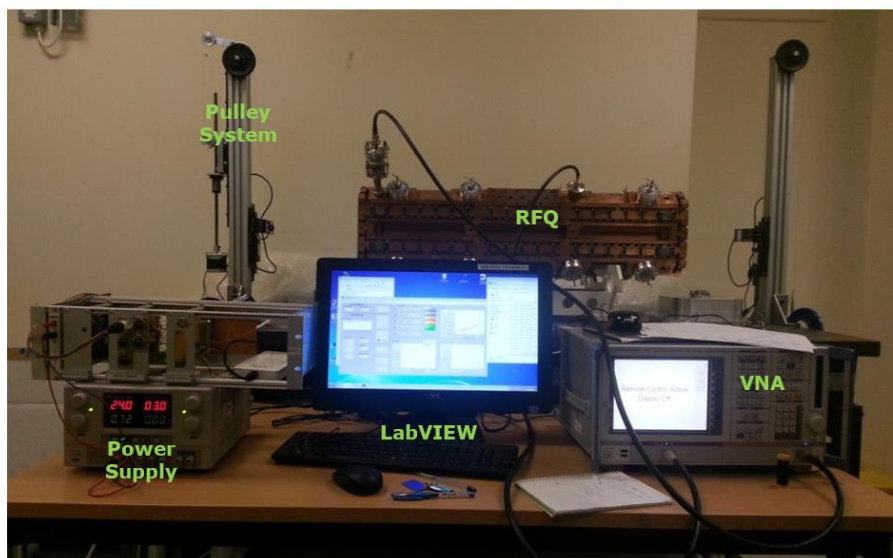


Figure 6.1: The Bead pull measurement setup for one section of the FETS RFQ.

The bead position was manipulated by four servo and one stepper motors. The stepper motor is used for the longitudinal direction. The servo motors (ATP-DC Servo Motor TDC001) [89] control the transverse dimensions; two motors for each X and Y axes at both ends. The servo motors are used for X and Y because the motion is much smaller than in Z, but must be more precisely known due to the strong dependence of the field strength on a radius. The stepper motor is suitable to control the Z direction because it is used for the high torque resulting from the heavy loads used to reduce the bead sag.

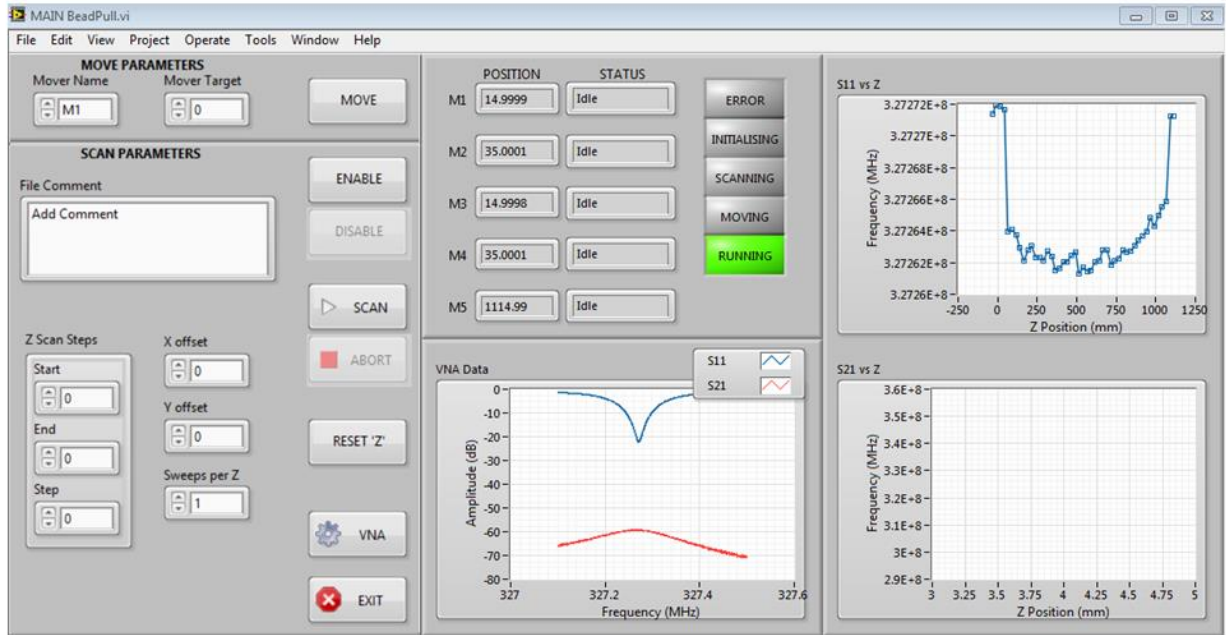


Figure 6.2: The LabVIEW window to setup and measure the parameters for the bead pull measurement of the FETS RFQ.

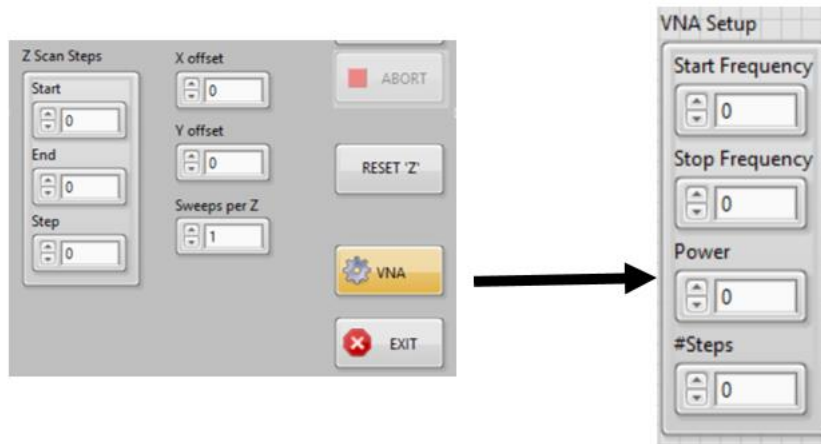


Figure 6.3: VNA pop-up window.

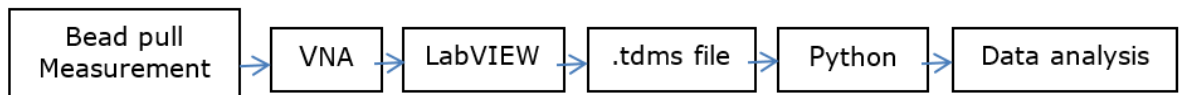


Figure 6.4: Bead pull analysis diagram of the one-metre FETS RFQ.

Figure 6.3 shows a pop-up window after clicking the VNA button as seen in orange colour. The start (F_{start}) and stop (F_{stop}) frequencies, provided power from VNA (dBm) and

number of frequency step ($\#Steps$) are filled in this window to control the VNA. The frequency resolution (F_{res}) which used in the error analysis is calculated by (6.1)

$$F_{res} = \frac{F_{stop} - F_{start}}{\#Steps} \quad (6.1)$$

From Figure 6.2 and Figure 6.4, the frequency and s-parameter in each Z position from the measurement are taken by the Rohde&Schwarz ZVB4 VNA [90]. Only S_{11} was collected because S_{21} port was not ready at that time. Then the LabVIEW programme which interfaced between the VNA, motors and computer would receive and convert the data to a readable file in a tdms form. The measurement was run only on one quadrant. The bead position then needed to be reset to move into the other quadrants.

Although the LabVIEW showed an analysis of the measurement, another programme is used to read and analyse the data in more detail offline. There are several programmes that could illustrate the results such as MATLAB, Python, C, R and etc. However, Python [91] is chosen for the following reasons. First of all, it is the programme that has been used by other colleagues. That means it will be convenient to exchange the code script and the results. Secondly, it is convenient to be used for reading the tdms file. Furthermore, the programme does not require a license, so, everyone can access it.

6.1.1.2 Tuners Adjustment

In 2015, the sixteen temporary tuners were inserted into the FETS RFQ section two. The scale was added, as seen in Figure 6.5. The length of each tuner was changed by hand. One turn equals one mm movement in the RFQ, and the number of turns needed to be counted. Otherwise, the length of the silver screw would have to be measured to calculate how far the tuners would be inserted. However, the scale was removed for the four-metre measurements.



Figure 6.5: A tuner with its scale.

6.1.2 Four-Metre Arrangement

After testing with the one-metre arrangement, the bead pull system was moved to the FETS area. Due to height limits, we cannot have at least two-metre posts for the motion, so, the string was looped over multiple wheels to reduce the height of the posts.

6.1.2.1 Four-metre Bead Pull Measurement

The pulley system was redesigned for the complete FETS RFQ in the following year. The aims were to extend its length to cover the four-module RFQ and reconstruct its layout to match the limitations in space. The Z stepper motor was changed from moving vertically to horizontally (Zaber X-BLQ1495-E01) [92], as seen in Figure 6.6 and Figure 6.7.

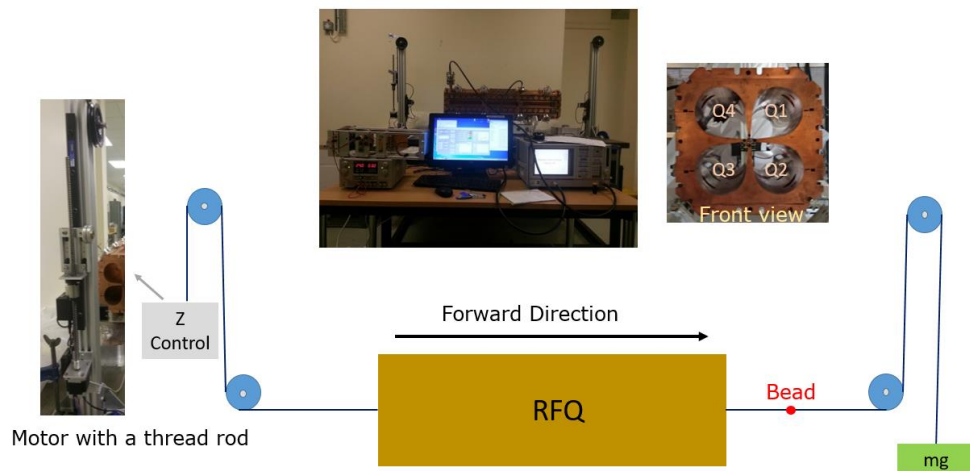


Figure 6.6: Old pulley system covering only one section of the FETS RFQ.

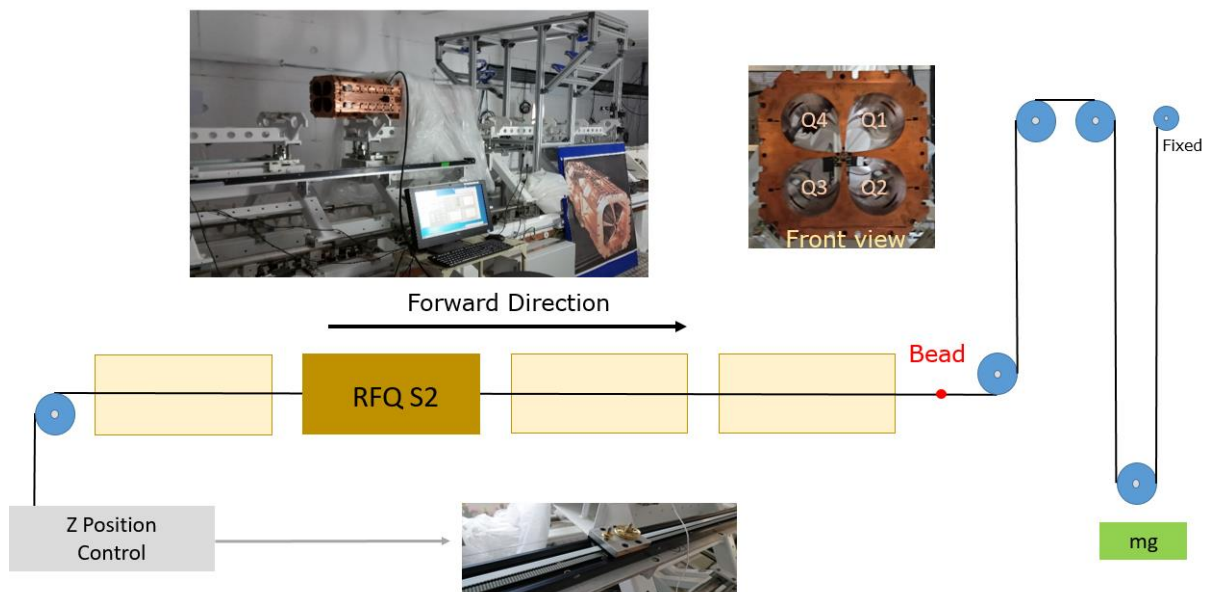


Figure 6.7: Pulley system on the FETS site.

Apart from the Z control layout, the main difference is the beginning of the Z position is not the same. In 2015, the Z began with the RFQ input, whereas, for the new set of bead pull measurements, an initial Z ($Z = 0$) was set at the end of the RFQ. In addition, the wheels were changed to bigger ones.

After the bead pull system was moved to the FETS area, section two of the FETS RFQ, which was available at that time, was placed on the rails to test the new bead pull system. The pulley layout then was disconnected and removed to provide some space for other experiments. Thus, when all modules of the RFQ are placed on the rails, the pulley system needed to be re-constructed again.

However, in 2018, only section one of the FETS RFQ, which was back from a manufacturer, was used to test the bead pull system again. This was to prepare for the final bead pull measurement.

6.1.2.2 Change in Four-metre Bead Pull Measurement

The bead pull then was reinstalled again in 2019. At that time, there were some changes to improve the test.

First of all, wheel supports were added, see Figure 6.8. This is because the previous wheels were not stable, and they might not move freely sometimes. This caused the problems in Z position when the measured and real Z might not be the same.

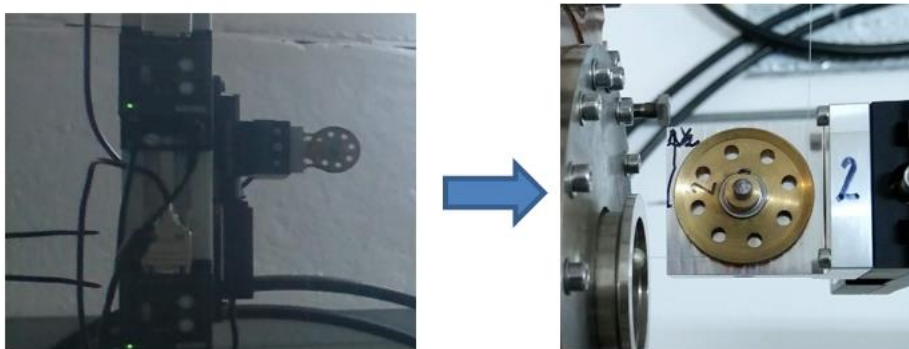


Figure 6.8: The change of the wheels in the FETS RFQ bead pull measurements.

Furthermore, the LabVIEW script has been changed. The new script was written by Alan Letchford. It was designed to be simpler. For example, the data from VNA was now collected in excel format rather than the tdms, as seen in Figure 6.9. Although the frequency was measured, as seen in Equation (5.14), the dependence of the electric field is

$E(z) \propto \sqrt{\frac{|f(z)-f_0|}{f_0}}$, to calculate the field and display that. This is more convenient to show how flat the field is, see Figure 6.10.

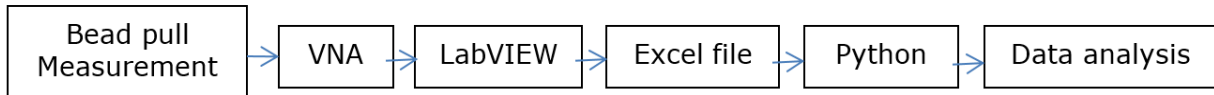


Figure 6.9: Bead pull analysis diagram of the four-metre FETS RFQ.

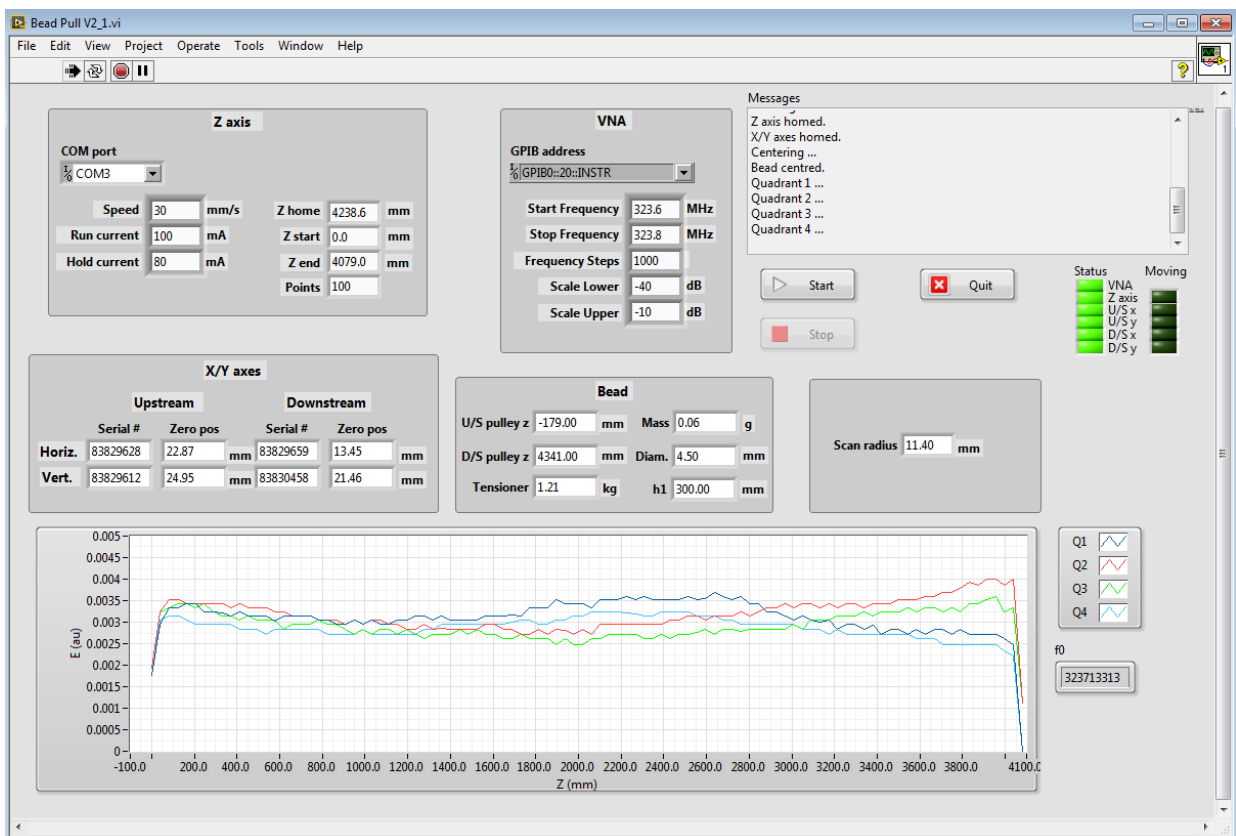


Figure 6.10: The new LabVIEW window to set the parameters for the bead pull measurement of the FETS RFQ.

The LabVIEW window was changed as shown in Figure 6.10. It allowed current and speed of the stepper motor to be changed. This allowed the weight of the load to be increased. The heavier the load is, the smaller the motor speed can be and the larger the current to support the load. The electric fan was added to reduce the temperature of the motor at higher currents. The longitudinal home position of the bead, Z_{home} from Z axis part in Figure 6.10 is a summation of the length of the RFQ, 54 mm which is the distance from the end of the FETS RFQ to the end plate and ΔZ which is the distance of the end plates to the bead as seen in Figure 6.11. The distance of ΔZ is variable depending on the type of the thread and how

weight the load is. ΔZ might be longer if the load mass is increased in that the wire might be lengthened.



Figure 6.11: The Zhome calculation.

The VNA area in Figure 6.10 shows the boundary of both the frequency (MHz) and s -parameters (dB in scale lower and upper) of S_{11} and S_{21} , which are set in the VNA monitor as seen in X and Y axes Figure 6.12 respectively. While the data of X/Y axes in Figure 6.10 are the initial position of the transverse section provided by the servo motors. The numbers of the X and Y which are the centre of the RFQ axis was determined using a laser survey. In the bead part, the mass of the bead (g) and load (kg) need to be entered to compensate for the sag of the thread over the four-metre FETS RFQ. The sag in the wire has been corrected by increasing the load and using a sag equation that was applied in the LabVIEW script. The vertical shift from the sag was calculated and compensated by moving the Y's motors during the bead motion. The motor current of longitudinal direction was increased to tolerate the heavy load.

The diameter of the bead is used for calculating the minimum of the radius of the bead position, which is at the right hand side, to prevent the bead touching the vanes when passing through the RFQ.

Everything needed to be set before running the bead pull. The bead pull starts running from quadrant one in the forward direction (from the output to the input of the FETS RFQ). The unperturbed frequency then is measured outside the RFQ cavity. When it finishes the forward scan of the first quadrant, the bead will be moved back to the end of the FETS RFQ to start the second quadrant. This process is repeated until finishing all four quadrants. Only forward scans are measured to avoid running times which are too long.

The new code provided both benefits and drawbacks. First of all, the size of the file was smaller. The new code took only important data such as the unperturbed frequency and the value of the peak frequency of S_{21} from the VNA and the Z position when the bead was in the RFQ cavity. They would then be converted to the fields, using the relationship of $E \propto$

$\sqrt{\frac{\Delta f}{f_0}}$, where f_0 is the unperturbed frequency, which was plotted on the LabVIEW window. The old code stored all S_{11} and S_{21} values of each frequency step in all Z positions. Thus, the resonant frequency can be precisely predicted by fitting a Lorentzian distribution rather than collecting only the peak data from the measurement. However, this causes a bigger size of the file from the previous code. In the new code, the frequency will not be very accurately determined if the frequency step size is too large, see Figure 6.12.

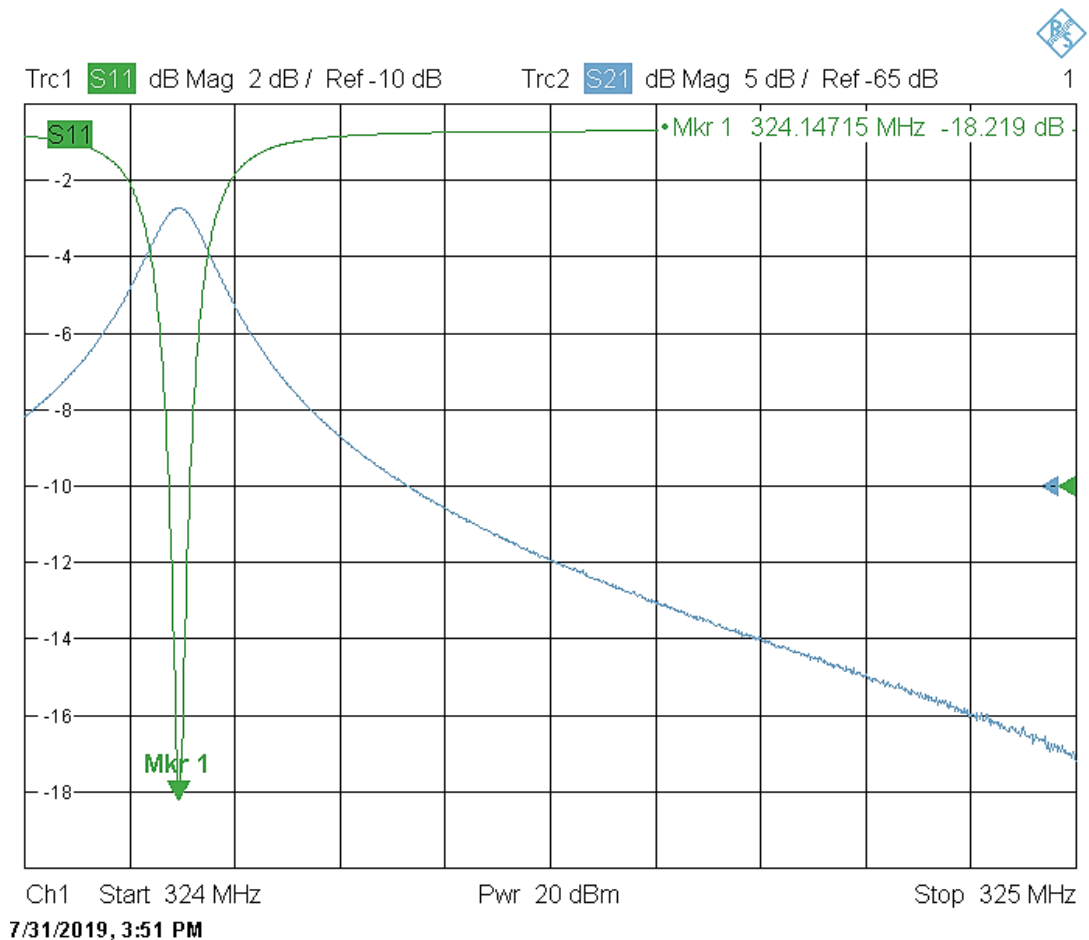


Figure 6.12: The operating frequency or the first quadrupole mode from the VNA with a maker (Mkr1) to detect the peak of s-parameter.

6.1.2.3 Tuner Adjustment

As it is not possible to directly measure how far the tuners extend into the RFQ from the inner surface, this has to be measured and adjusted externally. This is done by a Vernier Caliper and spanner. Figure 6.13 illustrates where the tuners are set on the coners of the FETS RFQ. The dynamic tuner is at a top left coner while others represent the manual tuners. The slug tuner can be inserted into the cavity about 29 mm. Beyond this, there is a risk of a

vacuum O-ring on the tuner falling into the FETS RFQ. As a result, 27 mm was set as the maximum in case of a mistake. At the start of the measurement, the tuners were inserted into the cavity a nominal 8 mm, which is the position where the edge of the tuner's tip touches the internal surface of the FETS RFQ.

The dynamic tuners are set differently from the slug tuners. It is difficult to measure how much length is inside the RFQ because there is an automatic feedback controller placed on the tuner. However, the length of the tuner corresponds to a bellow gap as seen in the black square of automatic tuner on the top left. The maximum length that can be inserted into the cavity is 15 mm from the FETS RFQ inner wall as shown in Figure 6.13 (top left). This relates to 17 mm of the bellow gap which is the shortest gap. This gap could be extended to 37 mm that means the automatic tuners can be move outward around 20 mm.

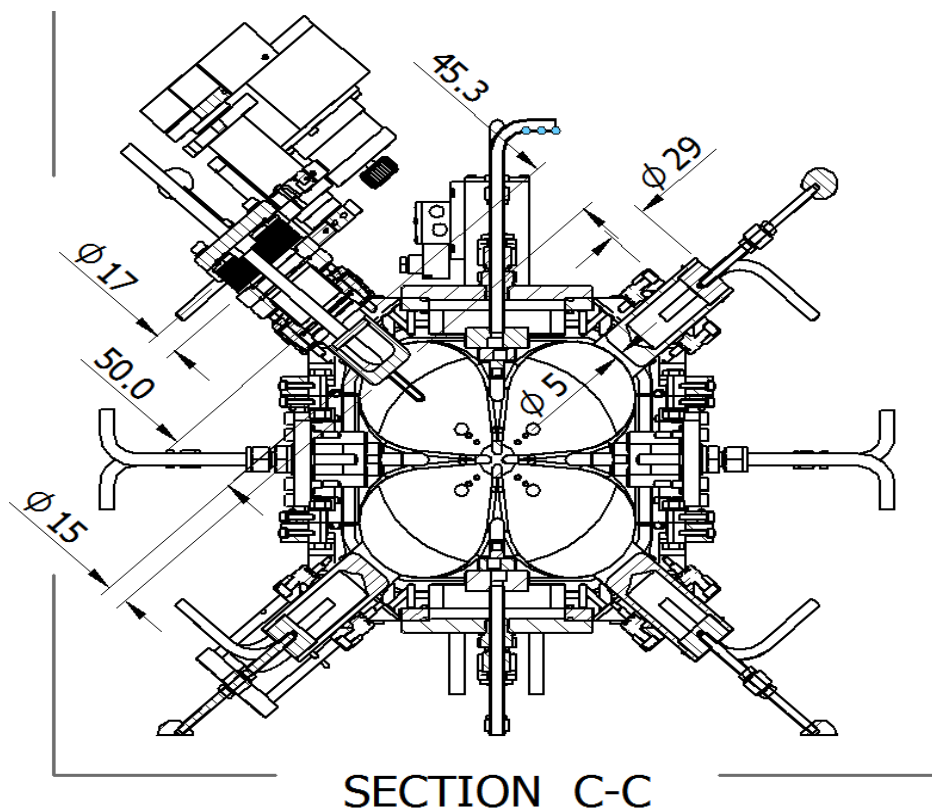


Figure 6.13: Dynamic and manual tuners layout [93].

The tuner adjustment is done as follows. As seen in Figure 6.14, the Vernier Caliper and spanner are used to change the length of the tuners. By tuning the nut screw, one turn equals one mm. If the tuner's length is needed to be in the cavity, the bottom nut screw would be turned. And the top nut screw has to be loosed to allow the sliver screw to move

down. The round back rubber at the end of the tuner can be taken off if the square brass reaches the end.

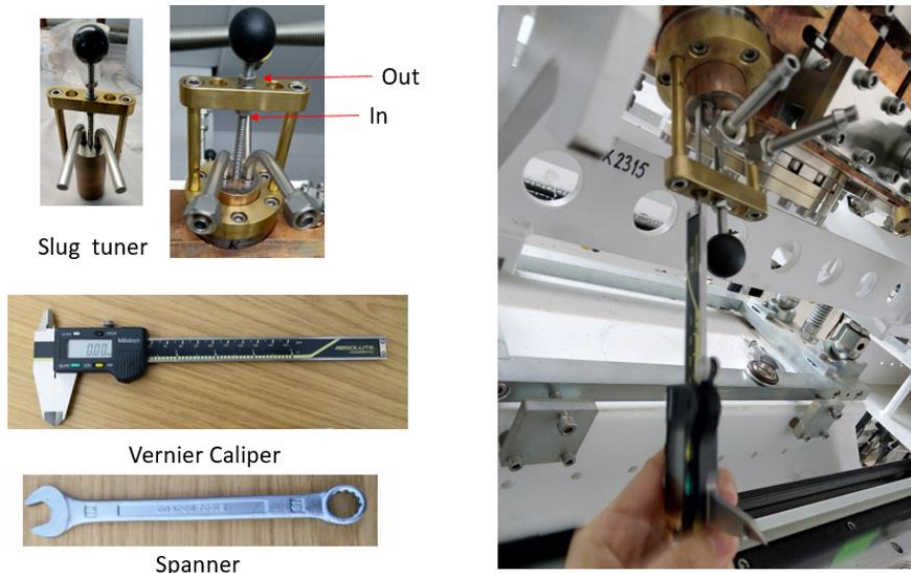


Figure 6.14: The instruments and way to adjust the slug tuner.

The way of measuring the automatic tuner's length is different from the manual tuners. The automatic tuner's length normally was changed by a motor. However, it could also be adjusted by hand by turning the end of the tuner as seen in a red arrow of Figure 6.15, left hand side. The Vernier Caliper is used to measure the gap, see Figure 6.15 (right).



Figure 6.15: The instruments and way to adjust the automatic tuner.

However, this can cause some errors in the measurement. It depends on the person who does this adjustment how they measure the length. This is because the end of the Vernier Caliper which touches the tuner is quite sharp and the surface of the tuner is not smooth.

6.2 Tuning Algorithm

In order to determine the new length of the tuner in the RFQ to flatten the fields, a FETS RFQ tuning algorithm from Chapter 5.3 is used. A Python script was used to do the analysis. The program uses the frequencies in each modes and the field shapes against the Z position. From the bead pull data, this is done as follows.

The resonant frequencies of the modes of the FETS RFQ are measured by the VNA. The results of the frequency modes are shown in Figure 6.16. This starts from dipole 1 (D11 and D12), dipole 2 (D21 and D22) which is rarely seen from S_{11} , dipole 3 (D31 and D32), quadrupole 1 (Q1) which is at the marker (Mkr), quadrupole 2 (Q2) and so on. The dipole consists of two frequencies as shown in the VNA, Dn1 and Dn2 where n is the number of the mode. These frequencies are used in the calculation, see Chapter 5.2. The way to judge which is Dn1 or Dn2 is the peak of the s-parameter. The higher peak of S_{21} means Dn1 because it is closer to the RF source, which is in quadrant one, than the Dn2. Q1 mode is at the green mark, and it provides only one frequency.

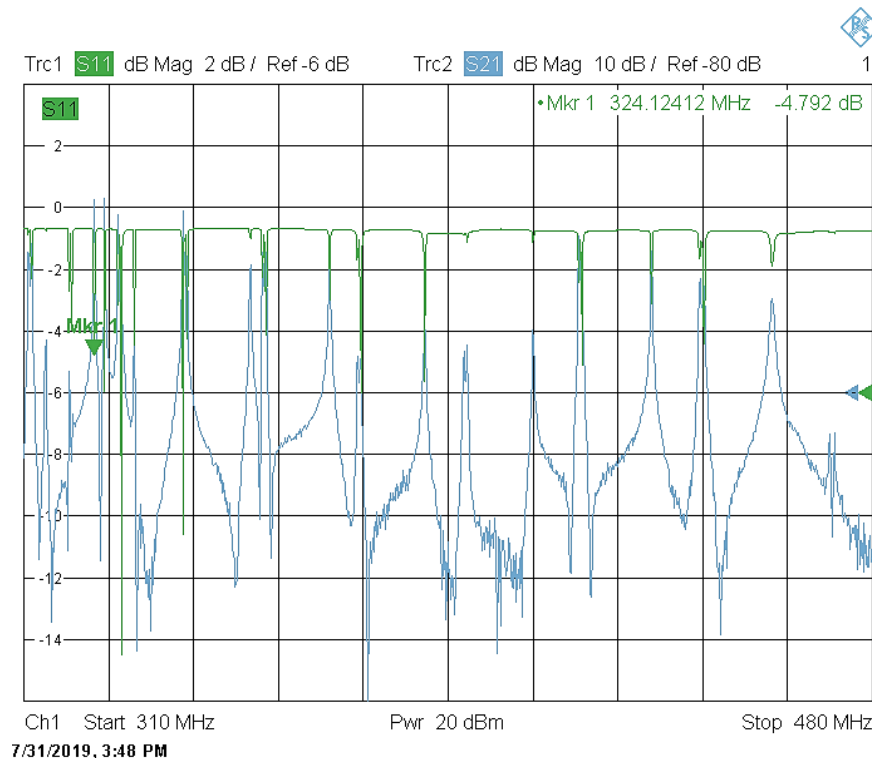


Figure 6.16: The first ten dipole and quadrupole modes from VNA.

Only the five first of quadrupole and dipole modes were collected from the VNA as they are the frequencies from the imperfect RFQ structure. This means the operating frequency is not 324 MHz leading the values of the frequencies in each five first modes are different from

the theory. The other modes were calculated by the theory of the waveguide based on the measurement data as in Table 5.1. This is because the higher modes provide less impact in the waveguide in that the predicted value is close to the measurement data, as shown in Table 6.2. The frequencies of the higher order modes are close to the predicted frequency from the calculation. Thus, the modes more than five are calculated, reducing the time taken. In the analysis, the longitudinal mode n consists of quadrupole (Q_n) and two dipoles (D_{n1} and D_{n2}). Thus, the number of modes should be at least three times more than number of the tuners for solving the effect tuners in each position. As seen in Figure 6.17 bottom left, the higher modes provide smaller magnitudes if compared with the very first modes.

Table 6.2: The frequencies of each mode between measurement and prediction.

n	Qn		Dn1		Dn2	
	Measured Freq.(Hz)	Predicted Freq.(Hz)	Measured Freq.(Hz)	Predicted Freq.(Hz)	Measured Freq.(Hz)	Predicted Freq.(Hz)
1	323.7237	-	311.0811	-	310.5706	-
2	325.5556	-	314.2342	-	313.3033	-
3	331.3814	-	318.8288	-	318.2282	-
4	341.1211	-	328.8589	-	328.4084	-
5	355.0551	-	342.5626	-	342.0020	-
6	370.9109	372.2337	357.5375	361.2926	358.3383	360.8531
7	389.9700	391.6794	376.5966	381.2966	377.1972	380.8803
8	411.5916	413.4833	397.8178	403.6617	398.4585	403.2684
9	435.5756	437.2928	421.0010	428.0179	421.7217	427.6470
10	460.1638	462.7984	445.2653	454.0449	446.2262	453.6953

The measured fields and modes are used in the algorithm, and an example of the results is shown in Figure 6.17. The top left is the results of the fields in each quadrant from the measurement, while the bottom left shows the 21 frequency modes. This is the minimum equations (21 times 3 modes) to calculate the 62 unknown parameters for the length of the tuners. The modes start from D_{11} , D_{12} , Q_2 , D_{21} , D_{22} , Q_3 and so on. Q_1 is not in the graph because the data are normalised by a quadrupole field mean. Thus, the Q_1 mode is always 1, so it can be ignored in the further calculation. For a flat field, all the modes shown in the graph should be zero.

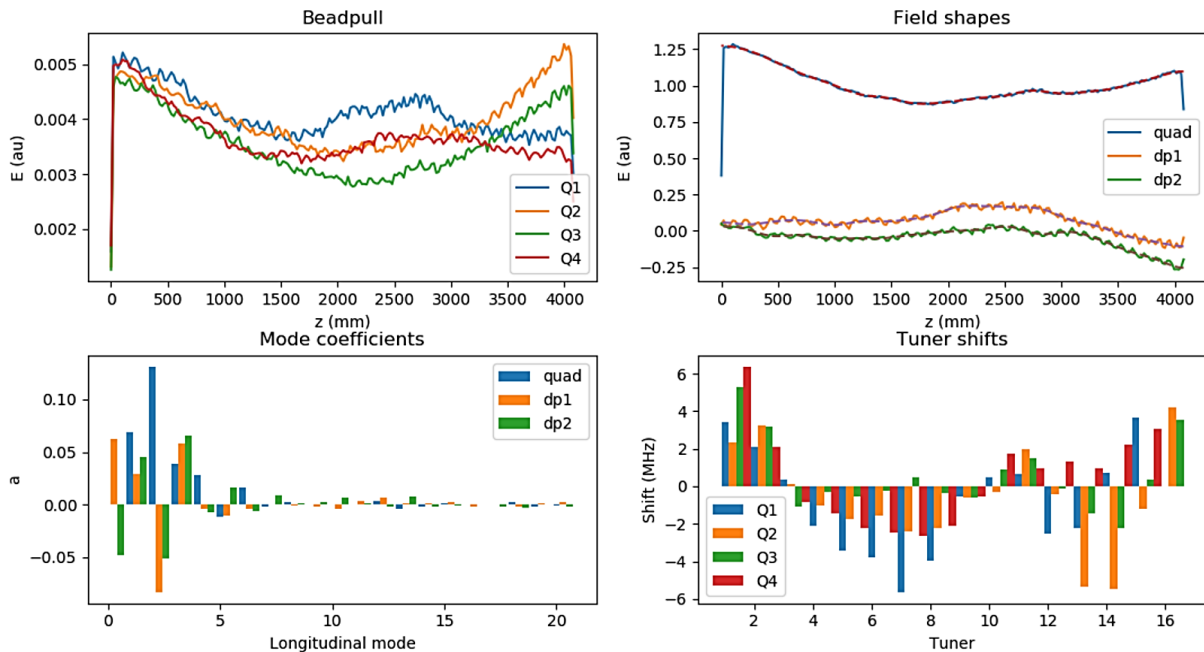


Figure 6.17: The results from algorithm code; Top left: the fields in each quadrant, Top right: the normalised quadrupole and dipole fields, Bottom left: Mode coefficients and Bottom right: the local frequency shift of each tuner.

The top right of Figure 6.17 is the calculated field from the measurement data. The blue line is normalisation of the fields by dividing the quadrupole field by its average. The orange and green are dipole fields which are normalised to the average of the quadrupole field. The quadrupole field is from the average of all four quadrants as in Equation 5.11. However, the dipole fields are from two quadrants. One is from quadrant one and three and another is from quadrant two and four, see Equations 5.12 and 5.13. The dotted lines are the reverse calculation from the frequency modes to confirm the fitted graph, as the fitting equation will be used for the tuning algorithm.

The calculation then uses a nonlinear least squares to fit the equation. This results in the new frequency shift of each tuner, see Figure 6.17 bottom right. An increase in frequency means a drop in the field.

The frequency shifts of each tuner in Figure 6.17 bottom right are the local frequency (f_{local}) changes. To convert these into a tuner movement, measured data are used. As these use the global frequency (f_{global}), the ratio of the diameter (L_T) of the tuner over the whole length of the FETS RFQ (L) is applied, as already seen in Equation (5.24) $f_{global} = \frac{f_{local} * L_T}{L}$. If the new length of the tuner is out of the allowable movement range, that tuner is ignored. The algorithm is rerun until all new tuner's lengths are adjustable.

The tuner algorithm provides a flat field, but the resonant frequency is not considered. After getting an acceptable flatness, in order to get the flat fields at the operation frequency, the new tuner's lengths need to be recalculated without the effect of the fields. To be simpler, all the tuners will be moved in the same direction and lengths to get the right frequency. If some of the tuners are out of limits, the length of other tuners will be calculated to compensate.

However, during the analysis, some issues have to be found. First of all, the sign of dipole modes on one pair of quadrants was incorrect. This is shown in Figure 6.18 as an example of the wrong sign of the quadrants. The minus signs were not used in quadrants two and four. This results in new frequency shifts, as seen in Figure 6.18 bottom right, which does not compensate the field shape.

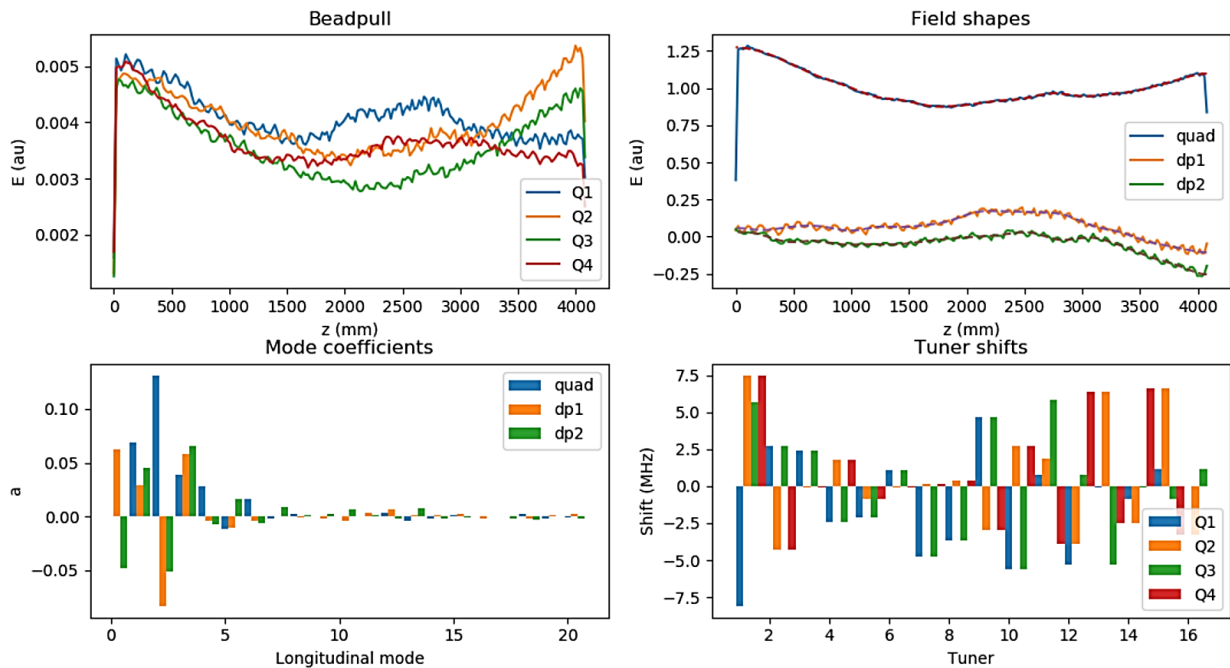


Figure 6.18: The results of incorrect dipole signs.

Secondly, the fitting of the field in terms of the frequency mode is also significant. As can be seen in Figure 6.19, some of both ends of the Z position are affected by the end of the RFQ and have to be taken out before fitting the graph because the graph should not drop at the end. The field shape should rather reach the highest amplitude at the end. The results of frequency shifts are sensible when taking out some Z points at both ends. Taking out different numbers of points gives different results. As a result, to determine the best fit, how many Z points to remove is decided on a case by case basis.

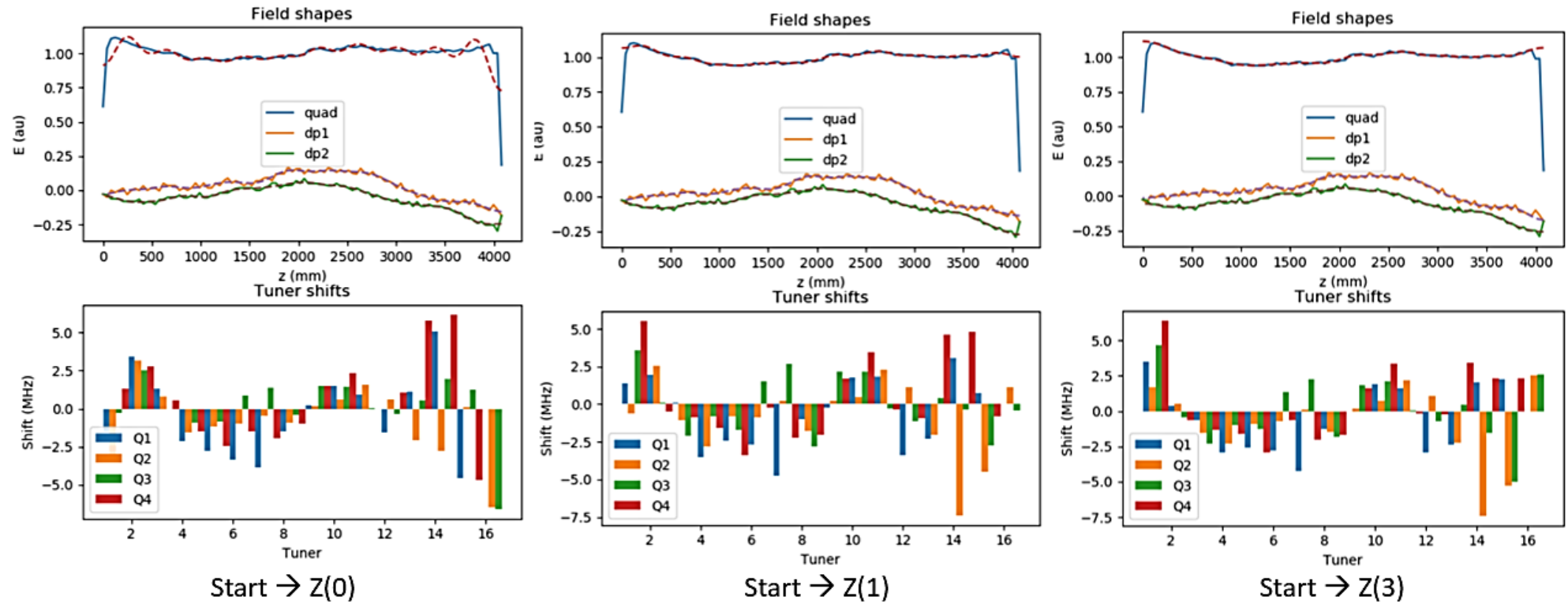


Figure 6.19: The field shape in different Z starting points.

A nonlinear least squares fit was used for the algorithm. A linear least squares optimisation was first considered as it was simpler, however, the result has not shown a good agreement with the frequency shifts, see Figure 6.20. The first tuner's length in each quadrant will compensate each other resulting in much larger and unrealistic frequency shifts to make any changes.

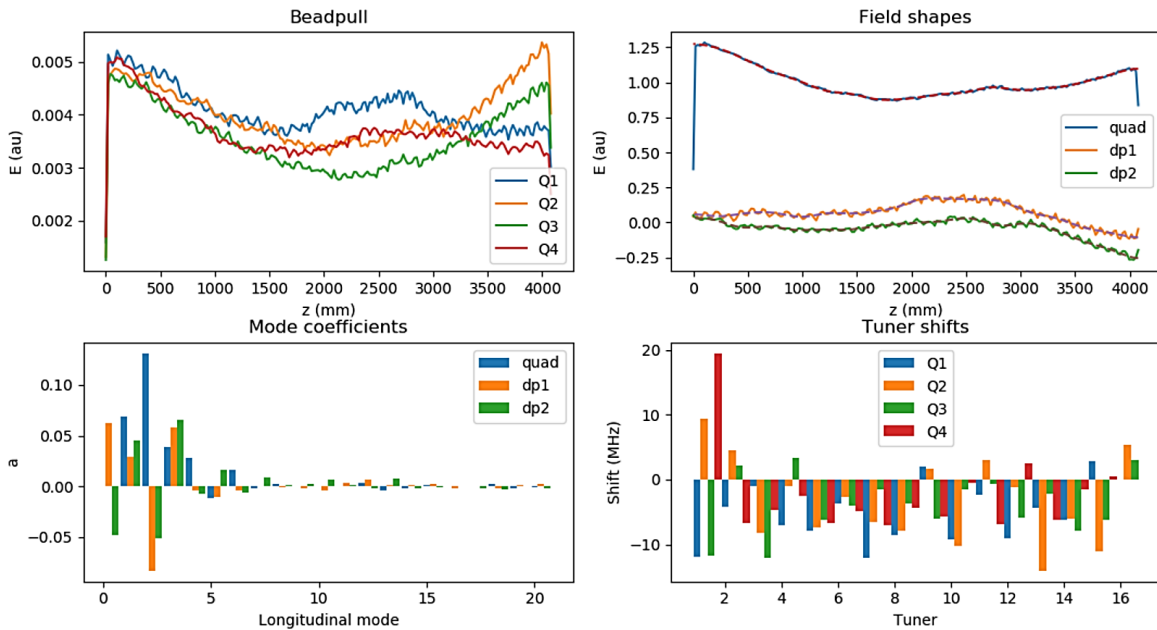


Figure 6.20: The results from algorithm code with a linear least squares optimisation.

6.3 Summary

The bead pull measurement has been created for one-metre to four-metre lengths in order to test the FETS RFQ bead pull. The goal is to obtain a flat field. There have been many changes in the bead pull measurement to improve the performance during these tests. For example, the layout of the pulley system needed to be modified to suit the FETS area. The LabVIEW window was also changed to produce the final measurement. The bead pull system was then accurately aligned with a laser survey.

The tuners, both slug and automatic, were measured by a Vernier Caliper from the outside of the FETS RFQ cavity. This is because it is impossible to measure from inside. The measured length then was converted to the real length for further calculation.

To get a flat field, the frequency modes and perturbation equation are applied. The first five modes were collected from the VNA while the others come from the calculation. The new frequency shifts were the local frequency, so they needed to be converted before use in

the real measurement. If the new frequency shift provided an out of limit value for the tuner's length, that tuner would be ignored, and the algorithm would be run again.

The results of the measurements will be discussed in the next chapter. This includes the final result from the bead pull measurement.

Chapter 7. One-Metre of Bead Pull Measurement

The bead pull measurements have been designed for producing the data required to determine the field flatness. Firstly, the pulley system was designed for one section of the FETS RFQ, which is about one-metre in length. The first measurements were only on section two, without the end plates closed to control the magnetic field. This is because it was the only module that was available at that time. After that, the pulley system was re-designed to cover the whole FETS RFQ.

The data were collected in tdms format from a LABVIEW program and analysed using Python scripts. Only S_{11} has been used because the coupler on the S_{21} port was faulty, resulting in noisy data.

7.1 Gaussian versus Lorentzian

The tdms file consists of the VNA frequency against S_{11} in each z position. The S_{11} was collected with different frequency steps and hence resolutions. The peak of the plot is the resonant frequency which needs to be determined for further analysis. Both Lorentzian and Gaussian functions have been fitted to the resonant plots to determine which gives the best fit. A Lorentzian equation is

$$|S_{11}(f)| = A_1 + A_2 f + \frac{|S_{max}| + A_3 f}{\sqrt{1 + 4\left(\frac{f - f_0}{\Delta f_{Lorent}}\right)^2}} \quad (7.1)$$

Where f_0 and Δf_{Lorent} are the resonant frequency and bandwidth, respectively. A_1 , A_2 , and A_3 are the constant background, slope on the background and skew [94]. A Gaussian equation is

$$|S_{11}(f)| = a * e^{-\left(\frac{(f-f_0)^2}{2*sigma^2}\right)} + b \quad (7.2)$$

Where f_0 is the resonant frequency and $sigma$ is the bandwidth. a and b are constant background and the background slope [95].

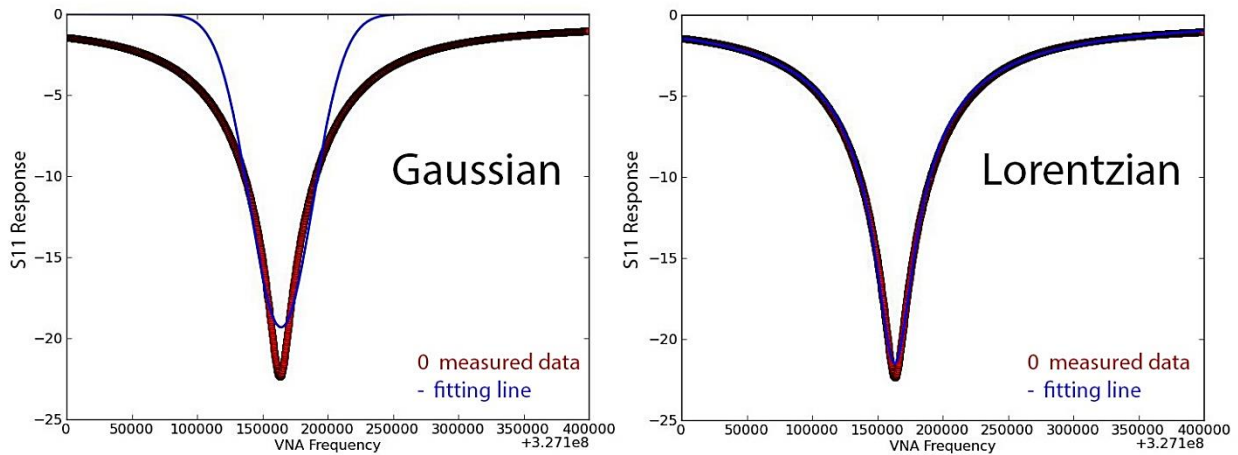


Figure 7.1: Results from fitting Gaussian (left) and Lorentzian (right).

In Figure 7.1, the red line presents the data taken from the measurement while the blue line is the fitting graph. The Lorentzian result provides a better fit when compared with the Gaussian one. Therefore, the Lorentzian function is chosen for the bead pull analysis. However, the peak values are similar. We need only the peak for application in further analysis.

7.1.1 Sweep Data

The analysis of the July 2015 data has shown that they are not smooth, as shown in Figure 7.2. One possible explanation of this was that the bead was still vibrating after it was moved to another position. As it was not plausible to delay the data-taking in LabVIEW to allow the bead to stabilise, instead multiple measurements at each position were implemented from August 2015, called a sweep function.

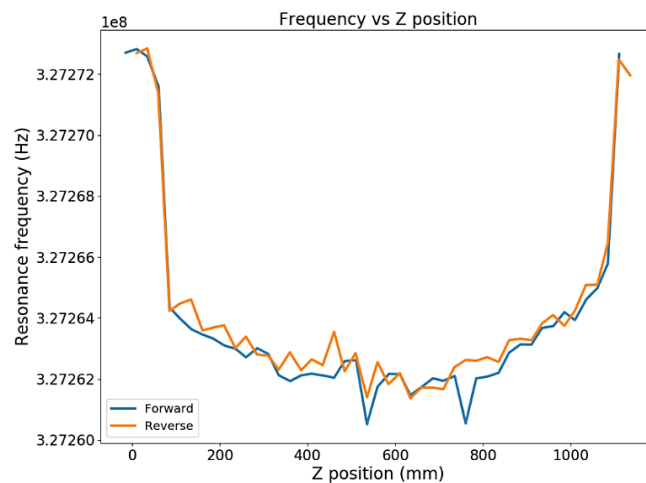


Figure 7.2: Results of resonant frequency against Z position of section two, quadrant three of the FETS RFQ in July 2015 with 200 Hz frequency resolution.

The LabVIEW programme was modified to use the sweep function. Though it is better to collect more data for calculating the average, the processing time was also important. As a result, five sweeps were used.

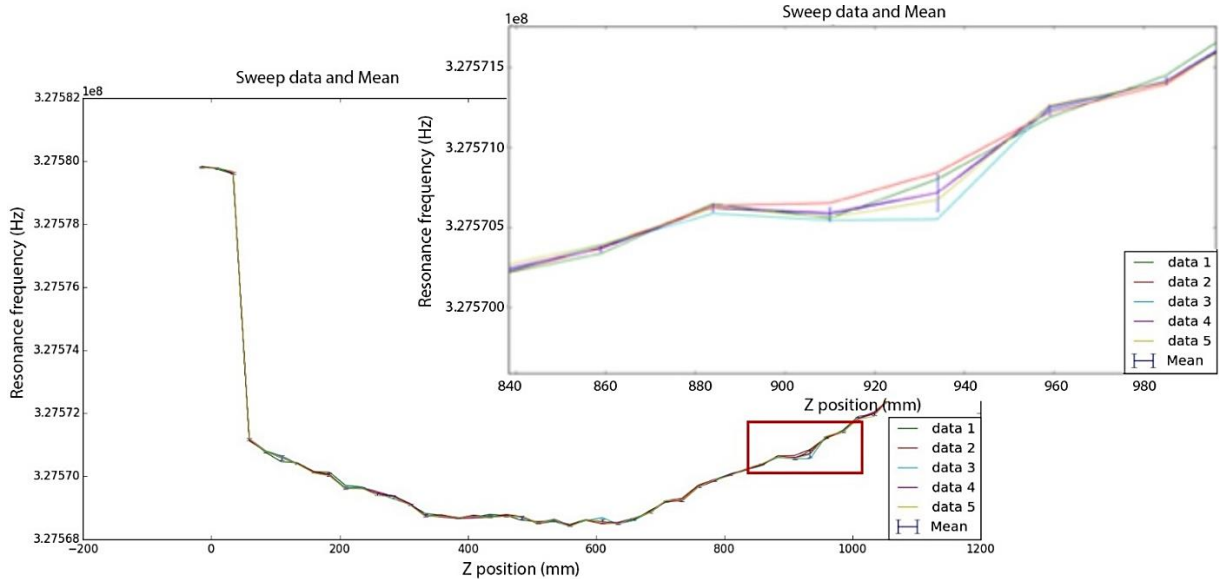


Figure 7.3: Sweep results of the reverse direction with 100 Hz frequency resolution in August 2015.

Figure 7.3 shows the data with five sweeps at each Z position in August 2015. Although they are sometimes not similar, the differences are much improved compared to Figure 7.2. The biggest frequency difference is at $z = 935$ mm with 291.44 Hz, while the lowest one is at $z = 385$ mm (33.99Hz). This indicates that bead stability is not the complete solution to the problem. As a result, more care was taken with the September measurements to avoid other sources that could have led to the discontinuities seen, with no movement around the RFQ being allowed, for example. In addition, the mean of the sweeps was used for the subsequent analysis.

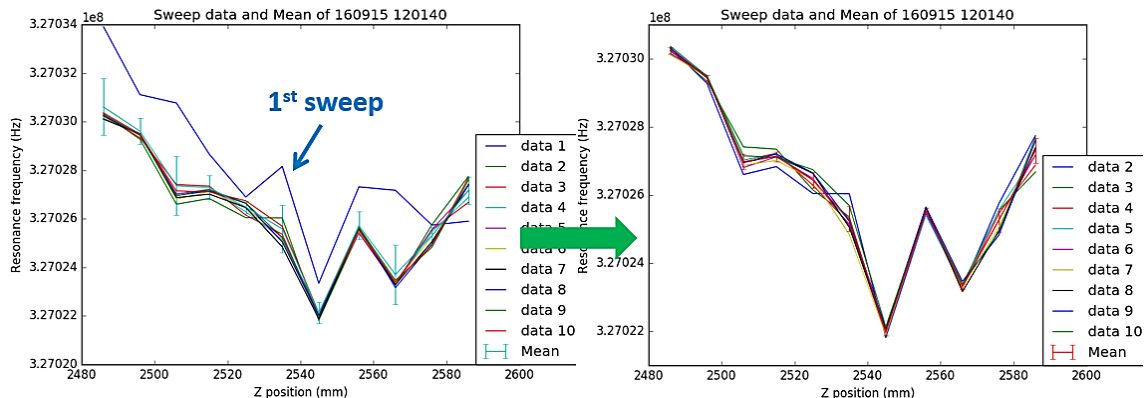


Figure 7.4: Sweep results of reverse direction with 500 Hz frequency resolution in September 2016.

In September 2015, the aim was to obtain as precise measurements as we could within a reasonable time scale to allow a better understanding of how the bead pull was functioning. The Z range was shortened while the steps in both Z and frequency scans were smaller than the previous measurements. In addition, the sweep number was increased from 5 to 10. If we focus on the sweep data itself, as seen in Figure 7.4, it clearly shows that the first sweep data significantly differs from the others. As the thread length needs to be extended to cover the complete FETS RFQ, this effect will get worse. This resulted in eliminating the first sweep data from further analysis. The control programme was corrected to allow more time for the stabilisation of the bead in further measurements.

7.2 Frequency resolution

The time of data-taking is significant for a measurement. For example, if it is run for a few hours, the temperature in the hall may change, and this will affect the results. This means the frequency resolution needs to be taken into account. The smaller the frequency resolution, the higher the period of time for one measurement. Thus, various frequency resolutions have been tested to determine the optimum.

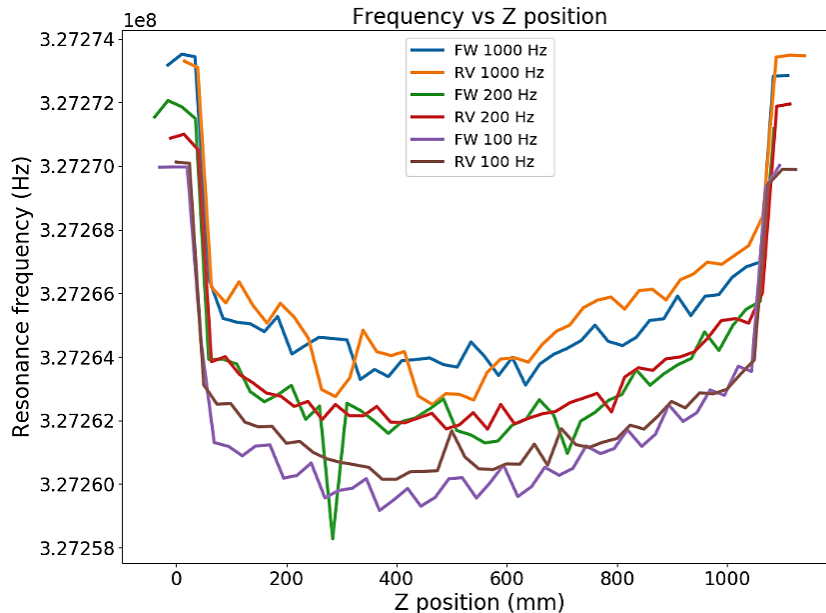


Figure 7.5: Results in different frequency resolutions of quadrant 1 in forward and reverse directions.

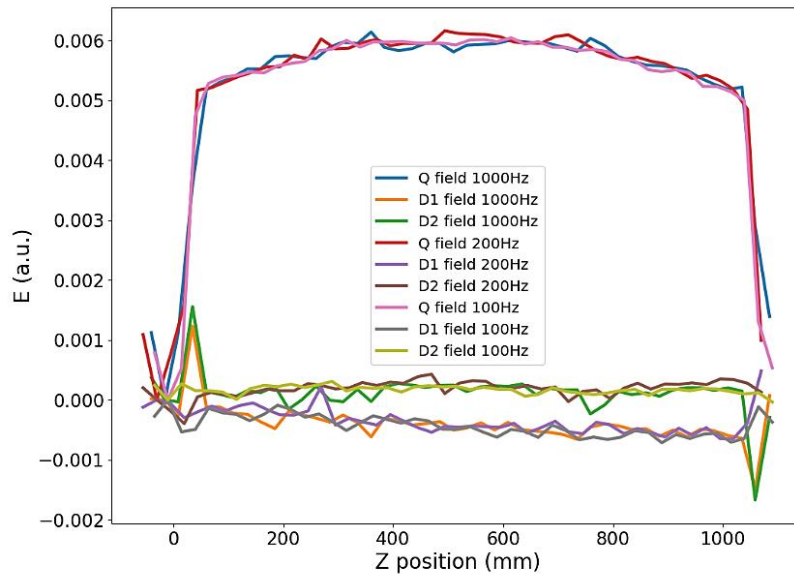


Figure 7.6: Fields against Z position in different frequency resolutions (1000, 200 and 100Hz) of the forward direction.

The results of changing the frequency resolution from 100, 200 to 1000 Hz are presented in Figure 7.5 in both forward and reverse directions. The fields, in the forward direction only, are shown in Figure 7.6. There are small improvements with better resolution, so as for the measurements with only one-metre length, the time duration is not such a problem, the frequency resolution was chosen depending on the required accuracy. For example, if we need to study the effect of the tuners, the smaller frequency resolution is better in that we will obtain more information. However, the small frequency resolution will affect the period of time of the measurement when running the full bead pull, see the next chapter.

7.3 Forward and Reverse Direction

In each longitudinal position, the measurement will take place in both the forward and backward directions. Ideally, the results should be the same.

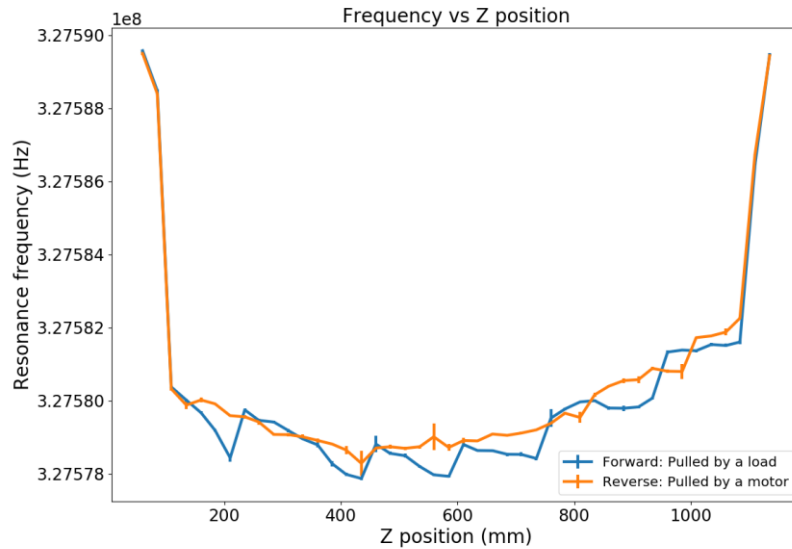


Figure 7.7: Result resonant frequency against Z position of quadrant 4 in September 2015 with 150 Hz frequency resolution.

In practice, the results from 2015 are not the same, see Figure 7.7. The reverse data provides more flatness in frequency than the forward one. In addition, forward data have some steps. These unsmooth lines occur in every result. This is thought to be due to slippage of the pulley systems. As a result, the bead pull was improved for future stages.

7.4 Tuner Effects

The tuners have been inserted to correct the uniformity of the fields along the RFQ. The idea behind this is decreasing the internal volume of the RFQ. The more the tuners are inserted into the RFQ, the higher frequency we obtain. The results from the sections above were either without tuners or with them flush to the internal surface level of the RFQ. This study then moved onto measuring the effects of each tuner in practice. Only the tuner 3 (T3) of quadrant 4 was adjusted by extending its length from the inner surface into the centre of the quadrant, see Figure 7.8.



Figure 7.8: The change of the tuner T3 of the quadrant 4 that affects the internal volume of the RFQ.

The third slug tuner would be turned for 5, 5, 5, and 4 turns, respectively for each measurement. That means the length of the tuner would be extended into the RFQ 5, 10, 15, and 19 mm. Subsequently, the volume of the RFQ is decreased.

The results from Figure 7.9 show an increase in frequency. These results further support the idea that the change in the tuner's length into the RFQ leads to the rise in the overall frequency due to the flatness of the lines in the graph, as shown in Figure 7.9 and Table 6.1.

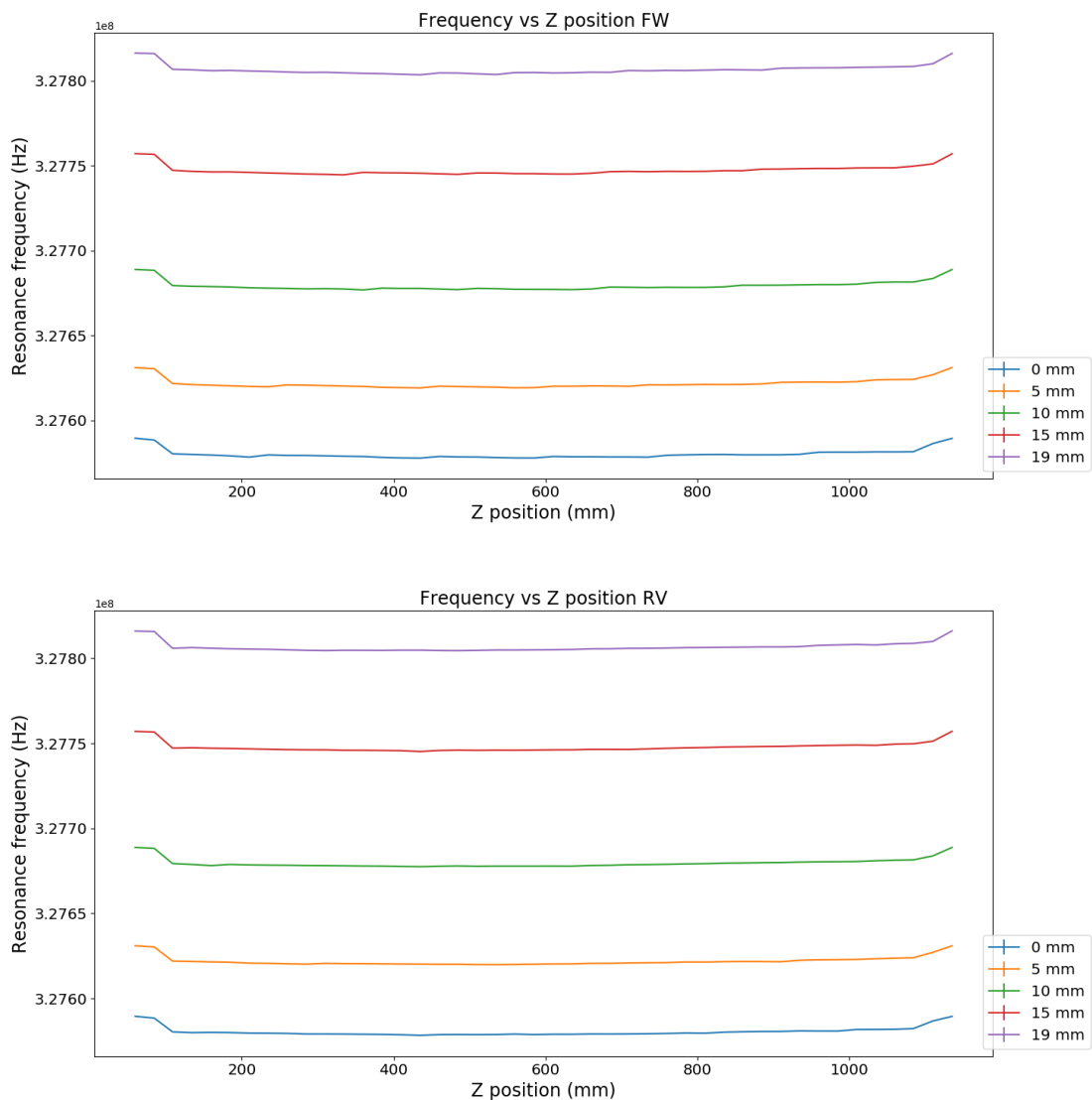


Figure 7.9: The results of adjusting the length of tuner 3 around 5, 10, 15 and 19 mm respectively from the internal surface of the RFQ in forward (top) and reverse (bottom) directions. Shown is the frequency as a function of longitudinal position.

Table 7.1: The inserted length of the tuner 3 with the average frequency.

Length of Tuner (mm)	Average Frequency (MHz)
0	327.58
5	327.62
10	327.68
15	327.75
19	327.81

The tuner 4 quadrant 3 (T4) was also adjusted but only 10 mm in length. Comparing with T3, the difference in frequencies are 99.11 and 86.99 kHz, respectively. Time limits meant that a more detailed comparison was not possible at that time.

7.5 Summary

In 2015, the one-metre tests of the bead pull measurements of FETS RFQ had been started, the Lorentzian distribution was chosen to fit the function of S_{11} versus the VNA frequency. Sweep data were used in further analysis to allow the bead to stabilise after movement. The first sweep was eliminated in the following year because of the unstable movement.

One of the 16 tuners of section 2 FETS RFQ was adjusted to see how the tuner's length relates to the frequency. The longer of the tuner's length is, the higher the frequency. However, we need more results from other tuners to do a more detailed analysis.

The one-metre bead pull apparatus was setup to help us become familiar with the test. It also allowed us to understand how the bead pull measurement should be applied and to prepare the data for the next experiments. However, the length of the pulley system needed an extension to measure all four sections of the FETS RFQ.

Chapter 8. Four-Metre of Bead Pull Measurement

The one-metre bead pull test was constructed to enable the system to be tested and to learn more about its use. After that, the system was moved to the FETS area with major changes to allow it to cover four modules. The changes of the pulley system are not only extending the length of the thread and Aluminium rods but also the system's layout because of the restriction on the space in the FETS area.

Measurements were made to understand how the bigger system works, sources of errors and to prepare for the final bead pull measurement. These measurements started with one section before moving to the full-section of the FETS RFQ. The results are discussed in this chapter.

8.1 One Section with Four-Metre of Bead Pull Measurement

Section two of the FETS RFQ was setup on the rails in the FETS area in 2016 before being return to complete the manufacture. In 2018, section one of the FETS RFQ, which was the first section that had been completely finished, was placed in the FETS area. There were no inserted tuners at that time.

8.1.1 Forward and Reverse Directions

The previous chapter, measurements in the forward and reverse directions were not the same, and it was unclear why that was. As a result, this test was repeated. In the previous chapter, the result when the bead was pulled by the motor seemed to be smoother. The weight of the load was increased for the four-metre measurement due to the much greater length of the thread.

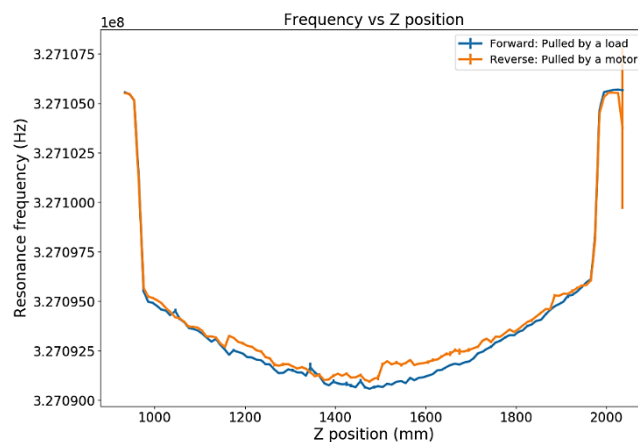


Figure 8.1: Result resonant frequency against Z position of the FETS RFQ section 2 quadrant 4 in July 2016 with 500 Hz frequency resolution.

In 2016, the graph in Figure 8.1 presents a similar trend in both directions. Due to the change in the mechanism, the bead pull system was slightly improved. The reverse data seems to provide more steps than the forward result but is smoother than the data of 2015 (the bead was pulled by the motor). It can be seen that the results have been improved but are still not perfect. This might be because of the environment around the experimental place such as the changes in temperature or weight of the load.

8.1.2 Angle versus frequency shift

Other studies were made using only a 100 mm range of the middle of the FETS RFQ to understand the fields better. Section 2 was used to study the frequency shift as a function of angle and radius. In addition, this is to allow higher resolution measurements that take a much longer time.

In order to calculate the X-Y offset between the RFQ centre and bead pull axes, we should know the effect of angle and radius of different positions. To begin with, the radius would be fixed to find the relationship between angle and frequency. $R = 11.31$ and $R = 14.14$ mm were chosen. At the former radius, the angle was varied from $34^\circ - 56^\circ$ in 1° steps, whereas for the latter, it was changed in 2° steps from $28^\circ - 62^\circ$, see Figure 8.2.

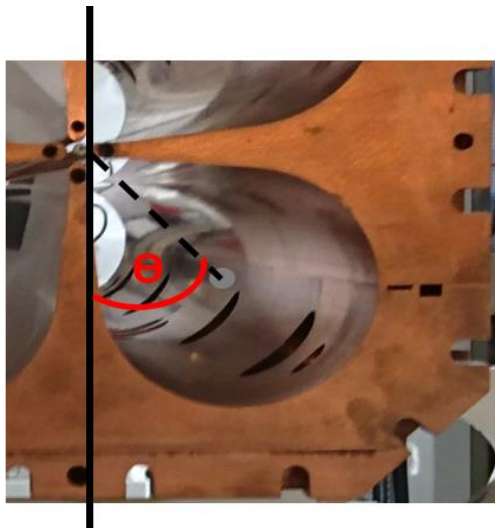


Figure 8.2: Angle measurement from a vertical line.

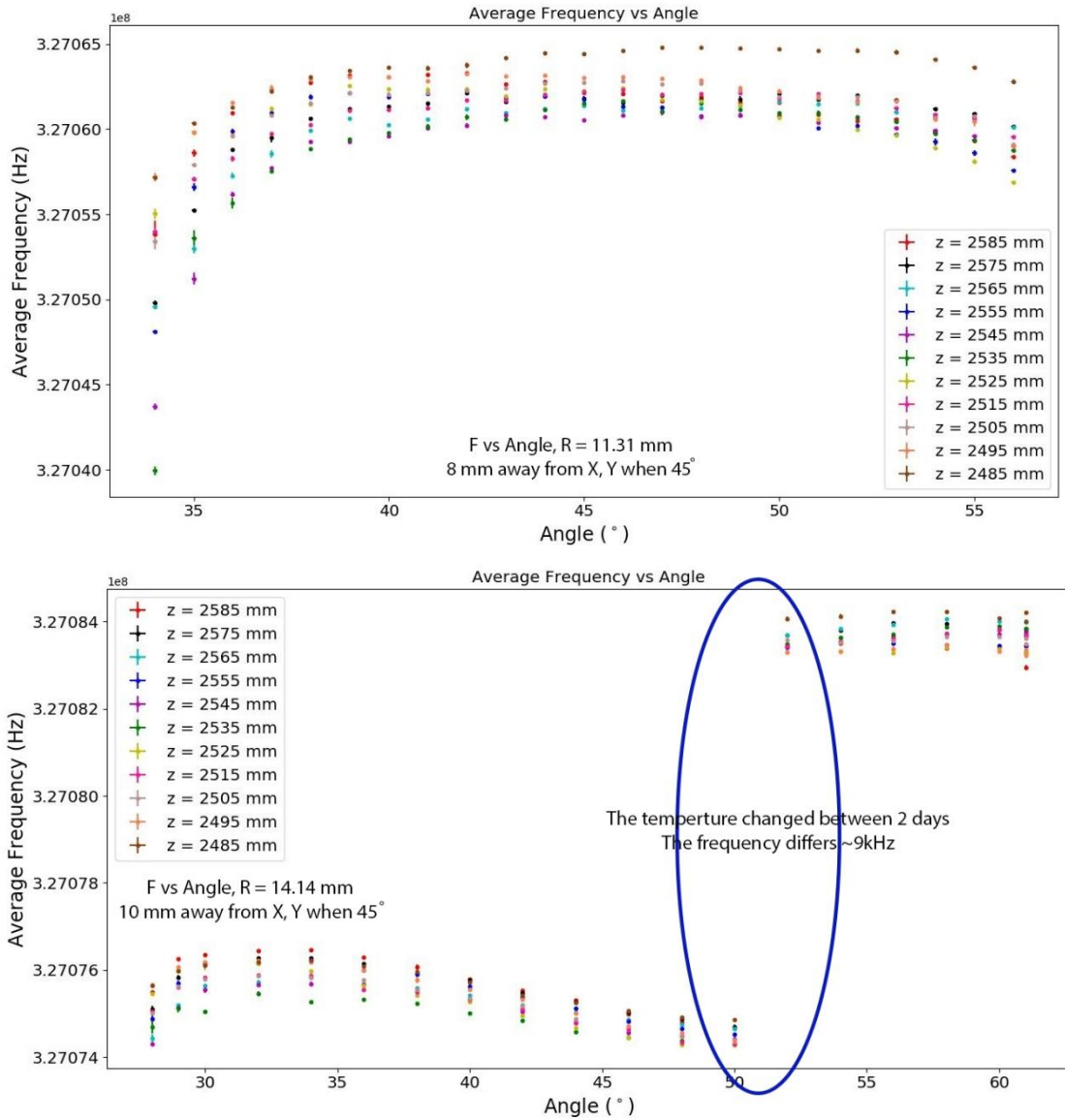


Figure 8.3: Angle against frequency in different Z position when the bead is 8 (top) and 10 (bottom) mm away from X and Y axes.

Surprisingly, the graph of $R = 14.14$ mm has a discontinuity. This is because the data were taken on different days, and the temperature in the hall was different, affecting the frequency measured. In addition, the graph in Figure 8.3 does not entirely show a similar trend. A major source of uncertainty is the bead position because of the manual adjustment of the bead pull axis. The bead might not be in the same radius when the angle was varied.

Moreover, the hole in the bead is bigger than the thickness of the string. This means the bead hung on the string. Thus, as we sweep the bead through the angle, the actual position of the bead comparing to what it should be is changed as the function of the angle.

The analysis, therefore, does not enable us to determine the relationship between the angle and frequency.

8.1.3 Temperature effect

As seen in Figure 8.3, the results change on different days even though measuring the same condition. This thought to be because of the temperature effect. In order to gain the results of the temperature effect, repeated measurement at $10\sqrt{2}$ or 14.14 mm radius (10 mm away from X and Y axes) from the RFQ centre were measured at different temperatures.

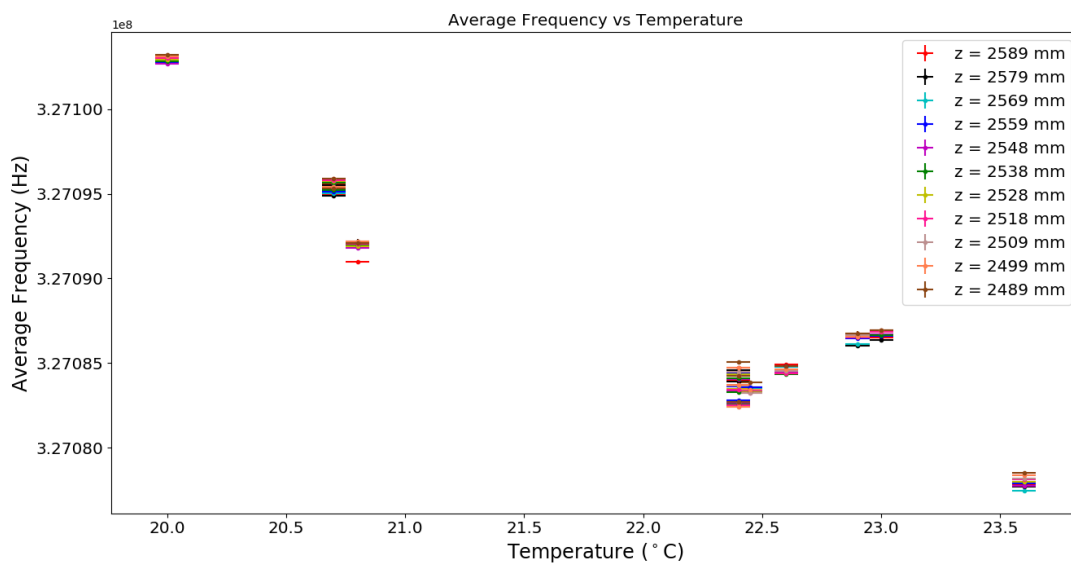


Figure 8.4: Frequency against temperature in different Z position when the bead is 10 mm away from X and Y axes.

The data in Figure 8.4 are noisy, as the thermometer used at that time had an inadequate accuracy, ± 0.5 °C, and could not be well connected to the RFQ. Nevertheless, the graph seems to indicate a linear relationship with temperature. A new thermocouple, with an acceptable error, was used in the later measurements.

8.1.4 Radius versus frequency shift

Finally, the radius between the bead and the RFQ centre was considered. With a 1 mm step, the data were measured from 7 to 20 mm away from X and Y axes in each Z position. Figure 8.5 shows the average frequency along Z at different radii. The frequency varies more with Z when the bead is close to the centre of the RFQ. This is due to the vane modulation. As a result of the strong dependence on radius at a small radius, subsequent measurements

were made at a larger radius, when possible, even though the fields nearer the vane are stronger.

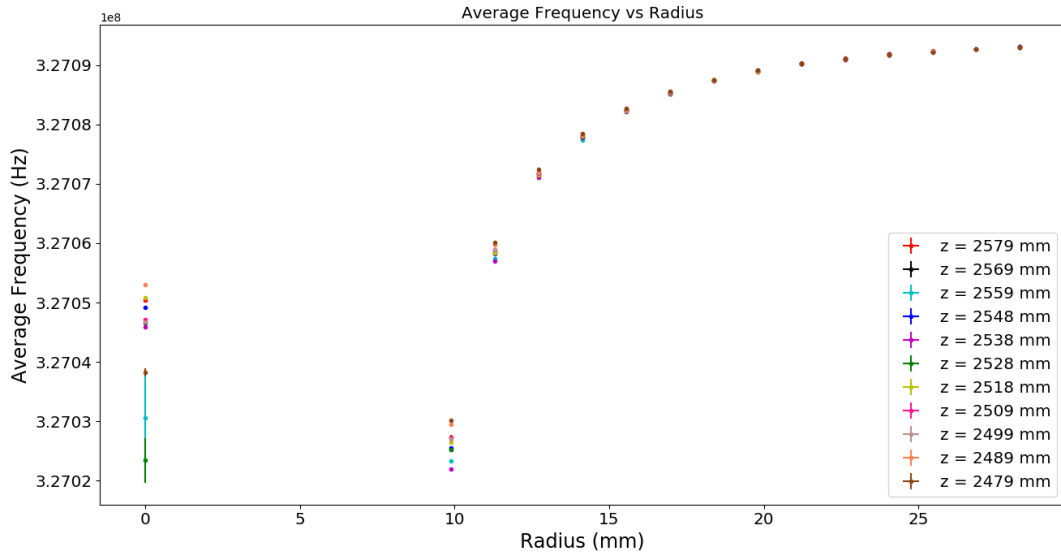


Figure 8.5: Radius (mm) against frequency (Hz) in different Z position in mm when the bead is at 45°.

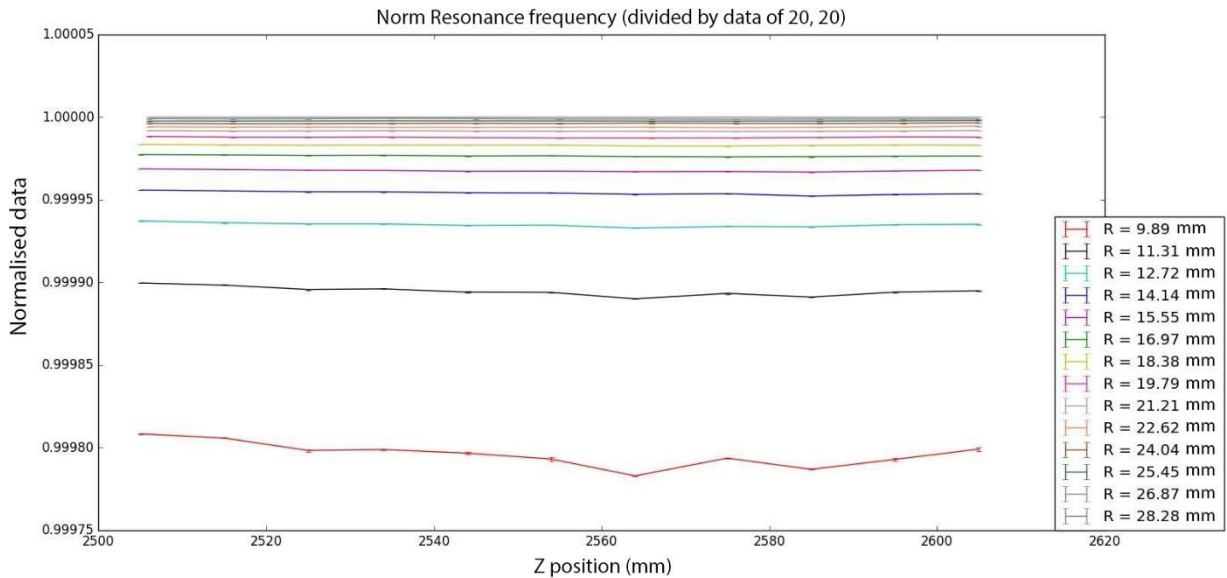


Figure 8.6: Normalised data in September 2016 along the Z position (in mm) in different radius (R in mm).

Dividing by the data of the furthest radius (20 mm away from X and Y axes), see Figure 8.6, the characteristic of the frequencies along the FETS RFQ are represented by the normalised data. We can compare it with the data in July 2016 because the various radius

was also measured in that Z range. However, there were only three radius (R = 14.14, 21.21 and 28.28 mm) that were taken from the measurements in July 2016.

After normalising the data, no significant differences were found between the results from July and September 2016, as shown from the orange arrows in Figure 8.7. This demonstrates that the surrounding environment does not influence the results after effects such as temperature are normalised out.

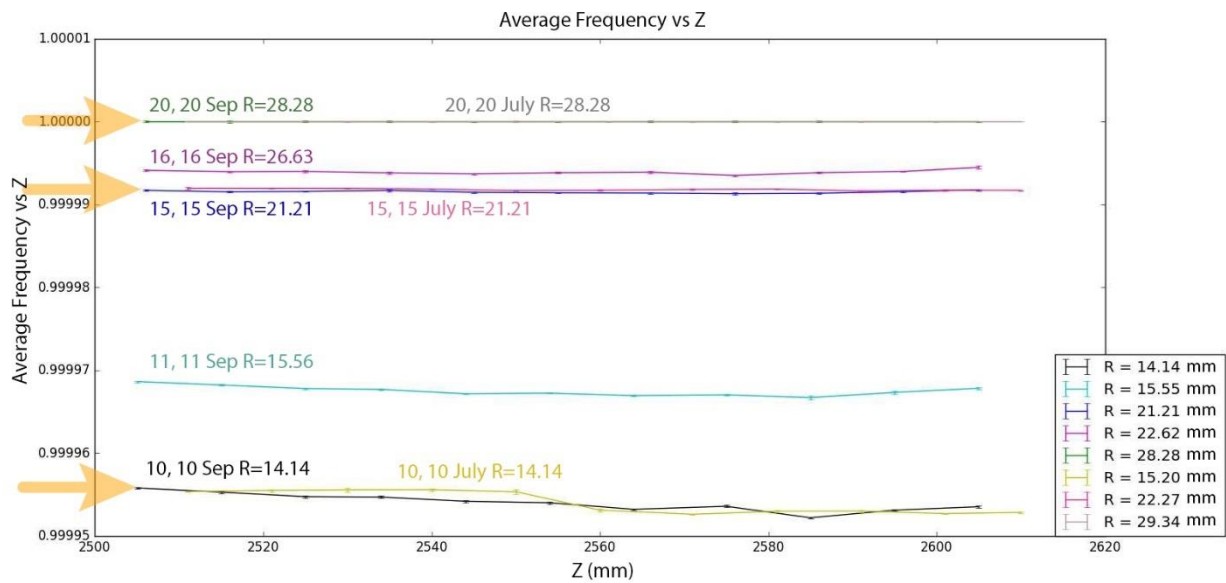


Figure 8.7: Normalised data in July and September 2016, R = 14.14, 21.21 and 28.28 mm as shown from the orange arrows.

8.1.5 FETS RFQ Section one and two

Section one and two of the FETS RFQ were individually tested in four-metre length bead pull apparatus in different years. The radius of X and Y was (10,10) in section one while the section two was measured at (8,8). The results of the fields are shown in Figure 8.9 and Figure 8.8.

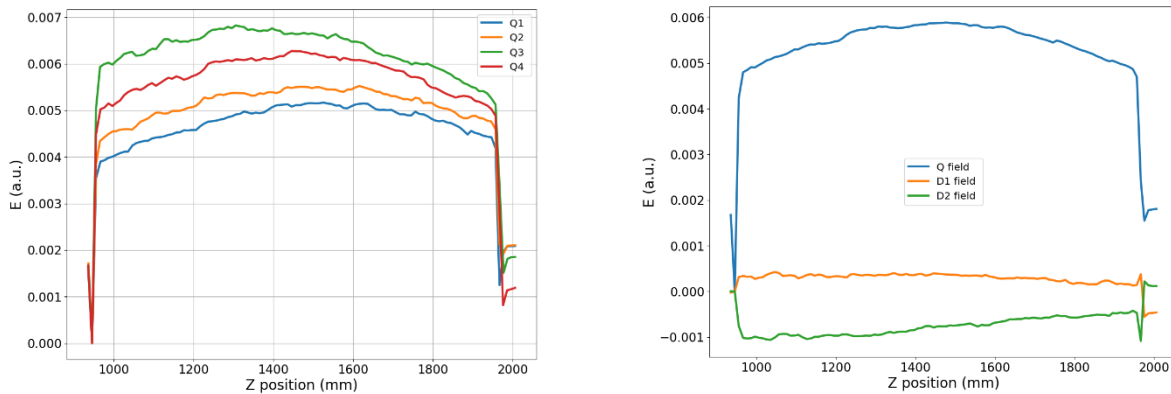


Figure 8.8: The fields of section two in 2016 at $r = (8,8)$ in the forward direction.

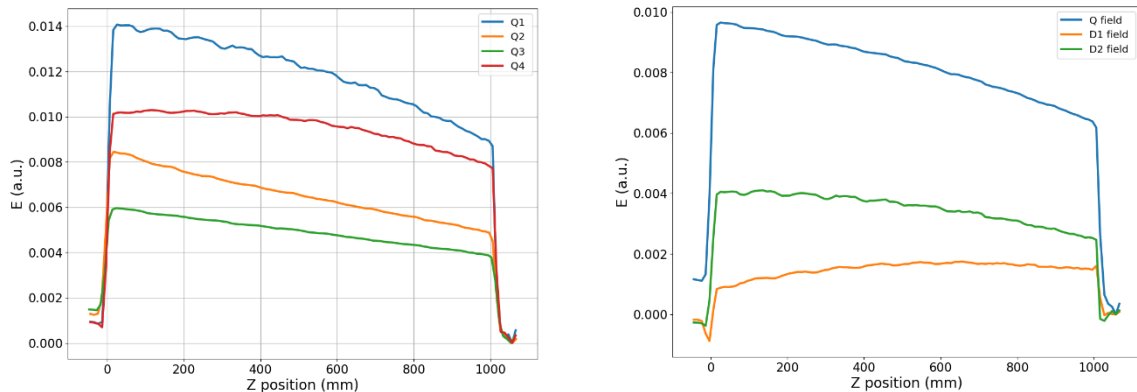


Figure 8.9: The fields of section one in 2018 at $r = (10,10)$ in the forward direction.

The fields in each section are not the same at this stage. However, the pulley position was setup by eye, so the bead may have not been correctly centred and may also have been at an angle, and the position may have been different between the two sections. This demonstrates the importance of correctly setting the pulley axis. As a result, it was done using a laser survey system for future measurement.

8.2 Four Sections with Four-Metre of Bead Pull Measurement

All sections of the FETS RFQ were completed and installed in 2019, enabling the measurement and tuning in order to obtain flat fields. The results of tuner studies, the sag correction and final results are discussed in this section.

The LABVIEW script had been changed by Alan Letchford in April 2019, while the old code was used until March 2019. The major difference is the way of collecting data which changed from tdms into excel format. Moreover, the automatic change in X and Y axes to

measure four quadrants continuously was introduced. The peak of s-parameter was taken directly from the VNA without using any fits, as explained in a previous chapter.

8.2.1 Forward and Reverse Directions

The forward and reverse measurements were run in March 2019 to decide which direction should be selected for further tests for time reduction. The weight of the load was increased so that it would pull the bead continuously without any discontinuous steps and to reduce the sag over four metres.

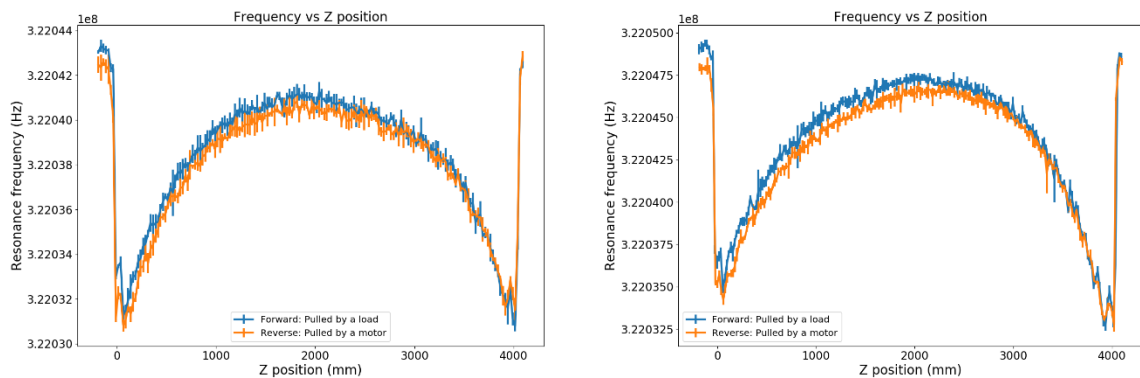


Figure 8.10: The frequencies of quadrant two (left) and three (right), section two of FETS RFQ in forward and reverse directions in March 2019.

As seen in Figure 8.10, the frequencies of quadrants two and three are measured along Z position. The forward and reverse directions provide a similar trend. The differences of the average frequencies between the forward and reverse directions are 403.78 and 631.69 Hz, respectively.

Thus, the only forward direction was chosen for the next experiments. This is due to the fact that it is more convenient for further analysis such as preventing confusion in the Z position when determining the tuner position. Moreover, it is the same direction as the beam propagation.

8.2.2 Measurement Errors

A number of sources of measurement error were identified and studied to determine their effect on the tuning process. These errors and their magnitude are as follows.

8.2.2.1 Error from VNA

From the VNA, the relationship between the S-parameter and frequency is measured. The peak frequency or the frequency where the value of S_{11} reaches the smallest point is compared with the data that is fitted by Lorentzian as seen in Equation (7.1). By using the data from 2016, the average errors of five sweep in along Z position is not more than ± 10 Hz

(± 7.0 - 9.5 Hz) which is very small if comparing with the frequency itself. In addition, they are also smaller than the frequency resolution. Therefore, the peak of the S_{11} from the VNA is selected for the further analysis as this error can be ignored.

The peak frequency is directly collected without fitting the distribution. This means the resolution on the frequency depends on the VNA parameters used, in particular the step size. The larger the size of frequency step is, the worse the resolution will be. As the time taken for each measurement is important, it is necessary to select the best start and stop frequencies and the number of frequency steps. The resolution required depends on what measurement is being made, but is particularly important for the tuning.

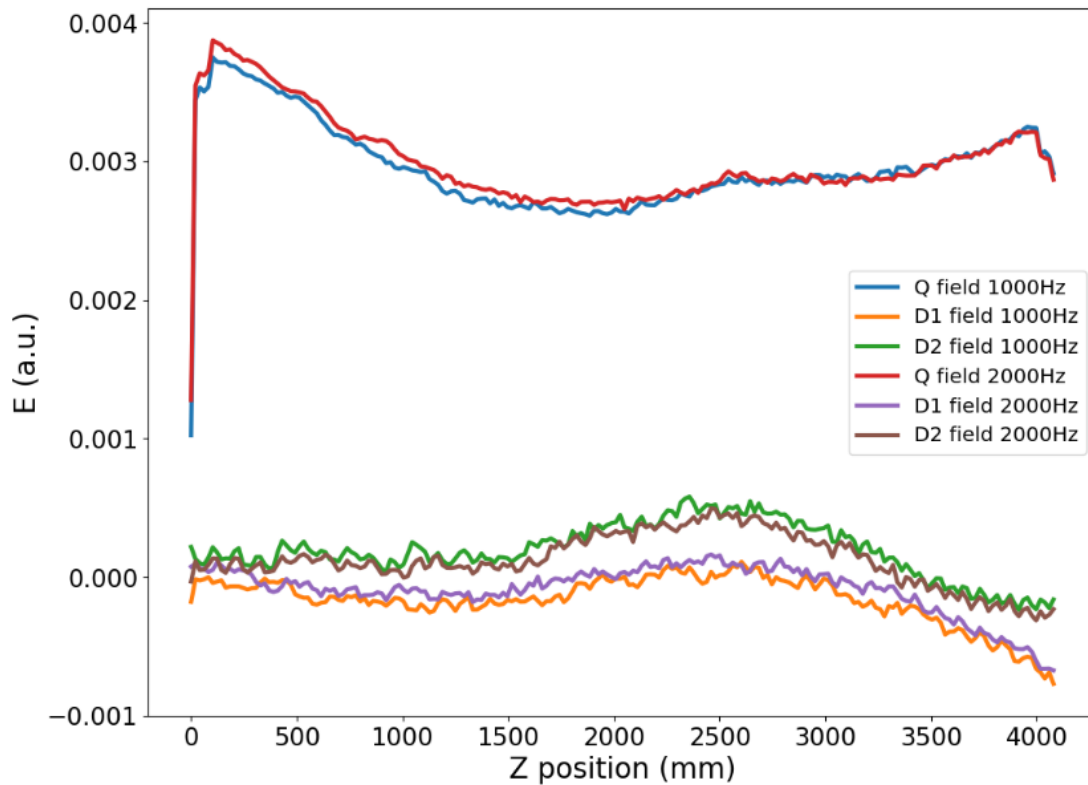


Figure 8.11: Results in number of frequency steps of four sections of the FETS RFQ in 2019.

The selection of the frequency step size affects the time duration. Reducing the step size by a factor of two doubles the acquisition time. To optimise the step size, Figure 8.11 shows the measured field for two step sizes, 1000 and 2000 Hz. Although the trends are the same, the smaller size tends to produce smoother curves. As a result, the suitable step size

was chosen depending on what experiment was being done, but the 1000Hz-step size was used for tuning, as a good compromise between speed and frequency resolution.

8.2.2.2 Bead and string oscillation

The bead and thread are being moved along during the measurement. Thus, when collecting the data or measuring the S-parameter, we must ensure that they are in a steady state otherwise the data would be incorrect. In the previous measurements, the first sweep data was eliminated to allow the bead to stop oscillating before the frequency was taken.

However, in 2019 the weight of the pulley load was increased providing more tension in the thread. In addition, the delay was increased at the beginning of the sweep data and reduced in between. Thus the time duration decreases overall. Figure 8.12 and Table 8.1 show the details of frequency in each sweep for an example measurement. This shows no different systematic error between the sweeps. However, the five sweeps are still measured.

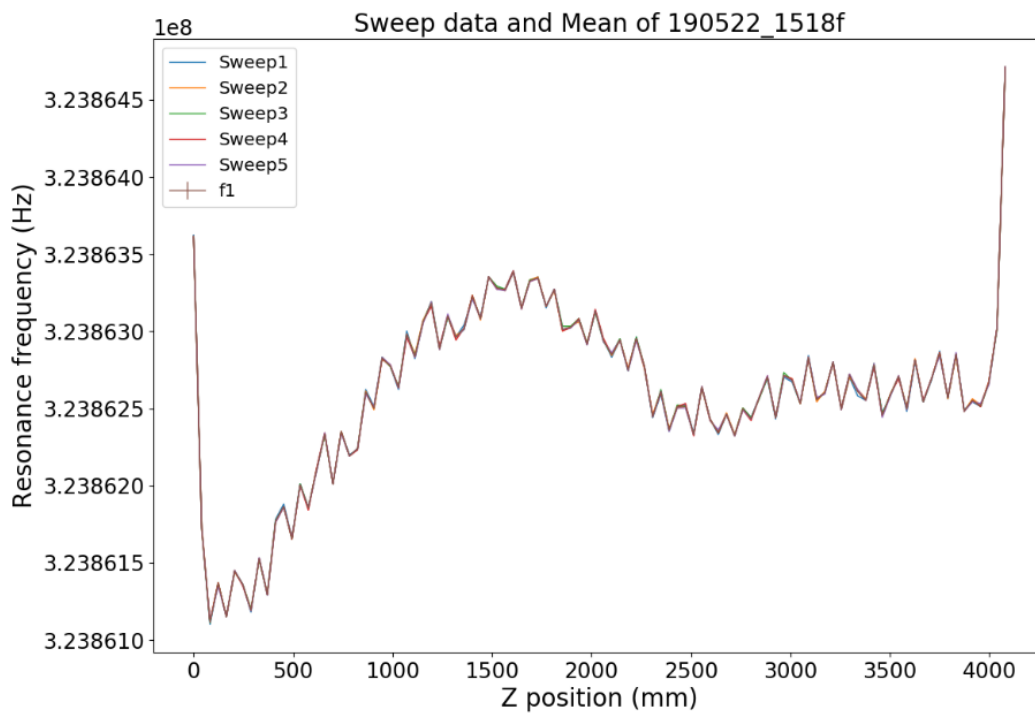


Figure 8.12: The sweep data of quadrant one with the new bead pull code.

Table 8.1: The frequency of each sweep data from the bead pull measurement.

Sweep	Frequency (Hz)
1st	323862597.63
2nd	323862599.13
3rd	323862599.75
4th	323862598.14
5th	323862597.42
Average	323862598.41

8.2.2.3 Wheel of the pulley system

After moving to the FETS area, the pulley system position sometimes did not correlate with the positions provided by the motors. This is because the wheels might not be freely moved when they were forced to rotate with the moving thread. Thus, all the wheels were changed to more flexible ones.

As seen in the data such as Figure 8.12, the graph has a ripple. This ripple seems to be in a periodic pattern which means it could be affected by the pattern of the RFQ structure or the pulley system. However, the ripple's wavelength is about 118 mm which is close to the circumference of the wheel (107 mm) of the pulley system.

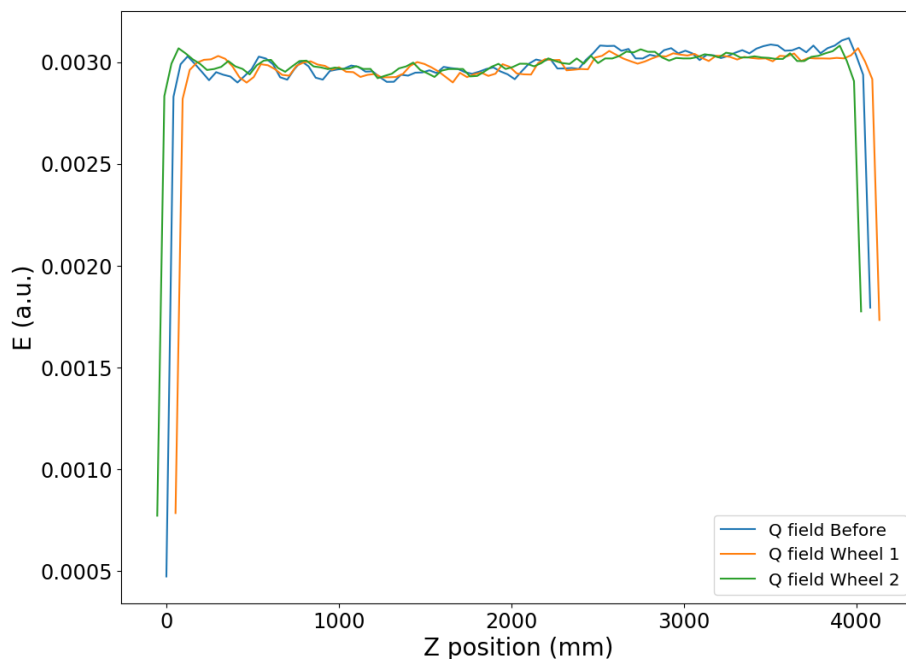


Figure 8.13: The results when rotating wheel 1 and 2 and shift the Z by 180 degrees.

Moreover, when two of the wheels were rotated by about 180 degrees and the measurements repeated, the ripples seem to shift by about 180 degrees with wheel 1. It is thought that a small flat spot on this wheel is creating the ripple. However, due to the size and systematic nature of the ripple, it is felt that this has a negligible effect on the field flattening compared to the other effects.

8.2.2.4 Motors

There are two types of motors used in the measurement, servo [89] and stepper motors [92]. The servo motors control the X and Y directions while the stepper motor is used for Z axis. These motors might affect the errors when changing the X, Y and Z position. However, the motors chosen are of high quality with good resolutions with small step size, see Table 8.2. Therefore, this source of error is negligible.

Table 8.2: The errors in step size of each motor.

Motor Type	Resolution	Step Size (μm)
Servo Motor (ATP-DC Servo Motor TDC001)	48 counts/revolution	± 4.0
Stepper Motor (Zaber X-BLQ1495-E01)	1/64 of a step	± 4.2

8.2.2.5 Human errors

The last errors to be considered in the measurement are the human errors. The human errors are significant because these errors are in the tuner adjustment part. We have to adjust and measure the tuners' lengths by hand. Therefore, the errors will be from the repeatability and the difference between the real and adjusted values.

8.2.2.6 Repeatability error

Each time of measuring the tuner's length, the results are not the same, since the end of Vernier Caliper is not flat and big enough to create a small angle. Moreover, the surface of the tuners is not definitely flat. When the measurement was taken by different people and even the same person, errors occur. Figure 8.14 and Table 8.3 show the different errors between one and two people by measuring five times in each tuner position.

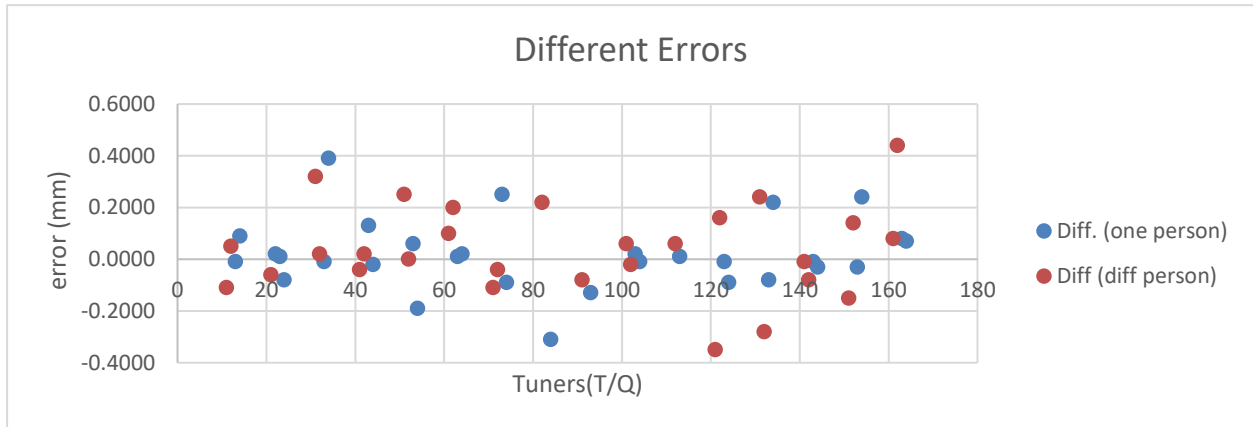


Figure 8.14: Different errors from one and different person in each tuner positions.

Table 8.3: Errors between one and different person.

Errors	RMS
One person	0.1345 mm
Different person	0.1736 mm

As seen from the graph above, the error from one person (± 0.1345) is smaller than the error from different people (± 0.1736), as expected. The experiments were all done by the same two people, so these errors have been used. This is the largest source of error found.

8.2.2.7 Real vs expected tuners' length

It is hard to adjust the length of the tuner in order to obtain the exact value from the algorithm. The error depends on many factors as discussed above. In addition, the length of the tuners relates to the turn from the screwdriver. One turn refers to one millimetre when done by hand. They are taken into account by the iterative procedure used for the tuning.

8.2.3 Sag Correction

For the bead pull measurement, the FETS RFQ was placed in the pulley layout. Even though the length of the pulley system is very long, about 4.2 metres, it is difficult to see the sag which supposes to be a curve rather than a straight line. The sag basically affects in the Y direction. The load at the end of the pulley system can compensate the sag if its weight is heavy enough. Since the sag cannot be seen directly, the frequencies against Y position from an upper quadrant to a lower quadrant are measured. If there is no sag effect, the average frequency between two quadrants should be symmetrical along the horizontal axis.

However, Figure 8.15 and Figure 8.16 shows the average average frequencies of quadrant one (the top right of the FETS RFQ) and two (the bottom right of the FETS RFQ) are

not symmetrical with both the load of 610 and 2330 g respectively. The average frequency decreases from the farthest Y and dramatically drops when the bead is close to the centre of the RFQ. In other word, when the bead is close to vane, the modulation of the vane affects the frequency leading to a large error in the average frequency. The drop of the frequency represents that the bead is close to the horizontal axis. In Figure 8.15 the frequency drops when the bead is between 7 and 7.5 mm in Y position (the top quadrant). While the large change in average frequency is located around -5 and -4.5 mm in the bottom quadrant. Therefore, there is the sag effect in the load of 610 g.

The sag improves when adding more weights, as shown in Figure 8.16. The position of the frequency drop in the upper quadrant decreases from 7 to 6 mm while it increases in the lower quadrant from -4 to -5 mm. However, the result from the load of 2330 g does not provide a symmetrical graph. Thus, there is still a sag effect that needs to be corrected.

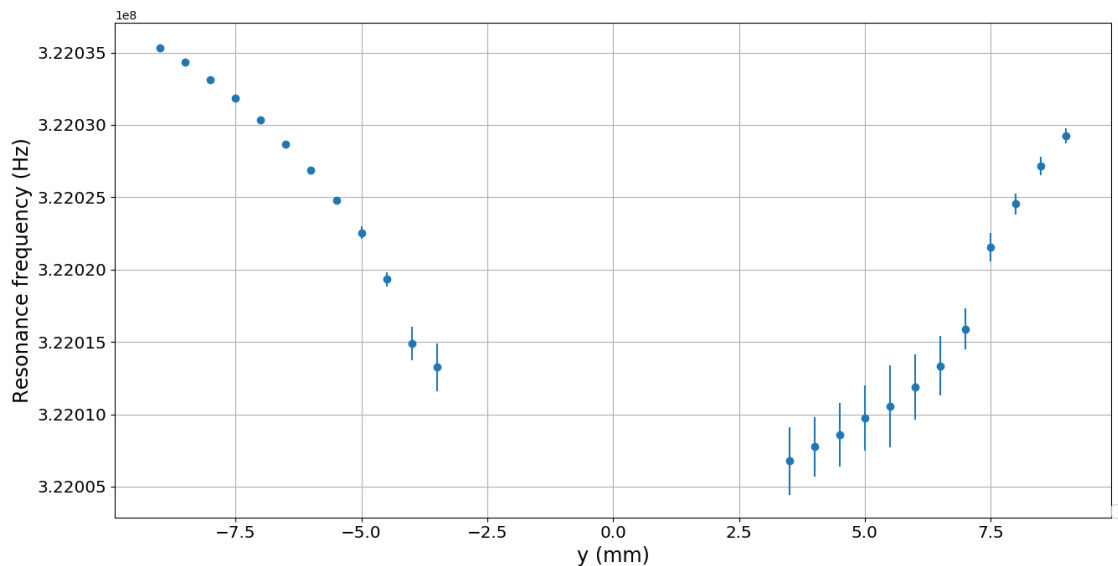


Figure 8.15: The average frequency in different Y position from 9 to -9 mm for the load of 610 g.

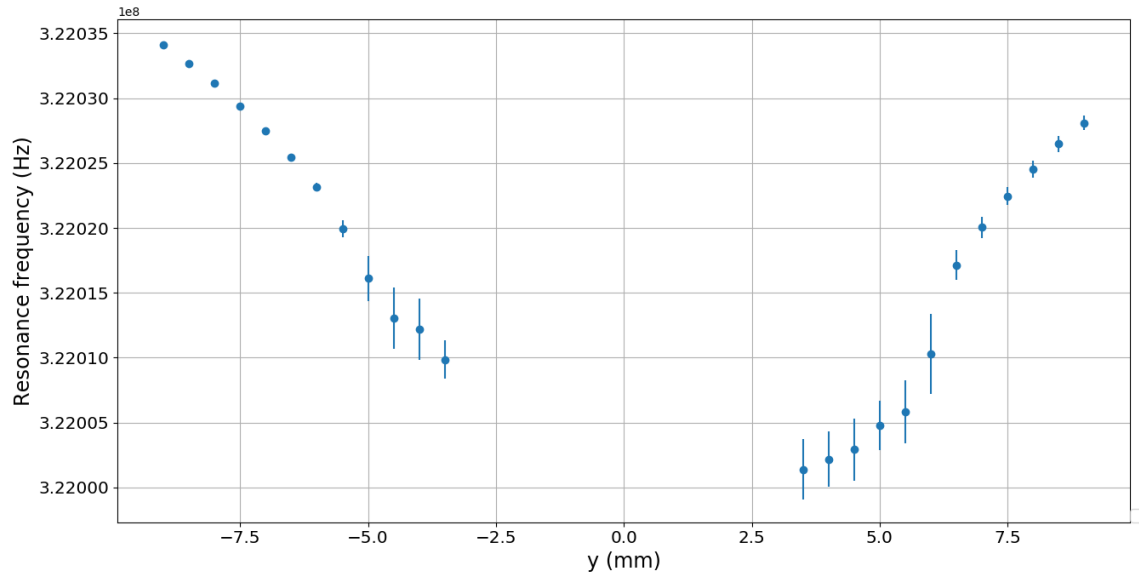


Figure 8.16: The average frequency in different Y position from 9 to -9 mm for the load of 2330 g.

Sag equation, from Equation (4.13), needs to be applied to correct this effect. This equation only shows the relationship between the sag and weight along the Z position. However, the frequency is measured to ensure whether there is the sag effect from the pulley system or not as seen Figure 8.15 and Figure 8.16. In order to confirm the theory, the relationship between the difference in frequencies against the difference in Y position, based on Y in 5 mm steps from the load of 610 g, is considered, in only the lower quadrant. The fitted graph of the difference in frequency against Y position is shown in Figure 8.17. The fitted line increases nonlinearly when the Y distance is higher. The fitted line slowly increases when the Y distance is higher. This can be fitted with horizontal asymptote function. However, principle polynomial function is considered as the -Y could be ignored because the data is not stable. This relationship is applied in the sag equation to find the difference in frequency from the sag that provided by the weights, see Figure 8.18. The propagation error from the fit is about ± 124.55 Hz. However, the error becomes ± 46.04 Hz when ignoring the first two points.

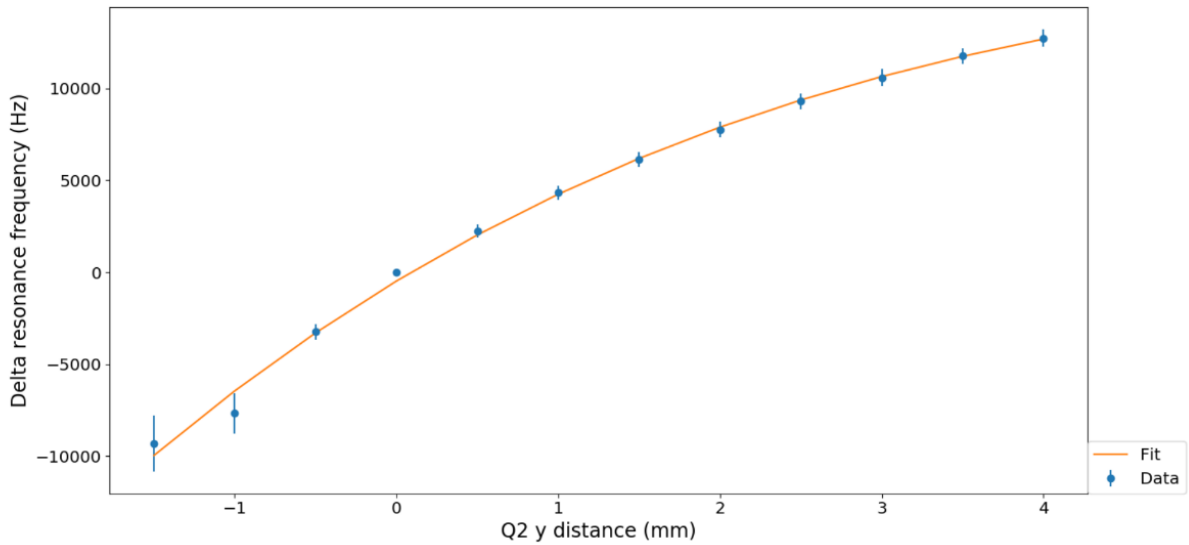


Figure 8.17: Fitting of different frequency against Y distance for the load of 610 g.

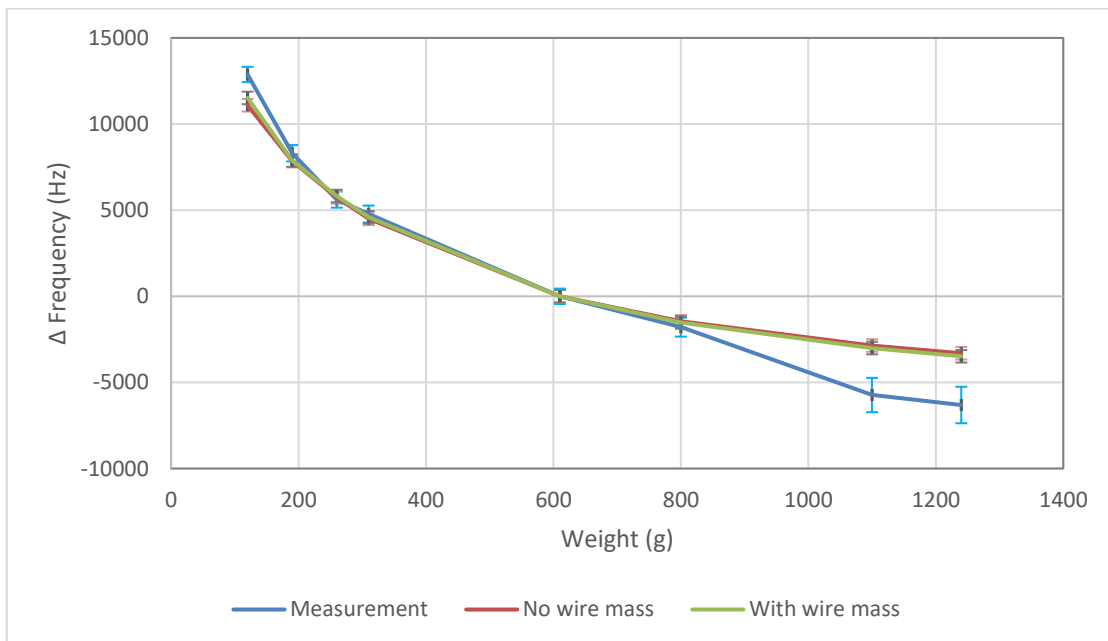


Figure 8.18: The comparison of sag correction from the sag equation with and without the weight of the thread and the results from the measurements.

Figure 8.18 illustrates how the sag would be with different weights. There are calculated from Equation (4.13) and the relationship between the difference in frequency and the change in Y position from the fit in Figure 8.17. The green and red lines show the results of the sag equation with and without wire mass, respectively. The data are close to each other, so, the wire mass can be ignored. The blue line provides the difference in frequency against the load. The high masses provide some variation which comes from the bead being

closer to the vanes and leads to results being different from the predicted outcome. Nevertheless, this demonstrates that the sag equation is correctly compensating for the sag.

8.2.4 Temperature Effects

The effect of temperature on the frequency of the RFQ has been studied. It is hard to detect an effect of the temperature because there are various environmental factors that impact the fields and frequency. The temperature is one of those. Figure 8.19 shows the temperature of the FETS RFQ and air from afternoon 25th July to afternoon 26th July. The air and FETS RFQ temperature provide a similar trend until 5 pm. The FETS RFQ temperature still increases with a similar trend, but the air temperature goes up gradually. Then, the air temperature drops at 9 pm whereas the FETS RFQ temperature starts decreasing around midnight. The idea behind why the RFQ and air temperature are not in a good agreement for all the day is the material of the RFQ. Further, the FETS RFQ is connected via the rails to other equipment and material, giving it a much higher thermal mass and a much slower response to temperature changes than the air.

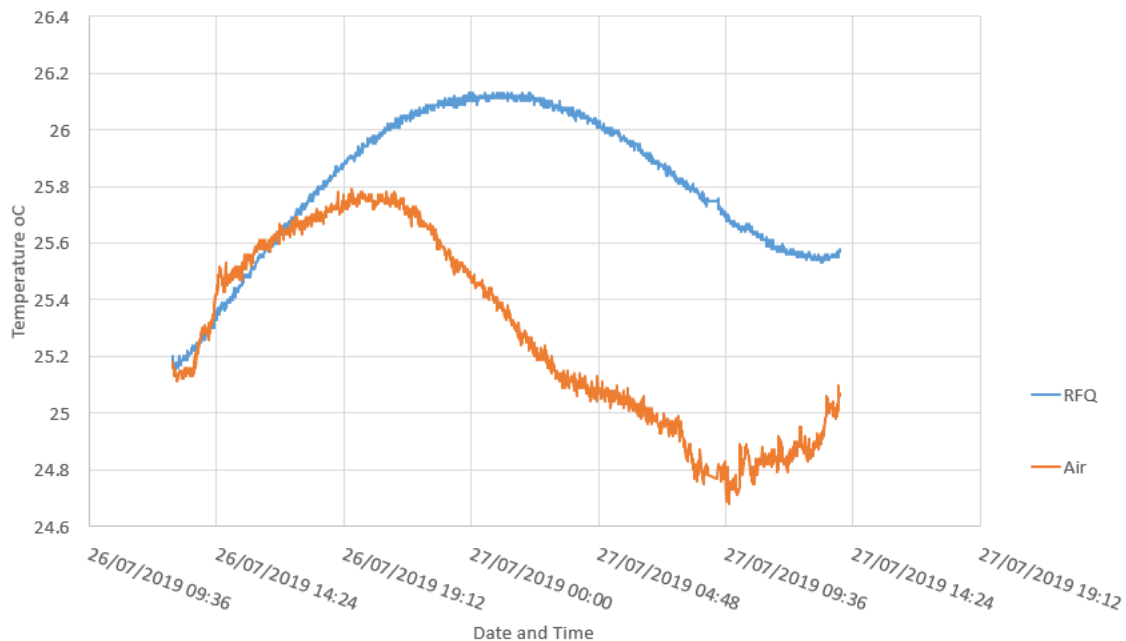


Figure 8.19: The temperature at FETS area overnight from noon 25th July to noon 26th July 2019 by a thermocouple.

The temperature does affect the fields. An example that illustrates the effects of the temperature on frequency has been shown by running the bead pull for a longer period. That measurement starts with a normal run speed, but the time for each step slowly increases due

to a bug in the software at that time. As seen in Figure 8.20 and Table 8.4, there is a significant change in the fields over a long period of measurement.

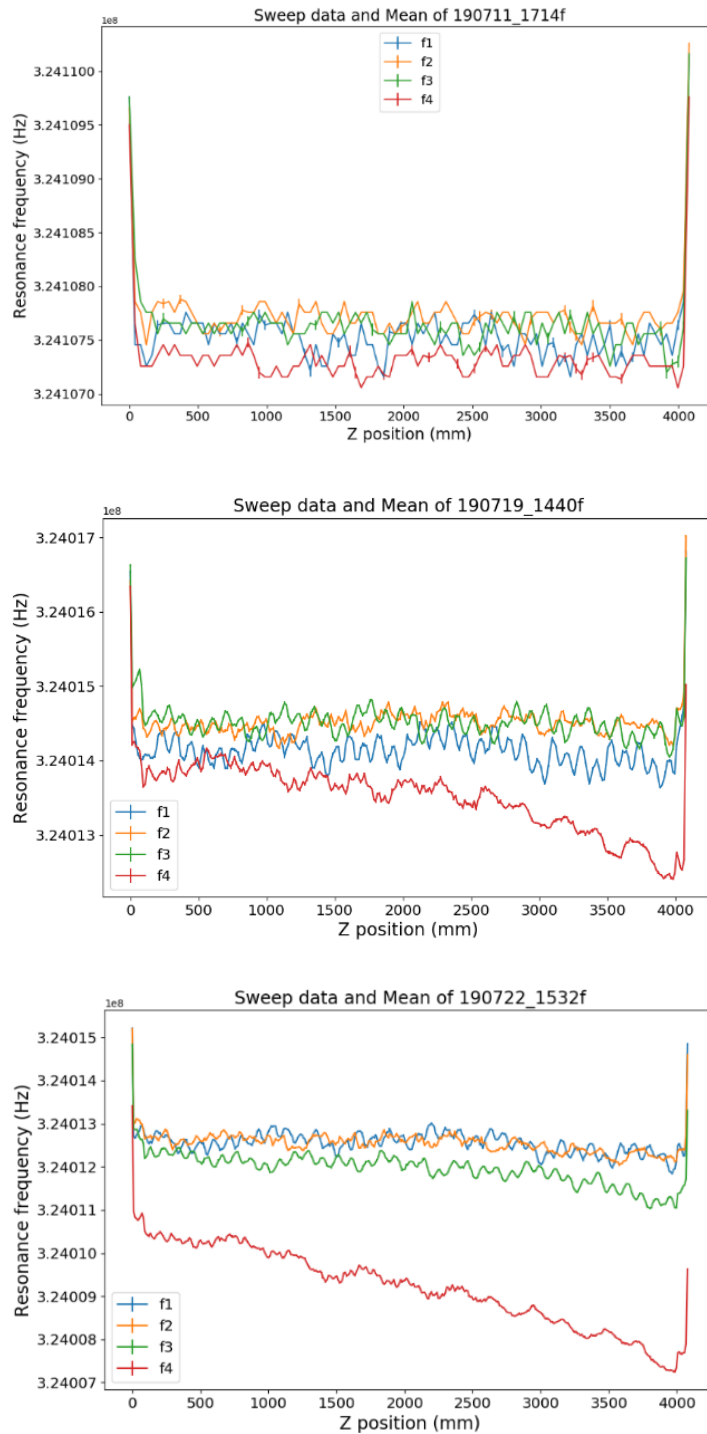


Figure 8.20: The frequency of the FETS RFQ along Z position in each quadrant when running over 15 minutes (top), 1 hour (middle) and 4 hours (bottom).

Table 8.4: The time period of the measurement in different time and quadrants.

File	190711 1714	190719 1440	190722 1532
Z points	100	300	400
Q1	16 m	40 m	52 m
Q2	16 m	48 m	1 h 10 m
Q3	17 m	1 h 2 m	2 h
Q4	16 m	1 h 37 m	3 h 40 m

The data was taken in the evening until night. The red line is data of quadrant 4 which has the longest period. The temperature of the FETS RFQ increased from the afternoon to midnight. Therefore, the frequency dropped as expected. The temperature effect is small if a running period is a short period and are acceptable when the running period was less than 1 hour and a half. This is set a limit for how long a run could be.

For the very final tuning, the RFQ was on a stable cooling water supply, so maintained at a constant temperature, eliminating this source of error.

8.2.5 Manual Tuners

The slug tuners were studied to find the relationship between the frequency and their lengths. Because of the limit of times, only tuner fifteen quadrant two (T15Q2) and tuner five quadrant four (T5Q4) were chosen to see the effects in frequency and field when their length has changed.

8.2.5.1 Local frequency

In the algorithm, the local frequency (ω_z) is used to find the new tuner length. The measured frequencies are converted to the local frequencies for further calculation.

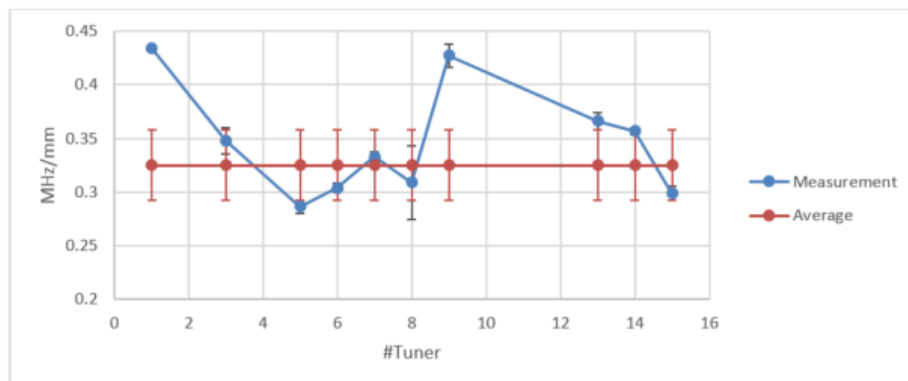


Figure 8.21: The ratio of frequency against the tuner's length from measurement and its average.

By measuring the frequency when each tuner was inserted in different lengths, Figure 8.21 shows the local frequency per unit length of each tuner along the RFQ. Ignoring the striking data from T1 and T9, the average of the measurement data would be applied to the algorithm to calculate by what length each tuner should be adjusted.

8.2.5.2 Effects on the FETS RFQ

The different lengths of tuner T15Q2 and T5Q4 were tested. By increasing in 2 mm steps, the results of their fields have been plotted in Figure 8.22. It is not easy to identify the effects of these tuner's length on the fields. However, the effects on the frequency are easier to determine.

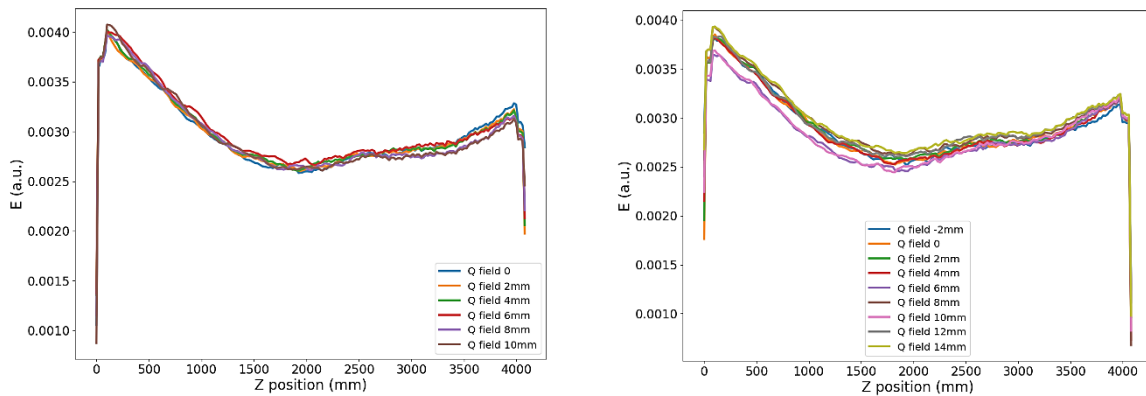


Figure 8.22: The quadrupole fields when inserting T15Q2 (left) and T5Q4 (right) by 2 mm.

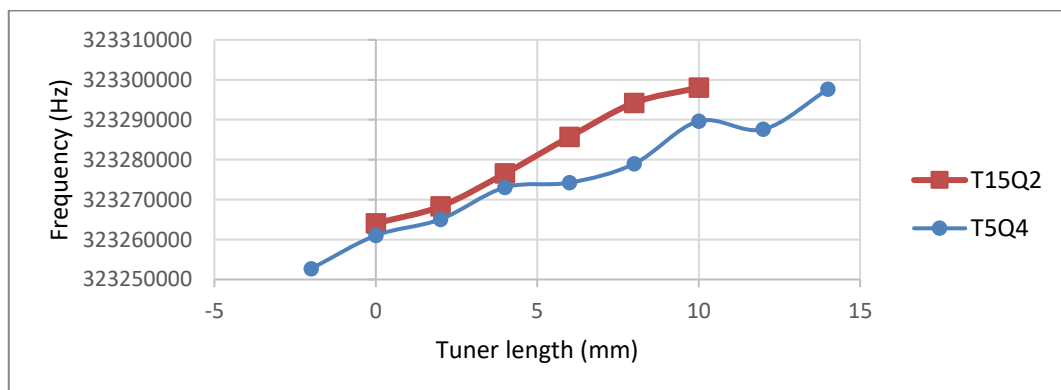


Figure 8.23: Relationship between frequency and tuner's length of T15Q2 and T5Q4.

Figure 8.23 illustrates the average frequency against the tuner's length in both T15Q2 and T5Q4. They are in a similar trend at the beginning. However, the data of T5Q4 seems to be different. This is because the data are taken on different days at a different temperature. Thus, the average of local frequency per unit length of tuners is used for the field flattening.

8.2.6 Automatic Tuners

The automatic tuners will be applied to correct the frequency during the operation. Ideally, the movement could be between 0 and 15 mm, see Figure 6.13, from the RFQ's surface or 17 to 37 mm from the external measurement. The inner and outer limit of all automatic tuners were measured to record what frequency change can be made with these tuners. The fields are shown in Figure 8.25. The average of each field is used to calculate the difference and sigma errors.

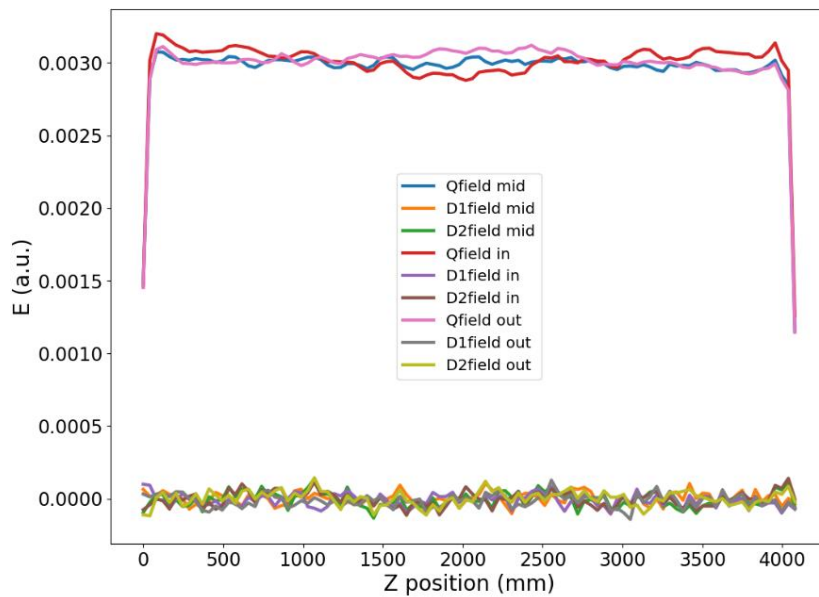


Figure 8.24: The field when the automatic tuners reach the inner and outer limit.

Table 8.5: Data when moving the automatic tuners.

Automatic Tuners	All mid	All in	All out
Frequency (MHz)	324.14706	324.26415	324.07983
Frequency Difference (MHz)	-	0.11709	-0.06723
Error of average Q field (%)	0.84	1.81	1.28
Relative error of middle tuner length (%)	-	2.08	1.31
Sigma error of Q field	0.0000299780	0.0000675129	0.0000461819

The maximum range of frequency that can be shifted by the dynamic tuners is around ± 0.19 MHz. When the automatic tuners are in, the percentage of the different error is higher than when the dynamic tuners are out. This is because the tip of the tuners is closer to the vane resulting in a bigger variation in frequency.

8.2.7 Results with the Tuning Algorithm

After running the algorithm by using measurement data, a new set of tuner positions is applied. This process is repeated until we cannot achieve a better sigma of the quadrupole field which should be a small value. This limitation comes from the human errors in the tuner adjustment, as it then becomes very difficult to make further improvements.

The goal of correcting the tuner's length is to provide a flat field as much as possible. The length of each tuner is changed by the algorithm until it is out of limits. Then, that tuner is ignored for the next calculation. The process is repeated until all of the new lengths are adjustable.

The tuning process was first calculated with all the tuners including the automatic tuners as seen in Table 8.6. The reference data was when all the tuners were in their middle lengths. The different and sigma errors, calculated using the variation of quadrupole fields from its mean, are seen to significantly improve with the first two tunings, from 7.42% to 1.51% and 0.84%, respectively. After that, they do not much improve as they reach the limit from human errors, as seen in Figure 8.25. Then it is hard to see the differences by eye.

Table 8.6: Results of each field after applying the algorithm and adjusting the tuners.

Conditions	Order #	Frequency (MHz)	Q field Error (%)	Sigma of Q field
With automatic tuners	Before	323.71371	7.42	0.0003085591
	1st	323.89389	1.51	0.0000553596
	2nd	324.01401	0.84	0.0000333814
	3rd	324.05405	0.81	0.0000297603
	4th	324.13413	0.81	0.0000293401
	5th	324.09409	0.99	0.0000362933
Moving the automatic tuners in the middle	1st	324.10822	1.21	0.0000469594
	2nd	324.11260	0.82	0.0000294956
	3rd	324.09409	0.83	0.0000311772
	4th	324.09409	0.82	0.0000312810
Reset position of automatic tuners (middle)	1st	323.97397	1.01	0.0000400131
	2nd	324.01401	0.81	0.0000298613
	3rd	324.01401	1.07	0.0000392155
	4th	324.01401	0.77	0.0000291461
	5th	324.05405	0.80	0.0000324030
	6th	324.05405	0.76	0.0000300466
Final	1st	324.12007	0.96	0.0000341278
	2nd	324.13213	1.12	0.0000427132
	3rd	324.13714	0.80	0.0000290486
	4th	324.14414	0.80	0.0000305578

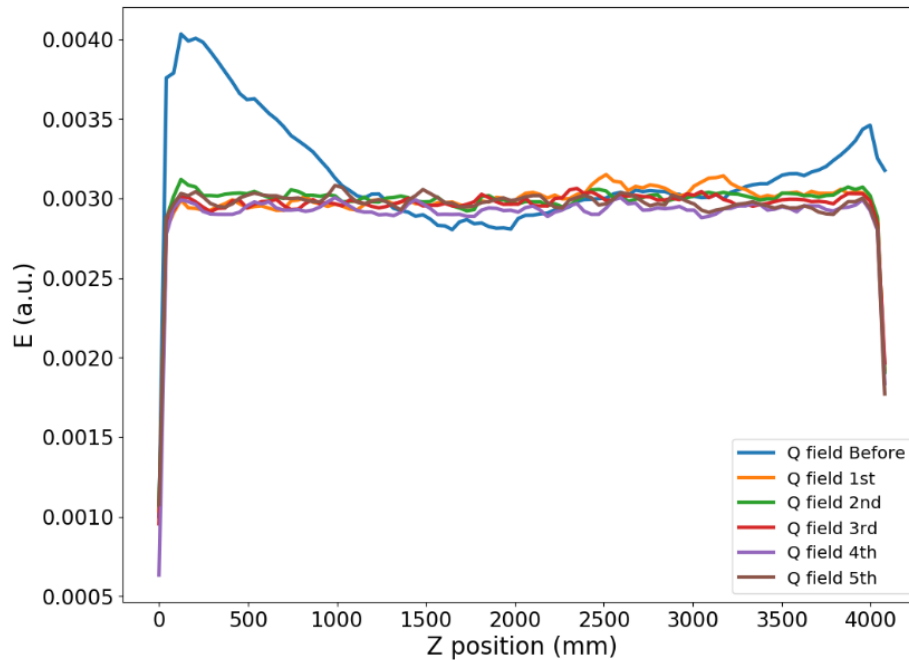


Figure 8.25: The quadrupole field results after tuning the RFQ with automatic tuners.

As this clearly shows that the algorithm is working, the next step as to set the automatic tuners at the middle length, the most convenient position to correct the field during operation. Following this, the limits of the automatic tuners were reset. The tuning was repeated for the “final” measurement.

The frequency is not easy to control as it can change in just a day depending on temperature. For example, the data from the first tuning of the final measurement and the last tuning with reset automatic tuner limits were taken in different weeks. The temperature differed from 25.4 °C to 23 °C, leading to an increase in frequency.

8.2.8 Final Tuning Results

The frequencies and fields before and after tuning are compared in Figure 8.26, Figure 8.27 and Figure 8.28. The frequencies and fields in each case are now flat. The frequencies difference decreases from 6 kHz to 0.5 kHz. This improves the imperfect structure of the FETS RFQ. All quadrupole and dipole fields are more uniform. The error bar from the graph before the tune is higher because the range of the frequency that has been used is longer than the final data.

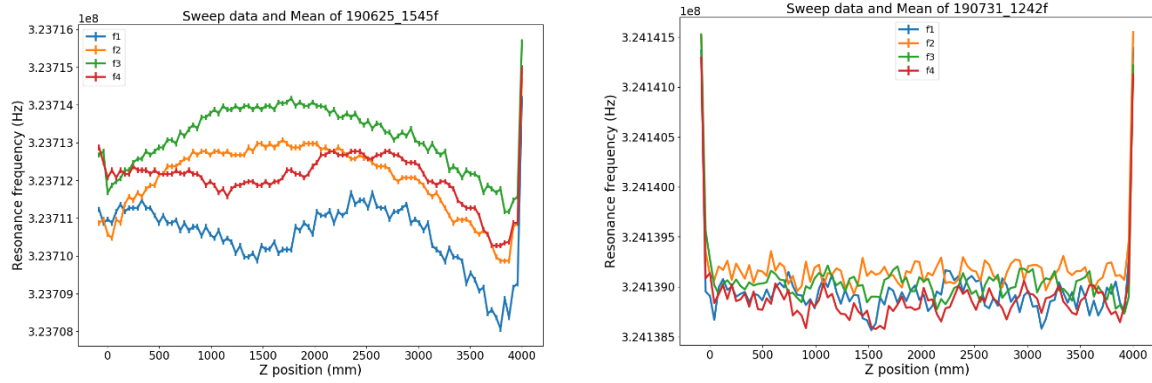


Figure 8.26: The frequencies of the RFQ before (a) and after (b) doing the field flatness in each quadrant.

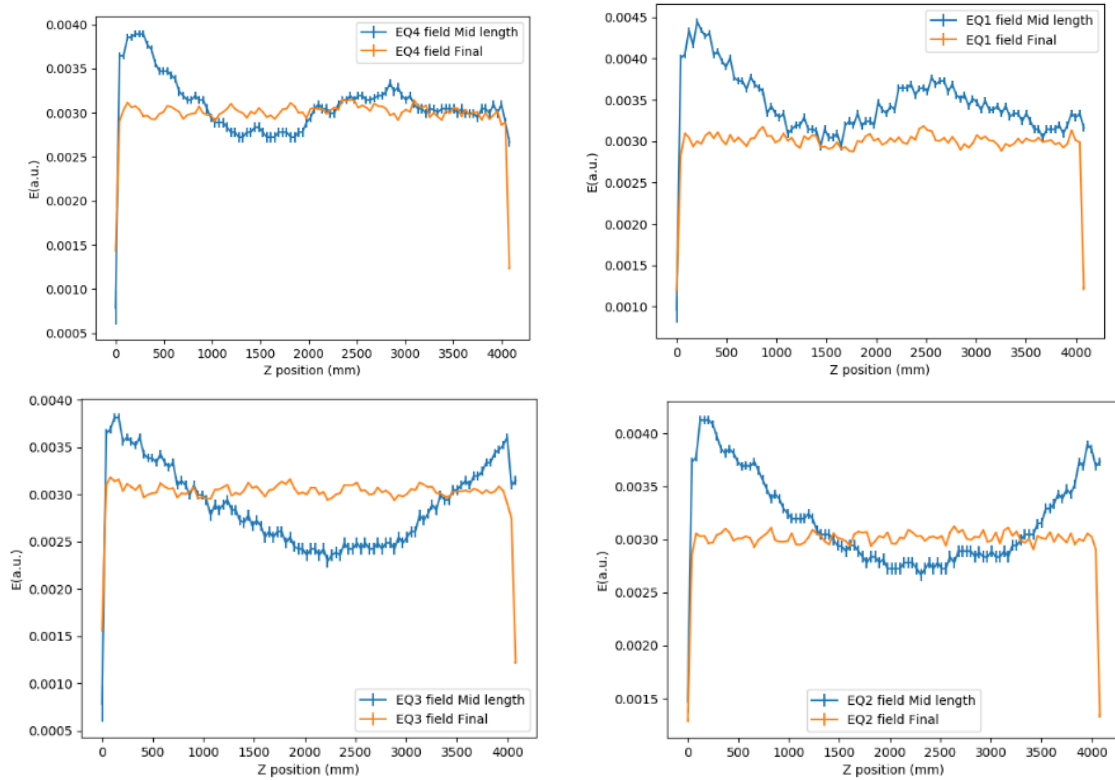


Figure 8.27: Quadrupole fields of before (blue) and after (orange) doing the field flatness in each quadrant.

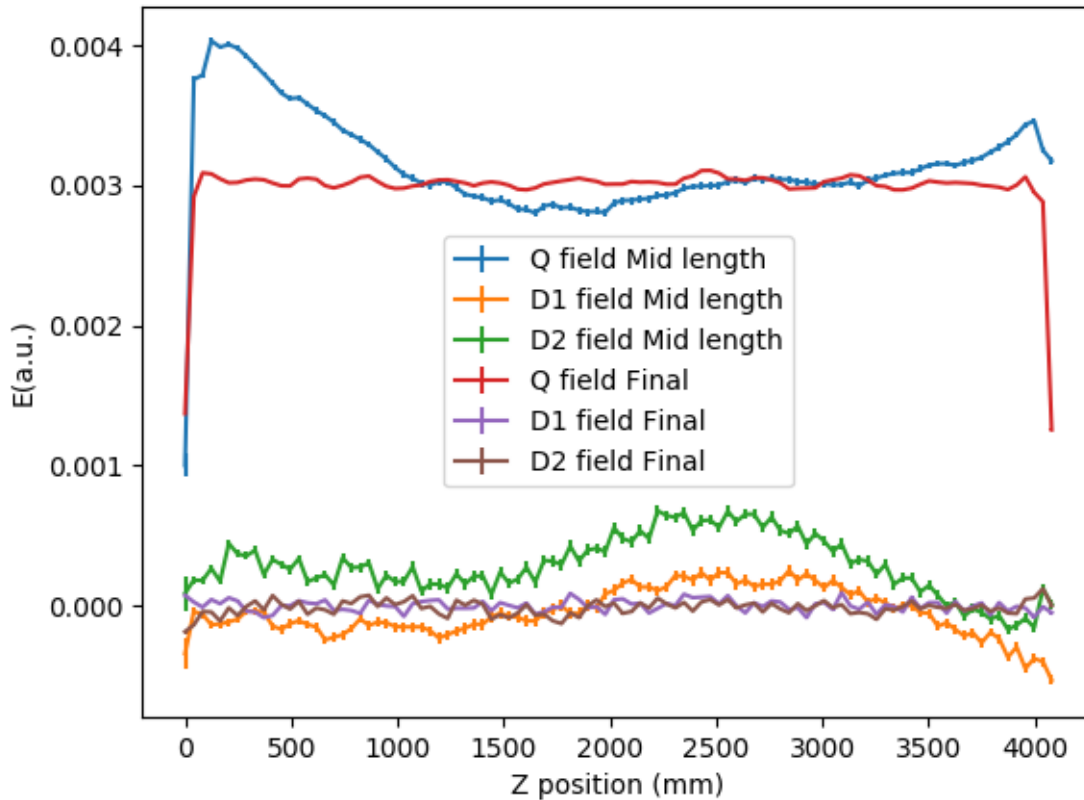


Figure 8.28: The comparison of the quadrupole and dipole fields between before and after doing the field flatness.

The idea of the algorithm is to only flatten the fields while the frequency depends on how the tuners are inserted. The final frequency can only be set when the RFQ is under power, with the cooling on, as only then temperature will be at its correct value. The algorithm has been re-written to calculate the length of the tuners to give the right frequency at 324 MHz. As the flat field is provided, the calculation would be changing the length of the tuners to meet the operation frequency without affecting the fields.

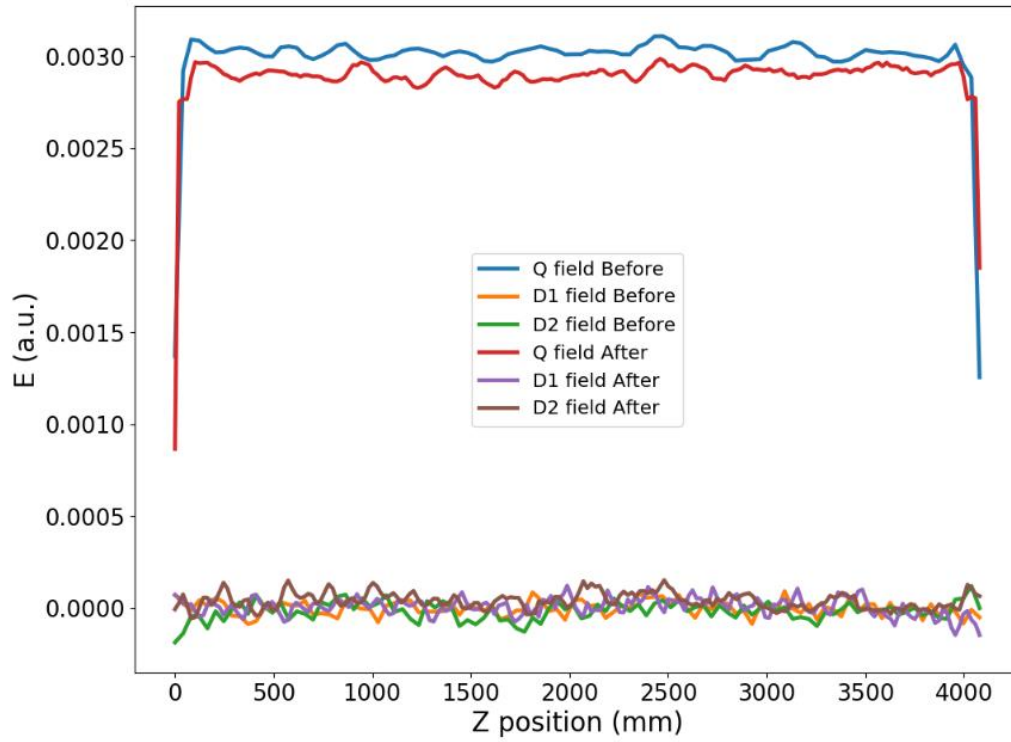


Figure 8.29: After added the cooling system.

In December 2019, the cooling system was installed with 20 °C operating temperature. The FETS RFQ needed to be tuned to meet 324 MHz with that temperature. Figure 8.29 illustrates the quadrupole and dipole fields of the data from the end of July and the final results with the cooling system. The error of the quadrupole field slightly increases from 0.8% to 0.93% which is still acceptable. With the new tuner adjustment, the frequency was 324.00137 MHz. It would be moved down by the automatic tuners which are in mid-length in the final process. After that, the bead pull test was dismantled and cannot be re-installed without a major intervention. The FETS RFQ then was in vacuum condition.

8.3 Summary

In 2016, the bead pull measurement with the required four-metre length was reconstructed. The setup was moved from the testing area to the FETS area, with major changes being required for the FETS site. The length of the pulley system was extended from one to four metres. The measurements were taken from one section to the complete FETS RFQ.

In one section of the FETS RFQ measurement, only sections one and two were mounted for the bead pull measurements, in different years. The forward and reverse directions were run to study their differences.

With the complete FETS RFQ, many measurements have been taken. The measurement data were used to calculate the new tuner's length to flatten the fields. The measurements of the forward and reverse directions were repeated. The possible errors in the bead pull measurements were studied to include the impact of errors in the calculation. The sag effect was an important in the long pulley system. The weight of the pulley load was varied to study the results from the sag. When the weight is high the frequency started varying which means the bead is close to the vane. The results show that a sag correction was still required and used to verify that this was being done correctly. The effect of temperature changes the overall frequency. This was a concern because the temperature in the hall changes, and the measurements were taken at room temperature.

Both the manual and automatic tuners were studied. The effects of the tuners, such as the length against the frequency, were used for further calculation. The results from the tuning algorithm gave a significant improvement. The error reduced from 7.42% to 0.8% and became stable from the fourth tuning. The final results are 0.8% and 0.93%, without and with the cooling system at about 324 MHz.

Chapter 9. Conclusions

This chapter summarises the work of this thesis and draws the conclusions from the work that has been done. It also identifies what further work still needs to be done and makes recommendations for future bead pull measurements of RFQs.

9.1 Summary

RFQs are designed to provide focusing, bunching and acceleration for proton and ion beams at low energy to allow further acceleration in standard linear accelerators. The acceleration and bunching fields are generated by the vane tip modulation along the RFQ. The focusing forces are from the quadrupole fields of the four-electrodes. A 324 MHz RFQ has been designed for the FETS project. This project aims to accelerate a 60 mA H⁻ beam to 3 MeV. It consists of five main parts: an ion source, LEPT, RFQ, MEPT and a diagnostic section.

The FETS RFQ is a four-vane structure with four modules, each one metre long. This RFQ type is suitable for an available RF source, a pulsed klystron. Rather than the standard technique of permanent brazing, the RFQ is bolted together and uses an O-ring to vacuum seal the major and minor vanes, making the FETS RFQ more convenient to transport. There are fifty-eight slug tuners and four automatic tuners inserted into the FETS RFQ cavity. The slug tuners must be adjusted by hand. The maximum inserted length is 27 mm. The automatic tuners with the feedback control are applied during operation, to compensate for environmental changes, etc. The inserted length is up to around 20 mm from the inner surface of the RFQ cavity. They are set in the middle of the RFQ and are automatically adjusted to make the RFQ operation at the correct frequency.

The idea of the tuner is the relationship between the inserted length and the frequency. The frequency increases when the tuner's depth increases. The RFQ fields can be calculated from the measured frequency obtained using a VNA. The quadrupole and dipole frequencies are also measured. They are decomposed into the summation of sinusoidal terms, leading to a measure of which modes, quadrupoles and dipoles, are dominant in the RFQ. By calculating the coefficient factors: $A(p)$, $B(p)$ and $C(p)$, the new local frequency, depending on the tuner positions, can be achieved by a least squares fit to compensate the old fields. The local frequency then is converted into the tuner's length. After adjusting all of the RFQ tuners, the bead pull is then re-run to measure the new fields. This process is repeated until sufficiently flat fields are achieved.

The bead pull measurements started with the one-metre long section two of the FETS RFQ. The experiment consisted of the pulley system, VNA and a LabVIEW system. There were five motors to control the bead: one stepper motor for the longitudinal direction and four servo motors for the transverse directions. The pulley system was about 1.5 metres long. The measurements were in 2015 and were for studying the bead pull system and program. In 2016, the pulley system was moved to the FETS area and redesigned as this site has a limitation in height and longitudinal space due to the LEBT and MEBT. Section two of the RFQ was tested at that time, followed by section one in 2018 and the full and complete FETS RFQ in 2019.

For the full FETS RFQ, measurements were only made in the forward direction to reduce the time taken. The sag and measurement errors were considered. This included wheel and human errors. Temperature data were also collected. Both the manual and automatic lengths were adjusted to study their effect on the frequency and fields. The relationship between the tuner's length and frequency was measured. The tuning algorithm was applied to adjust the tuners and improve the field. The difference from flat fields was reduced dramatically from 7.42% to 0.8%, the limit that could be obtained with the system used for adjusting and measuring the tuner positions.

The final results with the cooling system in operation gave a similar result. The tuning algorithm flattened not only the overall field, but also the fields in each quadrant, as seen in Figure 8.27 and Figure 8.27. Comparing with the four-vane PXIE bead pull measurement where the flat fields improved from 94.6% to 96% [82], the tuned fields of the FETS RFQ are surprisingly uniform overall and in each individual quadrant.

9.2 Future Work and Suggestions

After the FETS RFQ bead pull measurements had been done, the pulley system was dismantled for the next FETS studies. The FETS RFQ is going to be commissioned with power and tested with a single beam from the ion source when the FETS interlocks are approved [96]. This aims to confirm the tuned fields are good enough and study the beam characteristics. After that, full commissioning will be undertaken.

The tuners' length might need to be adjusted depending on the temperature with the RFQ under full power. The previously measured data can be used as the reference. However, the bead pull FETS RFQ measurement has already been tested with the cooling system on. The fields' pattern might not change, but the manual tuners may need to be used if the

automatic tuner correction range is insufficient. In addition, the temperature will be tracked during operation, in order to adjust the length of the automatic tuners.

Though the FETS RFQ bead pull measurements have been completed successfully, there are some changes that could be made to improve a similar system in the future and make it easier to use.

The design of the slug tuner is a problem from the point of the length adjustment and measurement. The adjustment needs to be easier and more reliable to do, and it should be easier to measure how big the adjustment is. For example, a scale could be added, as done with the CERN 750 MHz HF-RFQ [86]. A displacement gauge can also be used to find how deep the tuner is [97]. These options were considered for FETS, but were not implemented due to the additional cost for the 58 tuners. Nevertheless, this has been determined as the limiting factor during this work and improvement in this area will reduce the time it takes to do the tuning and increase the accuracy. The tuning algorithm used is different to what other groups have done and requires fewer measurements than the CERN technique, for example. This iterative technique has proved very successful.

The environmental measurements are also important. The temperature of the RFQ and air pressure and humidity need to be measured more precisely than done in this project. This is because there was no temperature control for most of these measurements, making some results harder to interpret.

Chapter 10. References

- [1] T. Amin, "Improving Hadron Therapy: Design of the Beam Transport System for a Biomedical Research Facility and PET Isotope Production," University of Huddersfield, 2019.
- [2] N. Ratcliffe, "Potential of a compact low energy proton accelerator for medical applications," University of Huddersfield, 2014.
- [3] S. Albright, "Security Applications of Novel Neutron Sources," University of Huddersfield, 2016.
- [4] T. P. Wangler, "RF Linear accelerators," pp. 232-281, 2008.
- [5] A. Sidorin, "Linear Accelerators," in *NUCLEAR PHYSICS METHODS AND ACCELERATORS IN BIOLOGY AND MEDICINE: Fifth International Summer School on Nuclear Physics Methods and Accelerators in Biology and Medicine*, 2010, vol. 1204, no. 1, pp. 83-90: AIP Publishing.
- [6] Y. Cheng, S. Jolly, A. Kurup, P. Savage, and J. Back, "The RAL Front End Test Stand," *Proceedings of EPAC04, Edinburgh, Scotland*, 2006.
- [7] M. Vretenar, "Linear Accelerators," *arXiv preprint arXiv:1601.05210*, 2016.
- [8] M. Lindroos *et al.*, "The European spallation source," *Nuclear Instruments and Methods in Physics Research Section B: Beam Interactions with Materials and Atoms*, vol. 269, no. 24, pp. 3258-3260, 2011.
- [9] A. W. Chao and K. H. Mess, *Handbook of Accelerator Physics and Engineering*. World scientific, 2013.
- [10] M. Weiss, "Introduction to RF linear accelerators," 1994.
- [11] J. W. Staples, "RFQs—An introduction," in *The Physics of Particle Accelerators: Based in Part on the US Particle Accelerator School (USPAS) Seminars and Courses in 1989 and 1990*, 1992, vol. 249, no. 2, pp. 1483-1532: AIP Publishing.
- [12] F. Gerigk, "Cavity types," *arXiv preprint arXiv:1111.4897*, 2011.
- [13] D. H. Sloan and E. O. Lawrence, "The production of heavy high speed ions without the use of high voltages," *Physical Review*, vol. 38, no. 11, p. 2021, 1931.
- [14] L. W. Alvarez, "The design of a proton linear accelerator," in *Physical Review*, 1946, vol. 70, no. 9-10, pp. 799-800: AMERICAN PHYSICAL SOC ONE PHYSICS ELLIPSE, COLLEGE PK, MD 20740-3844 USA.
- [15] J. Staples, "Chapter 7 - Accelerator Structures III - RFQ," Available: http://uspas.fnal.gov/materials/11ODU/Proton_9.pdf
- [16] I. Kapchinskii and V. Teplyakov, "A linear ion accelerator with spatially uniform hard focusing," *Prib. Tekh. Eksp.*, vol. 1970, no. SLAC-TRANS-0099, pp. 1-17, 1969.
- [17] L. D. Hansborough, "Development of 400-to 450-MHz RFQ resonator-cavity mechanical designs," Los Alamos National Lab., NM (USA)1982.
- [18] A. Schempp, "Radio-frequency quadrupole (RFQ)," 1992.
- [19] Y. Kondo, T. Morishita, S. Yamazaki, T. Hori, Y. Sawabe, and A. Takagi, "BEAM TEST OF A NEW RFQ FOR THE J-PARC LINAC," *MOPP091, in these proceedings*, 2014.

-
- [20] A. Lombardi *et al.*, "Beam dynamics in a high frequency RFQ," in *Proceedings of 6th International Particle Accelerator Conference, Richmond, 2015*.
- [21] A. Letchford, D. Faircloth, D. Findlay, M. Perkins, A. Stevens, and M. Whitehead, "Testing, installation, commissioning and first operation of the ISIS RFQ pre-injector upgrade," in *Proceedings of the 2005 Particle Accelerator Conference, 2005*, pp. 695-697: IEEE.
- [22] F. Float and A. Market, "Advanced Oncotherapy," 2017.
- [23] *Advanced Oncotherapy*. Available: <https://www.avopl.com/en-gb/>
- [24] C. Prior and A. Adelman, "High Intensity Proton Studies at RAL," in *Proc. of ICFA Advanced Beam Dynamics Workshop (HB'18)*, 2018: JACoW.
- [25] J.-B. Lagrange *et al.*, "Progress on Design Studies for the ISIS II Upgrade," in *10th Int. Particle Accelerator Conf. (IPAC'19), Melbourne, Australia, 19-24 May 2019*, 2019, pp. 2075-2078: JACOW Publishing, Geneva, Switzerland.
- [26] R. Edgecock, "Neutrino factory R&D in Europe," *Nuclear Physics B Proceedings Supplements*, vol. 149, pp. 49-53, 2005.
- [27] D. Findlay, M. Clarke-Gayther, and D. Faircloth, "The RAL Front End Test Stand," *Proc. NuFact04, Osaka University, Japan, 2004*.
- [28] A. Letchford *et al.*, "STATUS OF THE RAL FRONT END TEST STAND," in *IPAC 2015, Richmond, VA, USA, 2015*.
- [29] A. Letchford, "RFQ Development at RAL: Proton Accelerators for Science and Innovation Second annual meeting," 2013.
- [30] A. Letchford *et al.*, "Proposal for continuation of the Front End Test Stand," 2015.
- [31] R. Scrivens, "Proton and ion sources for high intensity accelerators," 2004.
- [32] G. J. R. o. s. i. Dimov, "Use of hydrogen negative ions in particle accelerators," vol. 67, no. 10, pp. 3393-3404, 1996.
- [33] D. Faircloth and S. J. N. J. o. P. Lawrie, "An overview of negative hydrogen ion sources for accelerators," vol. 20, no. 2, p. 025007, 2018.
- [34] I. Gardner, C. Planner, G. Rees, and D. J. P. A. Gray, "The Relevance Of Isis Experience To The Design Of Future High intensity synchrotrons," vol. 31, pp. 227-234, 1990.
- [35] B. Jones, D. Adams, and C. Warsop, "Injection optimisation on the ISIS synchrotron," in *Proc. of EPAC, 2008*, vol. 8.
- [36] D. Faircloth *et al.*, "The front end test stand high performance H- ion source at Rutherford Appleton Laboratory," vol. 81, no. 2, p. 02A721, 2010.
- [37] A. Letchford *et al.*, "Current status of the RAL front end test stand (FETS) project," *LINAC2012, Israel, to be published*, 2012.
- [38] S. Jolly, M. Easton, S. Lawrie, A. Letchford, J. Pozimski, and P. Savage, "Novel integrated design framework for radio frequency quadrupoles," *Nuclear Instruments and Methods in Physics Research Section A: Accelerators, Spectrometers, Detectors and Associated Equipment*, vol. 735, pp. 247-251, 2014.
- [39] P. Savage, "2011 FETS RFQ Design Review," 2011.
- [40] S. Alsari, J. Pozimski, P. Savage, and M. Aslaninejad, "RF delivery system for FETS," *IPAC2014, Dresden, June, 2014*, 2014.

-
- [41] M. Weiss, "Radio-frequency quadrupole," 1987.
- [42] M. Vretenar, "The radio-frequency quadrupole," *arXiv preprint arXiv:1303.6762*, 2013.
- [43] K. Wang *et al.*, "RF design of radio-frequency quadrupole accelerator for heavy ion medical machine," *Nuclear Instruments and Methods in Physics Research Section A: Accelerators, Spectrometers, Detectors and Associated Equipment*, vol. 927, pp. 375-381, 2019.
- [44] J. Staples, "Chapter 9 - Structures IV - Tuning and Stabilization," Available: http://uspas.fnal.gov/materials/11ODU/Proton_9.pdf
- [45] A. Schempp, "Radio-frequency quadrupole linacs," 2005.
- [46] S. Lawrie, "Summary of Recent RF Simulations of the FETS RFQ," ed, 2011, p. 16.
- [47] O. Delferriere, M. Desmons, A. France, and R. Ferdinand, "A New RF Tuning Method for the End Regions of the IPHI 4-vane RFQ," in *Tenth European Particle Accelerator Conference "EPAC'06"*, 2006, pp. 285-287.
- [48] G. Romanov *et al.*, "The Fabrication and Initial Testing of the HINS RFQ," *LINAC08, Victoria, BC, Canada*, 2008.
- [49] T. Morishita *et al.*, "Fabrication of the New RFQ for the J-PARC Linac," in *Proc. of 2010 International Particle Accelerator Conference, Kyoto, Japan*, 2010, p. 783.
- [50] S. Turner and E. O. f. N. Research, *CAS: CERN Accelerator School : RF Engineering for Particle Accelerators : Exeter College, Oxford, UK, 3-10 April, 1991 : Proceedings*. CERN, 1992.
- [51] N. Wells, "Radio Frequency Quadrupole and Alternating Phase Focusing Methods Used in Proton Linear Accelerator Technology in the USSR," DTIC Document 1985.
- [52] E. Boltezar *et al.*, "Performance of the CERN RFQ: RFQ1 project," 1984.
- [53] E. Tanke, M. Weiss, and M. Vretenar, "Performance of the CERN high-intensity RFQ," 1990.
- [54] R. Gough, "Design and operation of the LBL heavy ion RFQ linac," 1984.
- [55] H. Haseroth, "Planning and proposals for the CERN heavy ion injector," CM-P000591521988.
- [56] A. Schempp, "RFQ ion accelerators with variable energy," *Nuclear Instruments and Methods in Physics Research Section B: Beam Interactions with Materials and Atoms*, vol. 40, pp. 937-942, 1989.
- [57] O. Hohn *et al.*, "Status of the Frankfurt 14 GHz-ECRIS-(ve) RFQ Facility," 1999.
- [58] M. Clarke-Gayther *et al.*, "The RAL front end test stand," *Nuclear Physics B-Proceedings Supplements*, vol. 149, pp. 323-325, 2005.
- [59] C. Bailey *et al.*, "THE RUTHERFORD RFQ TEST STAND," 2000.
- [60] K. Bongardt *et al.*, "The ESS project. Vol. 3. Technical report," 2003.
- [61] S. Jolly *et al.*, "Detailed study of the RF properties of the FETS RFQ cold model," *Proceedings of EPAC08, Genoa, Italy, THPP024*, pp. 3422-3424, 2008.
- [62] A. Letchford and A. Schempp, "A Comparison Of 4-Rod and 4-Vane RFQ-Fields," in *EPAC*, 1998, vol. 98, p. 1204.

-
- [63] S. Jolly, M. Easton, J. Pozimski, and A. Letchford, "Integrated design method and beam dynamics simulations for the FETS radio frequency quadrupole," *IPAC2010, Kyoto, May*, 2010.
- [64] S. Jolly, M. Easton, S. Lawrie, A. Letchford, J. Pozimski, and P. Savage, "Novel integrated design framework for radio frequency quadrupoles," *Nuclear Instruments and Methods in Physics Research Section A: Accelerators, Spectrometers, Detectors and Associated Equipment*, vol. 735, pp. 240-259, 2014.
- [65] S. Alsari, M. Aslaninejad, and J. Pozimski, "Use of phase information with a stepper motor to control frequency for tuning system of the Front End Test Stand Radio Frequency Quadrupole at Rutherford Appleton Laboratory," *Nuclear Instruments and Methods in Physics Research Section A: Accelerators, Spectrometers, Detectors and Associated Equipment*, vol. 775, pp. 105-111, 2015.
- [66] W. Promdee, A. Letchford, T. Edgecock, G. Boorman, and J. Pozimski, "Bead Pull Measurements of the FETS RFQ at RAL," 2017.
- [67] A. Letchford, P. Savage, J. Pozimski, and Y. Cheng, "Mechanical design and RF measurement on RFQ for front-end test stand at RAL," in *Proceedings of EPAC*, 2006, vol. 6.
- [68] M. Puglisi, "The radiofrequency quadrupole linear accelerator," 1987.
- [69] A. Letchford, "Cavity tuning and field flattening. What's it all about?," presented to FETS Meeting, Rutherford Appleton Laboratory, 2014.
- [70] A. Lombardi, "The Radio Frequency Quadrupole (RFQ)," *CAS, CERN Accelerator School: Small Accelerators: Proceedings: Zeegse, The Netherlands, 24 May-2 June 2005*, no. 12, p. 201, 2006.
- [71] F. Caspers, "RF engineering basic concepts: S-parameters," *arXiv preprint arXiv:1201.2346*, 2012.
- [72] F. Caspers and P. Kowina, "RF Measurement Concepts," 2014.
- [73] L. Young, "Tuning and Stabilization of RFQ's," in *Proceedings of the 1990 Linear Accelerator Conference*, 1990, pp. 10-14.
- [74] S. Biedron and S. Milton, "RF Cavities," Accessed on: 26 June Available: <http://www.engr.colostate.edu/ECE581A3/Labs/RF%20Cavities.pdf>
- [75] L. C. Maier Jr and J. Slater, "Field strength measurements in resonant cavities," *Journal of Applied Physics*, vol. 23, no. 1, pp. 68-77, 1952.
- [76] D. Meidlinger, "A general perturbation theory for cavity mode field patterns," *Proceedings of SRF2009, Berlin, Germany, THPPO05*, 2009.
- [77] J. B. Tatum, "The Catenary," 2019, Available: <http://orca.phys.uvic.ca/~tatum/classmechs/class18.pdf>.
- [78] R. Ainsworth *et al.*, "BEAD-PULL TEST BENCH FOR STUDYING ACCELERATING STRUCTURES AT RHUL," *Proceedings IPAC2011, MOPC049*, 2011.
- [79] D. Bazyl, I. Gonin, T. Khabiboulline, V. Poloubotko, and G. Romabov, "Notes on the Bead-Pull Systems Design for PXIE RFQ," 2013.
- [80] K. R. Shin, Y. W. Kang, S.-H. Kim, and A. E. Fathy, "Investigation of Electromagnetic Field Perturbation With Respect to Mechanical Imperfections in Radio-Frequency Quadrupole (RFQ) Structure," *IEEE Transactions on Nuclear Science*, vol. 59, no. 5, pp. 2428-2434, 2012.

-
- [81] F. Simoens, F. Ballester, A. France, J. Gaiffier, and A. Sinanna, "A fully automated test bench for the measurement of the field distribution in RFQ and other resonant cavity," in *Proc. of the 8th European Particle Accelerator Conf*, 2002, pp. 3-7.
- [82] P. Berrutti *et al.*, "PXIE RFQ BEAD PULL MEASUREMENTS," *Proceedings LINAC2014, TUPP047*, 2014.
- [83] P. M. Lapostolle, "Proton linear accelerators: a theoretical and historical introduction," 1989.
- [84] P. M. Lapostolle and A. L. Septier, "LINEAR ACCELERATORS," 1970.
- [85] S. Zhi-Rui, P. Jun, and F. J. C. P. C. Shi-Nian, "Matrix method for the solution of RF field perturbations due to local frequency shifts," *Chinese Physics C*, vol. 33, no. 9, p. 798, 2009.
- [86] B. Koubek, A. Grudiev, and M. Timmins, "rf measurements and tuning of the 750 MHz radio frequency quadrupole," *Physical Review Accelerators and Beams*, vol. 20, no. 8, p. 080102, 2017.
- [87] C. Li *et al.*, "Radio frequency measurements and tuning of the China Material Irradiation Facility RFQ," *Nuclear Instruments and Methods in Physics Research Section A: Accelerators, Spectrometers, Detectors and Associated Equipment*, vol. 890, pp. 43-50, 2018.
- [88] R. Ainsworth *et al.*, "Bead-pull test bench for studying accelerating structures at RHUL," *Proceedings IPAC2011, MOPC049*, 2011.
- [89] I. Thorlabs, "ATP-DC Servo Motor TDC001," 2020.
- [90] ROHDE&SCHWARZ. (2020). *R&S®ZVB4 Vector Network Analyzer 4 ports, 4 GHz*. Available: https://www.rohde-schwarz.com/dk/product/zvb4-4-port-productstartpage_63493-9747.html
- [91] Python Software Foundation. (2015, 20 December). *Python*. Available: <https://www.python.org/>
- [92] Z. T. Inc. (2020). *X-BLQ1495-E01: Motorized, belt-driven, linear stage, integrated motor encoder and controller, 1495 mm travel*. Available: <https://www.zaber.com/products/linear-stages/X-BLQ-E/details/X-BLQ1495-E01>
- [93] M. Dudman, "Dynamic and Manual Tuner Assy dims," ed, 2019.
- [94] P. J. Petersan and S. M. Anlage, "Measurement of resonant frequency and quality factor of microwave resonators: Comparison of methods," *Journal of Applied Physics*, vol. 84, no. 6, pp. 3392-3402, 1998.
- [95] C. Walck, "Hand-book on statistical distributions for experimentalists," 1996.
- [96] E. Wilson, E. J. Wilson, and E. Wilson, *An introduction to particle accelerators*. Clarendon Press, 2001.
- [97] Y. Cheng, P. Savage, A. Kurup, J. Pozimski, and A. Letchford, "RFQ cold model RF measurements and waveguide-to-coaxial line transition design for the Front-End Test Stand at RAL," in *2007 IEEE Particle Accelerator Conference (PAC)*, 2007, pp. 1655-1657: IEEE.